INSTITUTO CARLOS CHAGAS

Doutorado em Biociências e Biotecnologia

ESTUDOS SOBRE A S-PALMITOILAÇÃO DE PROTEÍNAS EM *TRYPANOSOMA CRUZI*

CASSIANO MARTIN BATISTA

Curitiba/PR

2018

Ministério da Saúde
FIOCRUZ
Fundação Oswaldo Cruz

INSTITUTO CARLOS CHAGAS

Doutorado em Biociências e Biotecnologia

ESTUDOS SOBRE A S-PALMITOILAÇÃO DE PROTEÍNAS EM *TRYPANOSOMA CRUZI*

CASSIANO MARTIN BATISTA

Curitiba/PR
Março-2018

Lombada

TESE D -ICC*	C.M. BATISTA	2018

INSTITUTO CARLOS CHAGAS

Pós-Graduação em Biociências e Biotecnologia

CASSIANO MARTIN BATISTA

Estudos sobre a S-palmitoilação de proteínas em *Trypanosoma cruzi*

Tese apresentada ao Instituto Carlos Chagas/Fiocruz-PR como parte dos requisitos para a obtenção do título de Doutor em Biociências e Biotecnologia.

Orientadores: Dr. Maurilio José Soares

Dra. Iriane Eger

CURITIBA/PR

2018

Batista, Cassiano Martin.

Estudos sobre a S-palmitoilação de proteínas em Trypanosoma cruzi / Cassiano Martin Batista. - Curitiba, 2018.
131 f.; il.

(Doutorado) – Instituto Carlos Chagas, Pós-Graduação em Biociências e Biotecnologia, 2018.

Orientador: Maurilio José Soares.
Co-orientadora: Iriane Eger.

Bibliografia: f. 12-22

1. Trypanosoma cruzi. 2. S-palmitoilação dinâmica. 3. Cavitação . 4. 2-bromopalmitato. 5. Palmitoil proteômica. I. Título.

Elaborada pelo Sistema de Geração Automática de Ficha Catalográfica da Biblioteca de Manguinhos/ICICT com os dados fornecidos pelo(a) autor(a).

“Se o plano A não funcionar, lembre-se que o alfabeto tem diversas outras letras.”

AGRADECIMENTOS

Agradeço a todos que contribuíram direta e indiretamente para o desenvolvimento desta tese, principalmente aos meus orientadores, Dr. Maurilio José Soares e Dra. Iriane Eger, pelo apoio e ensinamentos durante o período.

RESUMO

S-palmitoilação é uma modificação proteica pós-traducional que consiste na adição de ácido palmítico a resíduos de cisteína através de ligação tioéster, regulando assim a localização subcelular e função das proteínas palmitoiladas, principalmente a inserção em membranas por conferir hidrofobicidade. Objetivo desta tese foi realizar um estudo global da S-palmitoilação em *Trypanosoma cruzi*. Análise *in silico* identificou 15 proteínas contendo o motivo DHHC ou DHYC em um domínio rico em císteína, além de regiões transmembrana, indicando que estas proteínas podem ser DHHC palmitoil transferases (PATs) de *T. cruzi*. Os genes codificantes para estas proteínas (TcPATs 1-15) foram identificados e amplificados por PCR, exceto para TcPAT1 (TcHIP, já caracterizada) e TcPAT6 (negativa no PCR). Formas epimastigotas foram transfectadas para expressar PATs fusionadas à etiqueta FLAG e a localização subcelular foi examinada por microscopia de fluorescência, sendo a maioria localizada na região anterior do parasita, próximo ao cinetoplasto, compatível com complexo de Golgi, bolsa flagelar e/ou vacúolo pulsátil. A mesma estratégia identificou duas palmitoil tioesterases (PPTs) em *T. cruzi*, ambas com localização dispersa por todo o corpo do parasita. Também foi desenvolvida uma metodologia de isolamento de amastigotas intracelulares por cavitação, os quais foram utilizados em ensaios de endocitose, tratamento com um inibidor de S-palmitoilação (2-BP) e palmitoil proteômica. Incubação de diferentes formas de *T. cruzi* com 2-BP interferiu em diversos eventos biológicos (morfologia, endocitose, diferenciação e infecção *in vitro*), indicando que S-palmitoilação é uma modificação bioquímica importante para o parasita. Ensaios por *Acyl Biotinyl Exchange* (ABE) em epimastigotas permitiram obter dados sobre a palmitoil proteômica de *T. cruzi* (abordagem PalmPISC), sendo identificadas 3097 proteínas, das quais 466 (15%) de alta confidencia ($p<0,01$). Destas, 35% (152) tinham função desconhecida e 13% (59) eram de metabolismo. Estes dados podem auxiliar na compreensão da função da S-palmitoilação em *T. cruzi*, uma vez que diversas proteínas de interesse podem estar palmitoiladas e envolvidas em importantes vias metabólicas, tais como endocitose, sinalização celular e movimento flagelar.

Palavras-chave: *Trypanosoma cruzi*, S-palmitoilação, PATs, PPTs, cavitação, 2-BP, palmitoil proteômica.

ABSTRACT

S-palmitoylation is an important post-translational protein modification consisting in addition of palmitic acid to cysteine residues, thus allowing the subcellular localization and function of palmitoylated proteins to be regulated, principally by inserting these proteins in membrane by hydrophobicity assembly. Aim of this thesis was to perform a global study of S-palmitoylation in *Trypanosoma cruzi*, the etiologic agent of Chagas disease. *In silico* analysis allowed to identify 15 proteins containing the DHHC or DHYC motifs in a cysteine-rich domain, in addition to transmembrane regions, thus indicating that these proteins may be PATs of *T. cruzi*. Genes encoding these proteins (TcPATs 1 to 15) were identified and amplified by PCR, except for TcPAT1 (TcHIP, already characterized) and TcPAT6 (negative on PCRs). *T. cruzi* epimastigotes were transfected to super-express the PATs fused to FLAG tags and the subcellular location of PATs was determined by fluorescence microscopy, most of them showing localization in the anterior region of the parasite, close to the kinetoplast, compatible with Golgi complex, flagellar pocket or contractile vacuole. The same strategy was used identify two palmitoyl thioesterases (PPTs) in *T. cruzi*, both with subcellular location dispersed throughout the body of the parasite. A methodology was developed to isolate intracellular amastigotes by cavitation and these parasites were used in endocytosis assays, treatment with 2-bromopalmitate (2-BP, an S-palmitoylation inhibitor) and palmitoyl proteomics. Incubation of different *T. cruzi* developmental forms with 2-BP affected several biological events (morphology, endocytosis, differentiation and infection *in vitro*), indicating that palmitoylation is an important modification for the parasite. Acyl Biotinyl Exchange (ABE) assays in epimastigotes allowed to obtain data on the palmitoyl proteomic (PalmPISC approach) of *T. cruzi*, with 3097 proteins identified, 466 of them (15%) of high confidentiality ($p < 0.01$). From these, 35% (152) had unknown function, and 13% (59) were part of metabolic pathways. The data could help future studies aiming to characterizae the S-palmitoylation function in *T. cruzi*, since several target proteins could be palmitoylated and involved in important metabolic pathways, such as endocytosis, cell signaling and flagellar movement.

Key words: *Trypanosoma cruzi*, S-palmitoylation, PATs, PPTs, cavitation, 2-BP, palmitoyl proteomics

LISTA DE FIGURAS

LISTA DE TABELAS

SUMÁRIO

I. Introdução

1.1. A doença de Chagas

A doença de Chagas, também conhecida como tripanossomíase americana, afeta 6 a 7 milhões de pessoas no mundo, principalmente na América Latina (OMS, 2017). Além disso, cerca de 70 milhões de pessoas estão em áreas sob risco de infecção (Pérez-Molina e Molina, 2017). Esta enfermidade, causada pelo protozoário hemoflagelado *Trypanosoma cruzi* (Euglenozoa: Kinetoplastea), foi descrita pelo médico e pesquisador brasileiro Carlos Chagas (1878-1934), que também relatou o complexo ciclo de vida deste parasito (Chagas, 1909).

A doença de Chagas apresenta as fases aguda e crônica. A fase aguda inicial se manifesta por 4 a 8 semanas, sendo geralmente assintomática, com detecção do parasito em exame de sangue e com sintomatologia variada e inespecífica. Cerca de 1 a 5% dos pacientes podem apresentar sintomas severos na fase aguda, como miocardite aguda, efusão pericardial e meningocefalites, com risco de morte de até 0,5%. Após aproximadamente três meses a parasitemia diminui e o parasito permanece latente em tecidos, dando início à fase crônica assintomática, também chamada de indeterminada. Após 10-30 anos da fase aguda, cerca de 30-40% dos pacientes podem desenvolver quadros clínicos típicos da doença como cardiomiopatias e problemas digestórios e/ou neurológicos (Pérez-Molina e Molina, 2017).

Existem dois fármacos disponíveis para o tratamento da doença: o nirfutimox (uso interrompido no Brasil) e o benzonidazol. Ambos apresentam baixa eficácia na fase crônica e efeitos colaterais exacerbados, além de existirem cepas do parasito resistentes a ambos os fármacos (Filardi e Brener, 1987; Murta e Romanha, 1998; Urbina, 2010). Diante desta problemática, é necessária a busca por terapias alternativas para a doença de Chagas, bem como investimento em linhas de pesquisa que visem elucidar a biologia celular do *T. cruzi* a fim de encontrar novos alvos terapêuticos.

1.2. O *Trypanosoma cruzi*

O protozoário *T. cruzi* pertence à família Trypanosomatidae. Outros protozoários patogênicos também pertencem a esta família, como o *T. brucei* (causador da doença do sono na África) e diversas espécies de *Leishmania* (que causam as leishmanioses). Os tripanossomatídeos possuem características morfológicas peculiares e específicas, sendo a principal delas a presença do cinetoplasto, uma região da mitocôndria onde se localiza

uma grande quantidade de DNA (k-DNA). Estes parasitos são uniflagelados e seu flagelo emerge de uma bolsa flagelar que alterna sua localização (anterior ou posterior) de acordo com a forma evolutiva do parasito. A bolsa flagelar sempre acompanha o cinetoplasto (De Souza, 2002).

A região anterior do corpo do *T. cruzi* (de onde o flagelo emerge) é de extremo interesse no estudo da biologia celular deste protozoário, pois neste local se concentram os portais de endocitose (bolsa flagelar e complexo citóstoma/citofaringe) e exocitose (complexo de Golgi e bolsa flagelar), os quais representam processos vitais para a sobrevivência do parasito (De Souza, 2009).

O *T. cruzi* possui um ciclo de vida complexo, com alternância entre um hospedeiro invertebrado e um vertebrado, podendo infectar diferentes espécies de mamíferos, inclusive humanos (Figura 1.1). No tubo digestório do hospedeiro invertebrado (insetos hemípteros da subfamília Triatominae) o parasito apresenta pelo menos duas formas evolutivas distintas: epimastigotas (replicativas) e tripomastigotas metacíclicas (infectivas), além de formas intermediárias. Já no hospedeiro vertebrado ocorrem as formas amastigotas intracelulares (replicativas e infectivas) e as formas tripomastigotas sanguíneas (infectivas) (De Souza, 1984). Recentemente demonstrou-se que formas epimastigotas recém diferenciadas são infectivas ao hospedeiro mamífero, tanto *in vitro* quanto *in vivo* (Kessler et al., 2017), representado assim um novo modelo para estudos que visem compreender a interação parasito-célula hospedeira. Além da transmissão vetorial também pode ocorrer transmissão transfusional, congênita ou oral, esta última caracterizada pela ingestão de alimentos contaminados com o parasito (como extrato de açaí), sendo essa via atualmente a principal responsável por surtos agudos da doença de Chagas no Brasil (Steindel et al., 2008; Coura e Viñas, 2010; Carter et al., 2012).

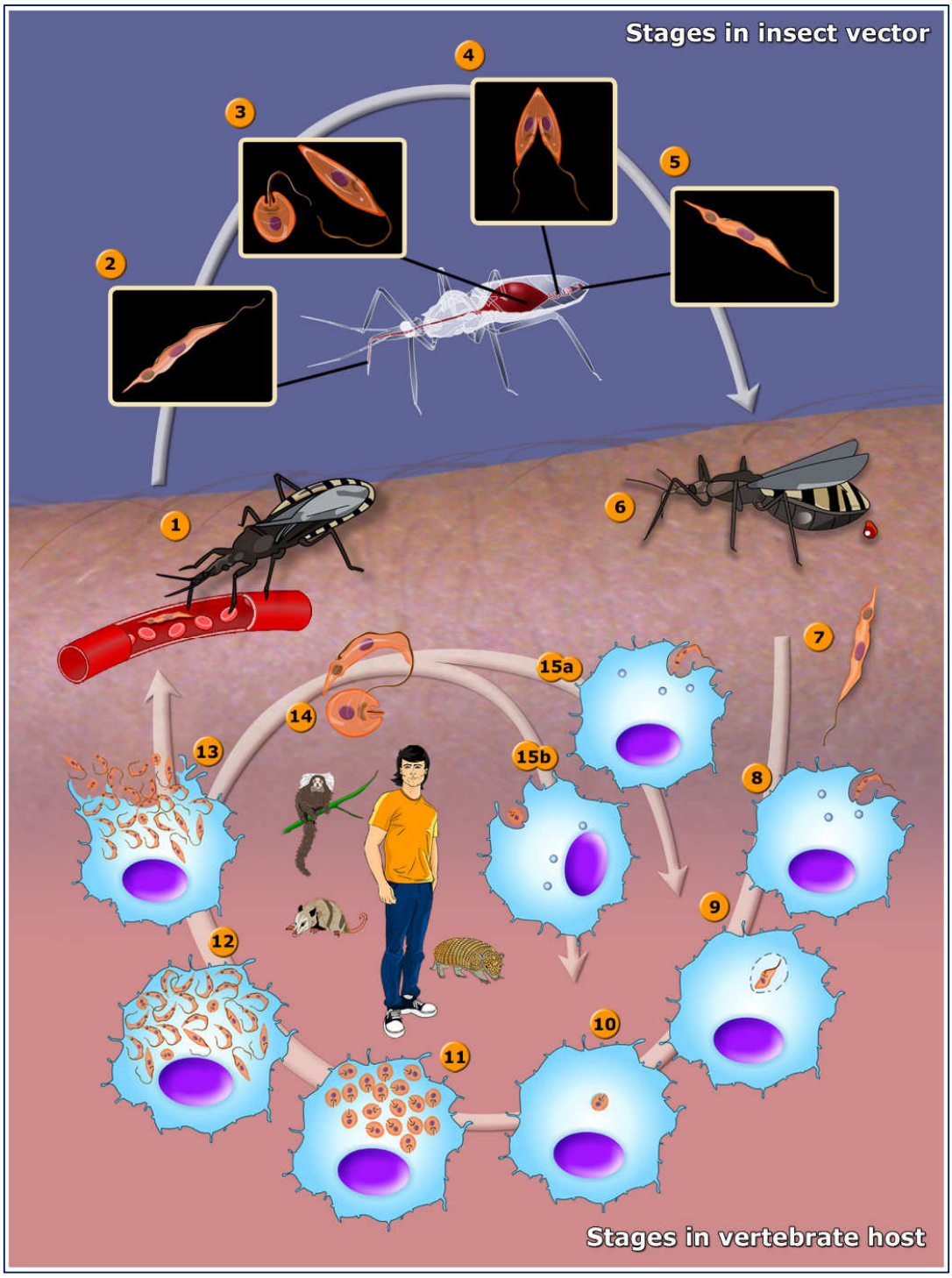

Figura 1.1. O ciclo de vida do *Trypanosoma cruzi*. O ciclo de vida do parasito é complexo, alternando entre hospedeiro mamífero e inseto vetor. No hospedeiro mamífero, as formas principais são as amastigotas intracelulares (replicativas e infectivas passivamente caso engolfadas pelos macrófagos) e tripomastigotas sanguíneos (infectivos). No inseto vetor, as principais formas são os epimastigotas (replicativas e infectivas se recentemente diferenciadas) e os tripomastigotas metacíclicos (infectivos). Adaptado de Texeira 2012 (Fonte de acesso: Atlas didático, disponível em http:// labspace.open.ac.uk/ mod/ resource/view.php?id=459540&direct=1).

As formas evolutivas de *T. cruzi* possuem organelas comuns às outras células eucarióticas, e outras específicas (Figura 1.2). A mitocôndria única do parasito se estende

por todo o corpo celular e concentra o k-DNA no cinetoplasto. O complexo de Golgi está sempre localizado lateralmente ao cinetoplasto, na região da bolsa flagelar (De Souza, 2002). Como na maioria das células eucarióticas, o complexo de Golgi de *T. cruzi* possui uma região de entrada *Cis* (*Cis Golgi Network*) associada a uma cisterna do retículo endoplasmático, e uma região de saída *Trans* (*Trans Golgi Network*) rica em vesículas exocíticas (Figueiredo e Soares, 1995). Também associado à bolsa flagelar encontra-se um sistema osmo-regulador, formado por um vacúolo contrátil alimentado por diversos túbulos coletores (Girard-Dias et al., 2012). As enzimas da via glicolítica se concentram em glicossomos (Michels e Opperdoes, 1991). Os acidocalcissomos são organelas ricas em cálcio e fosfato e possuem pH ácido, estando presentes em maior quantidade em epimastigotas (Docampo e Moreno, 1999). Os reservossomos são organelas peculiares de epimastigotas e amastigotas intracelulares, localizados na porção posterior da célula, concentrando a reserva de nutrientes ingeridos por endocitose (Soares e De Souza, 1988; Soares e De Souza 1991; Soares et al., 1992; Batista et al., 2015).

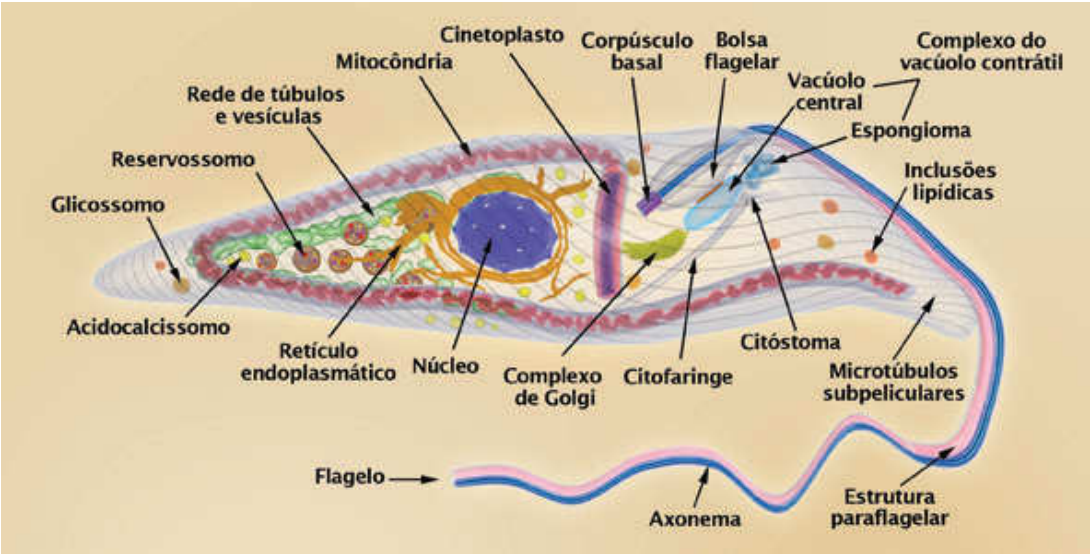

Figura 1.2. Esquema estrutural de epimastigota de *T. cruzi*. O parasito possui organelas comuns de células eucariotas (núcleo, retículo endoplasmático, mitocôndria, complexo de Golgi) e também organelas e estruturas específicas (glicossomos, reservossomos, cinetoplasto e complexo citóstoma/citofaringe). Fonte: Atlas didático: http://labspace.open.ac.uk/mod/resource/view.php?id=459544-.

1.2.1. A endocitose em *Trypanosoma cruzi*

A endocitose em *T. cruzi* está bem descrita em formas epimastigotas e amastigotas (Soares e De Souza 1991; De Souza et al., 2009; Batista et al., 2015). Em formas epimastigotas, a mais estudada, existem dois portais de endocitose de macromoléculas: a bolsa flagelar, como descrito em outros tripanossomatídeos, e o citóstoma, que é

específico de formas epimastigotas e amastigotas. O citóstoma é uma invaginação da membrana plasmática na região anterior da célula, revestida por microtúbulos especiais e que penetra na célula atingindo a região nuclear, formando o complexo citóstoma/citofaringe (Milder e Deane, 1969; Girard-Dias et al., 2012; Alcantara et al., 2014). Macromoléculas são rapidamente internalizadas em pequenas vesículas que brotam a partir da citofaringe e/ou da bolsa flagelar.

Macromoléculas ingeridas possuem um destino final específico em *T. cruzi*: os reservossomos (Soares e De Souza, 1988; Soares e De Souza, 1991). Estas organelas são classificadas como compartimentos pré-lisossomais ou endosomos tardios, devido ao pH ácido em torno de 6,0, mantido por uma bomba de prótons ATPase tipo P (Soares et al., 1992; Vieira et al., 2005) e também devido à presença de enzimas lisossomais, tais como a cruzipaína, a principal cisteína proteinase de *T. cruzi* (Cazzulo et al., 1990; Soares et al., 1992). A reserva energética dos reservossomos é consumida durante o processo de diferenciação *in vitro* (metaciclogênese) de epimastigotas para tripomastigotas metacíclicos (Figueiredo et al., 1994; Soares, 1999; Figueiredo et al., 2004). Os reservossomos também estocam lipídeos, formando inclusões lipídicas, além de armazenar grandes quantidades de colesterol (Soares e De Souza, 1988; Sant'Anna et al., 2008; Pereira et al., 2011).

1.3. S-palmitoilação

1.3.1. Definição

S-palmitoilação é uma modificação pós-traducional de proteínas descrita há mais de 30 anos que consiste na ligação covalente de ácido palmítico (C:16) a resíduos de cisteína através de ligação tioéster (Linder e Deschenes, 2003). Esta modificação regula a localização subcelular, a estabilidade, a ancoragem em balsas lipídicas, a função, a agregação e a interação das proteínas modificadas com proteínas efetoras (Aircart-Ramos et al., 2011), principalmente por conferir hidrofobicidade e inserir as proteínas alvo em membranas. Existem três sítios de palmitoilação propostos: tipo 1) padrão “X-CC-X”; tipo 2) padrão “CXXC”; tipo 3) padrão randômico “XCX”. Análises proteômicas dos alvos da S-palmitoilação em diferentes organismos têm revelado uma grande variedade de substratos, envolvidos em diversas funções celulares (Roth et al., 2006; Emmer et al., 2011), tais como tráfego de vesículas e endocitose, o que indica a importância desta modificação.

A S-palmitoilação de proteínas está envolvida em processos tais como localização em membranas e tráfego vesicular (Aircart-Ramos et al., 2011), os quais são muito importantes para a internalização de macromoléculas, ligação a receptores e direcionamento de proteases e macromoléculas internalizadas via endocitose. Em mamíferos a S-palmitoilação está envolvida na endocitose em células cardíacas (Lin et al., 2013) e fibroblastos BHK (Hilgemann et al., 2013), no transporte retrógrado do receptor de manose-6-fosfato cátion-independente (McCormick et al., 2008), na endocitose dependente de balsas lipídicas (Tankamony e Knudson, 2006; Kim et al., 2013; Oddi et al., 2017) e na reciclagem do receptor de transferrina diférrica (Alvarez et al.,1990).

1.3.2. Metodologias de Estudo

A primeira metodologia para detectar proteínas palmitoiladas utilizou palmitato tritiado seguido de imunoprecipitação e revelação de sua radiação, o que podia durar dias ou semanas. Por esta técnica foi detectada a S-palmitoilação das proteinas H-ras e G-alfa-s (Wedegaertner e Bourne, 1994; Baker et al., 2003). Uma alternativa mais recente é a técnica ABE (*Acyl Biotinyl Exchange*), que utiliza a propriedade da hidroxilamida de clivar a ligação tioéster entre a cisteína e o ácido palmítico, seguido da substituição por biotina e enriquecimento utilizando estreptavidina (Figura 1.3), o que permitiu identificar muitas proteínas palmitoiladas por abordagens proteômicas (Drisdel e Green., 2004; Wan et al., 2007). Outra abordagem é o uso do ácido graxo alcinil 17-octadecinóico (17-ODYA: 17-*octadecynoic acid*) (Martin e Cravatt, 2009). O 17-ODYA é inicialmente incorporado em células *in vitro* em sítios endógenos de S-palmitoilação. Em seguida as células são lisadas e as proteínas palmitoiladas são acopladas à etiquetas azida ($N3^-$) por *click chemistry*, um método de conjugação de pequenas moléculas em macromoléculas, no caso específico catalisado por cobre. As proteínas palmitoiladas são detectadas por fluorescência em géis, por conjugação da azida com rodamina, ou enriquecidas por conjugação da azida com biotina, o que também permite abordagens proteômicas. As técnicas ABE e 17-ODYA/*click chemistry* possuem suas vantagens e desvantagens, detectam perfil similares de proteínas e são melhor utilizadas em combinação (Jones et al., 2012; Martin, 2013).

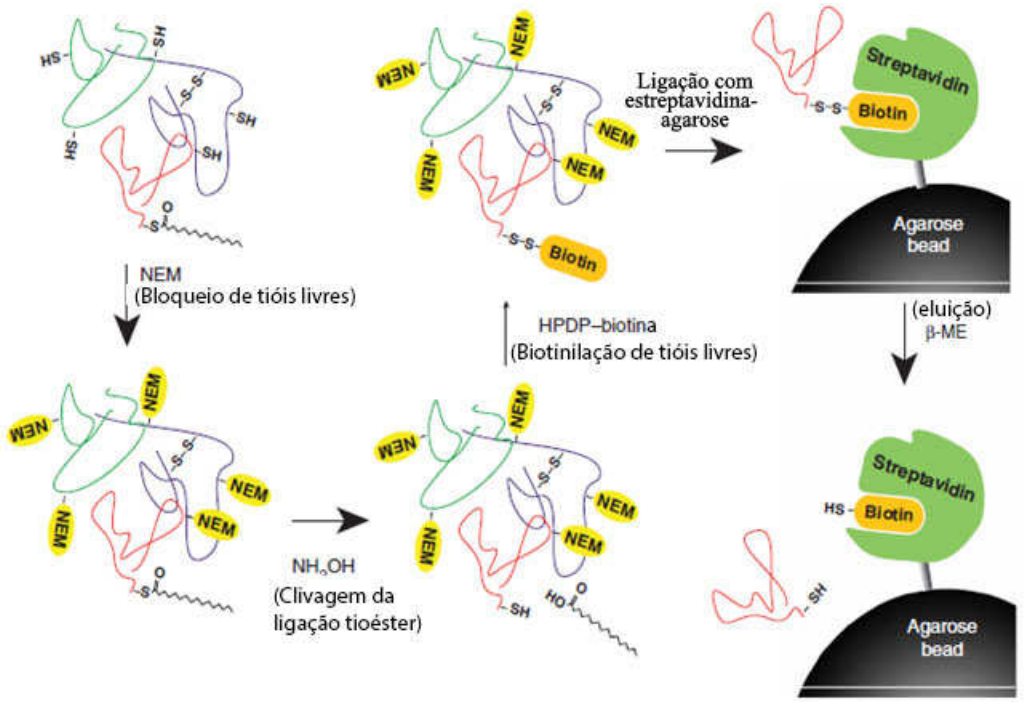

Figura 1.3. Enriquecimento de proteínas palmitoiladas pela metodologia "Acyl–biotinyl Exchange" e análise proteômica. Esta metodologia possui três passos: (i) bloqueio de tióis livres com N-etilmaleimida (NEM); (ii) clivagem das ligações tioésteres cis-palmitoil com hidroxilamina e; (iii) marcação dos tióis expostos resultantes com biotina-HPDP. Após a marcação, as proteínas marcadas são purificadas em colunas de afinidade com estreptavidina, identificadas por espectrometria de massas (MS/MS) e analisadas por bioinformática. Modificado de Wan et al., 2017.

Técnicas mais avançadas envolvem *single-cell in situ imagining* (Gao e Hannoush, 2014), baseada em *click chemistry* com uso de anticorpos primários para detecção de proteínas específicas, geração de anticorpos contra S-palmitoilação com aplicação em proteômica (Fang et al., 2016) e melhoria de ABE utilizando alterações no protocolo (PalmPISC, do inglês *Palmitoyl Protein Identification and Site Characterization*), na qual a etapa de tripsinização é antecipada ao passo de biotinilização para que os sítios de S-palmitoilação sejam identificados (Yang et al., 2010).

1.3.3. Enzimas envolvidas

As zDHHC palmitoil transferases (PATs) são enzimas que realizam a S-palmitoilação (Greaves e Chamberlain, 2011). Estas proteínas são transmembrana, possuem um motivo de ligação ao zinco (C_2H_2), o motivo catalítico aspartato-histidina-histidina-cisteína inserido em um domínio rico em cisteína (CRD-DHHC) ao lado citosólico das enzimas e normalmente estão localizadas no complexo de Golgi, organela que parece ser o centro de S-palmitoilação das células (Aircart-Ramos et al., 2011). Para transferir o grupo palmitato-CoA às proteínas alvo, as PATs primeiramente sofrem auto-palmitoilação (Figura 1.4) (Fukata et al., 2016). Motivos estruturais como DPG e TTxE

estão presentes (Merino et al., 2014), embora não se saiba o seu papel para a funcionalidade destas enzimas. Normalmente, as PATs são numerosas nos organismos, como por exemplo 9 em *Giargia lamblia* (Merino et al., 2014), 12 em *T. brucei* (Emmer et al., 2011) e 17 em *Leishmania major* (Goldston et al., 2014). Entre as enzimas, a conservação de aminoácidos se concentra próxima ao motivo DHHC, com o consenso "Cx2Cx3(R=K)PxRx2HCx2Cx2Cx4DHHCxW(V=I)xNC(I=V)Gx2Nx3F" (Mitchel et al., 2006).

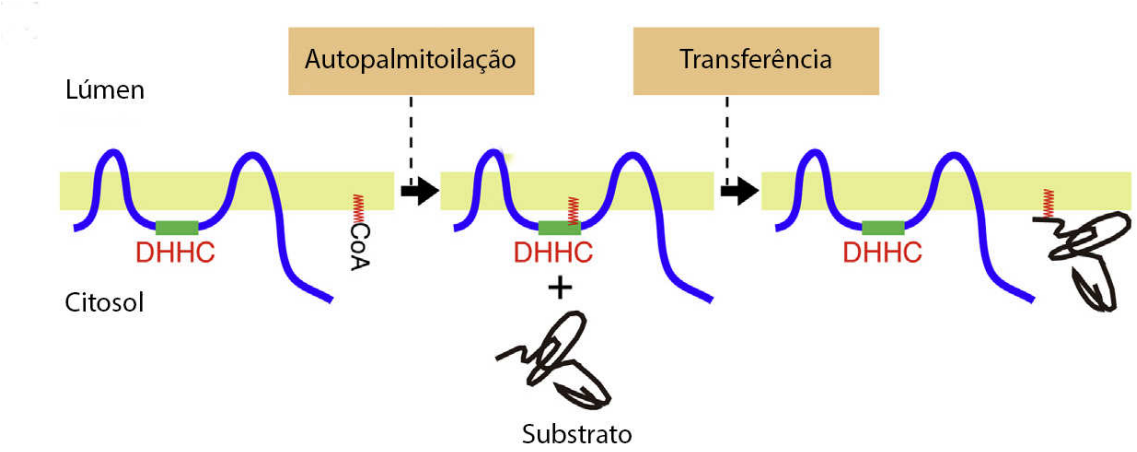

Figura 1.4. Transferência de ácido palmítico pelas DHHC palmitoil transferases (PATs). Primeiramente as PATs sofrem autopalmitoilação e em seguida transferem o ácido palmito ao substrato através de uma ligação tioéster entre um resíduo de cisteína e o ácido palmítico. Essa modificação confere hidrofobicidade, determina localização em membranas e a função das proteínas modificadas. Modificado de Fukata et al., 2016.

As palmitoil tioesterases (PPTs, do inglês *palmitoyl-protein thioesterases*) são enzimas que fazem a depalmitoilação (Lin e Conibear, 2015). Elas pertencem à superfamília das serino hidrolases (SH, do inglês *serine hydrolases*) caracterizadas por conter um sítio ativo de serina usado para a hidrólise do substrato, podendo clivar 2011). Os substratos das PPTs são menos conhecidos do que os das PATs (Lin e Conibear, 2015). A existência de ciclos de S-palmitoilação/despalmitoilação introduziu um novo conceito na literatura: S-palmitoilação dinâmica (Fig 1.5) (Conibear e Davis, 2010).

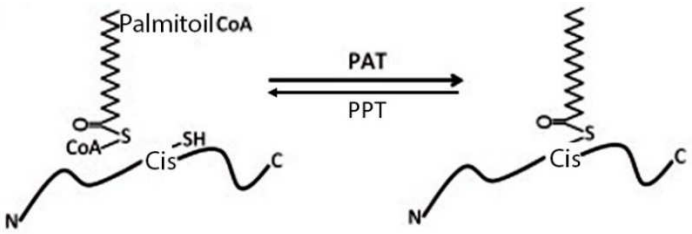

Figura 1.5. S-palmitoilação dinâmica. Ciclos rápidos de S-palmitoilação pelas PATs e despalmitoilação pelas PPTs conferem dinamismo a esta modificação. Modificado de Young et al., 2012.

1.3.4 Inibição da S-palmitoilação

O 2-bromopalmitato (2-BP, Fig 1.6), um análogo do palmitato, é um conhecido inibidor da S-palmitoilação (Webb et al., 2000). Existem dois mecanismos propostos para o mecanismo de ação do 2-BP: inibição direta das PATs ou bloqueio da incorporação do ácido palmítico por competição covalente direta com palmitato (Davda et al., 2013). Foi sugerido que 2-BP também inibe as PPTs, pois dificultou o ciclo de S-palmitoilação da proteína GAP-43 ao nível da despalmitoilação e, consequentemente, sua cinética de associação à membrana (Pedro et al., 2013). 2-BP já foi utilizado em diversos estudos (Webb et al., 2000, Emmer et al., 2011, Alonso et al, 2012; Davda et al., 2013), mas sua alta toxicidade torna imprescindível a busca por novos compostos para utilização em enfermidades relacionadas à S-palmitoilação, tais como as doenças neurodegenerativas, como Huntington, Alzheimer e Parkinson (Cho e Park., 2016). Estudos recentes demonstraram compostos em potencial, tais como os compostos V (Jeannings et al., 2009) e os compostos 13, 14 e 25, os quais são piperazinas bis-cíclicas que inibem a auto-S-palmitoilação de Erf-2, uma PAT de *S. cerevisae*, e seu alvo Ras (Hamel et al., 2016).

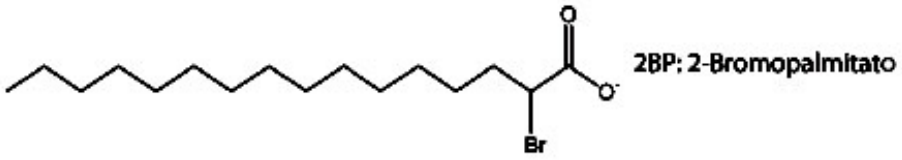

Figura 1.6. Estrutura química de 2-bromopalmitato. Note a presença de um grupo bromo no carbono 14 do ácido palmítico. Modificado de Hamel et al., 2016.

1.4. S-palmitoilação em protozoários Apicomplexa e tripanossomatídeos

A S-palmitoilação está descrita em *Toxoplasma* e *Plasmodium* spp. (filo Apicomplexa), com estudos globais envolvendo as PATs e abordagens proteômicas que identificaram proteínas palmitoiladas (Frénal et al., 2013; Jones et al., 2012; Caballero et al., 2016). Em *Toxoplasma*, estudos proteômicos foram realizados utilizando ABE (Caballero et al., 2016) e 17-ODYA/*click chemistry* (Foe et al., 2015) e muitas proteínas com provável função na invasão celular foram identificadas, indicando que a S-palmitoilação pode ter um papel chave na interação parasito-célula hospedeira. Um estudo global das palmitoil transferases de protozoários do grupo Apicomplexa revelou que a maioria das enzimas está localizada no complexo de Golgi e que uma delas, a TgDHHC7, é essencial para a invasão celular (Frénal et al., 2013). Além disso, tratamento com o inibidor 2-BP (50 e 100 µM) alterou os processos de deslizamento (*gliding*) prévio à invasão e de invasão (Alonso et al., 2012).

Uma grande variedade de proteínas foi identificada em *Plasmodium falciparum* utilizando ABE e *click chemistry*, envolvidas em diversos processos biológicos tais como transporte/secreção (SNAREs e RABs), desenvolvimento em formas esquizontes e invasão (Jones et al., 2012). O tratamento com 2-BP, mesmo em baixas concentrações, inibiu a invasão em eritrócitos e afetou fortemente o perfil da palmitoil proteômica, principalmente em relação a proteínas relacionadas à invasão (Jones et al., 2012). Um estudo global das PATs de *P. berghei* demonstrou que algumas apresentam localizações importantes na interação com a célula hospedeira, tais como no complexo de membranas interiores (IMC, do inglês *Inner Membrane Complex*) (PfDHHC3) e roptrias (PfDHHC7) (Frénal et al., 2013).

Em protozoários tripanossomatídeos, a S-palmitoilação está melhor descrita em *T. brucei*, e pouco descrita em *T. cruzi* (ver item 1.5 abaixo) e *Leishmania* spp (Goldston et al., 2014). Em *T. brucei*, por RNAi, a TbPAT7 foi caracterizada como responsável pela palmitoilção da calflagina (Emmer et al., 2009). Em um estudo posterior do mesmo grupo, realizando palmitoil proteômica após ABE, foram identificadas 132 proteínas estatisticamente significantes, muitas delas envolvidas em sinalização (p. ex. calflaginas), proteases (p. ex. calpaínas e precursores de cisteína protease), tráfego de vesículas (p.ex.t-SNARE), e outras proteínas de superfície, de membrana e de metabolismo de lipídeos (Emmer et al., 2009). Nesse mesmo estudo, 2-BP inibiu o crescimento em 50% (CI_{50}) em formas procíclicas (a 197 µM) e sanguíneas (a 226 µM) do parasito (Emmer et al., 2009). A presença de S-palmitoilação já foi caracterizada em outras proteínas de *T. brucei*, tais como glicosilfosfatidilinositol fosfolipase C-resistente (Fergunson, 1992; Doerrler, 1996), proteínas semelhantes a calpaínas (Liu et al., 2010), metacaspase 4 (Proto et al., 2011) e uma proteína componente da membrana exterior da mitocôndria (POMP39) (Albisetti et al., 2015).

Em *Leishmania* sabe-se apenas que um grupo de proteínas, denominado família de proteínas de superfície aciladas hidrofílicas, as SMP-2, é palmitoilado e miristoilado (Denny et al., 2000) e que *L. major* possui 20 genes codificadores para possíveis PATs em seu genoma (Goldston et al., 2014).

1.5. S-palmitoilação em *Trypanosoma cruzi*

Em *T. cruzi* apenas uma possível PAT (TcHIP) foi estudada (Batista et al., 2013), apesar da existência de 15 possíveis PATs codificadas em seu genoma (Goldston et al.,

2014). A TcHIP possui o motivo aspartato-histidina-tirosina-cisteína (DHYC), que já demonstrou ser funcional em *Saccharomyces cerevisae* (Roth et al., 2002) e domínios anquirina, típicos em palmitoil transferases (Putilina et al., 1999). A TcHIP é expressa em diferentes formas evolutivas de *T. cruzi* e a sua localização subcelular é no complexo de Golgi (Batista et al., 2013). Entretanto, ainda não houve o estabelecimento de sua função no parasito. Duas proteínas são sabidamente palmitoiladas em *T. cruzi*: *Trypanosoma cruzi Flagellar Calcium Binding Protein (*TcFCaBP) (Maric et al., 2011), envolvida em mobilidade, e *T. cruzi* fosfatidil inositol fosfolipase C (TcPI-PLC) (Martins et al., 2010), envolvida em evasão ao sistema imune do hospedeiro.

II. Justificativa

Pelo descrito acima fica evidente que pouco se sabe sobre a S-palmitoilação em *T. cruzi* e seu papel em processos envolvidos na biologia do parasito, apesar da palmitoilação certamente poder influenciar funções importantes para a sobrevivência do parasito, tais como tráfego de vesículas, endocitose e infectividade. Neste sentido, o objetivo geral desta tese foi realizar uma análise global da S-palmitoilação neste patógeno, tanto em relação à caracterização das enzimas DHHC palmitoil transferases que podem realizar este processo, assim como das palmitoil tioesterases, que revertem a reação, quanto em relação às proteínas que são palmitoiladas. Para isto, ferramentas de genética reversa foram implementadas, como a utilização dos vetores plasmidiais da plataforma pTcGW (Batista et al., 2010; Kugeratski et al. 2015) para determinar a localização subcelular das DHHC palmitoil transferases. Também foi realizada análise do efeito do inibidor de S-palmitoilação 2-BP na morfologia, crescimento, fisiologia, diferenciação e infectividade de *T. cruzi*. Além disso, foi utilizada a metodologia ABE e sua melhoria PalmPISC para enriquecimento de proteínas palmitoiladas, seguida de análise proteômica (Yang et al., 2010).

Uma etapa importante nesta tese foi o desenvolvimento e padronização de um método físico com base na cavitação para lisar células infectadas e obter amastigotas intracelulares viáveis e purificados, o que permitiu realizar ensaios biológicos envolvendo endocitose e palmitoilação em amastigotas intracelulares.

Os resultados obtidos nesta tese foram organizados e descritos em forma de capítulos, conforme artigos publicados, submetidos e em desenvolvimento.

III. Referências Bibliográficas

AIRCART-RAMOS, C. et al. 2011. Protein palmitoylation and subcellular trafficking. **Biochemical and Biophysical Acta.** 1808: 2981-2994.
Disponível em: < https://www.ncbi.nlm.nih.gov/pubmed/21819967>

ALBISETTI, A. et al. 2015. A component of the mitochondrial outer membrane proteome of *T. brucei* probrably contains covalent bound fatty acids. **Experimental Parasitology.** 155:49-57.
Disponível em: < https://www.ncbi.nlm.nih.gov/pubmed/25982029>

ALCANTARA, C.L. et al. 2014. Three-dimensional structure of the cytostome-cytopharynx complex of *Trypanosoma cruzi* epimastigotes. **Journal of Cell Science**. 127: 2227-2237.
Disponível em: < https://www.ncbi.nlm.nih.gov/pubmed/24610945>

ALONSO, A.M. et al. 2012. Protein palmitoylation inhibition by 2-bromopalmitate alters gliding, host cell invasion and parasite morphology in *Toxoplasma gondii*. **Molecular and Biochemical Parasitology.** 184:39-43.
Disponível em: < https://www.ncbi.nlm.nih.gov/pubmed/22484029>

ALVAREZ, E. et al. 1990. Girones N, Davis RJ. Inhibition of the receptor-mediated endocytosis of diferric transferrin is associated with the covalent modification of the transferrin receptor with palmitic acid. **The Journal of Biological Chemistry.** 265:16644-16655.
Disponível em: < https://www.ncbi.nlm.nih.gov/pubmed/2398066>

BATISTA, C.M. et al. 2013. Identification and subcellular localization of TcHIP, a putative Golgi zDHHC palmitoyl transferase of *Trypanosoma cruzi*. **Experimental Parasitology.** 134:52-60.
Disponível em: < https://www.ncbi.nlm.nih.gov/pubmed/23428831>

BATISTA, C.M. et al. 2015. *Trypanosoma cruzi* intracellular amastigotes isolated by nitrogen decompression are capable of endocytosis and cargo storage in reservosomes. **PLOS ONE.** DOI:10:e0130165.

Disponível em: < https://www.ncbi.nlm.nih.gov/pubmed/26057131>

BATISTA, M. et al. 2010. A high-throughput cloning system for reverse genetics in *Trypanosoma cruzi*. **BMC Microbiology.** 10: 259.
Disponível em: < https://www.ncbi.nlm.nih.gov/pubmed/20942965>

BAKER, T.L. et al. 2003. Distinct rated of palmitate turnover on membrane bound cellular and oncogenie II-Ras. **The Journal of Biological Chemistry.** 278: 19292-19300.
Disponível em: < https://www.ncbi.nlm.nih.gov/pubmed/?term=12642594>

CABALLERO M.C. et al. 2016. Identification of new palmitoylated proteins in *Toxoplasma gondii*. **Biochimical and Biophysical Acta.** 864:400-408.
Disponível em: < https://www.ncbi.nlm.nih.gov/pubmed/26825284>

CARTER, Y.L. et al. 2012. Acute Chagas disease in a returning traveler. **American Jounal of Tropical Medine Hygiene.** 87:1038-1040.
Disponível em: < https://www.ncbi.nlm.nih.gov/pubmed/23091192>

CAZZULO, J.J. et al. 1990. Some kinetic properties of a cysteine proteinase (cruzipain) from *Trypanosoma cruzi*. **Biochemical and Biophysical Acta.** 1037: 186-191.
Disponível em: < https://www.ncbi.nlm.nih.gov/pubmed/2407295 >

CHAGAS, C. 1909. Nova tripanozomiaze humana: estudos sobre a morfolojia e o ciclo evolutivo do *Schizotrypanum cruzi* n. gen., n. sp., ajente etiolojico de nova entidade morbida do homem. **Memórias do Instituto Oswaldo Cruz**. 1: 159-218.
Disponível em: <http://www.scielo.br/pdf/mioc/v1n2/tomo01(f2)_159-218.pdf >

CHO, E. e PARK, M. 2016. Palmitoylation in Alzheimer's disease and other neurodegenerative diseases. **Pharmacological Research.** 111:133-151.
Disponível em: < https://www.ncbi.nlm.nih.gov/pubmed/?term=27293050>

CONIBEAR, E. e DAVIS, N.G. 2010. Palmitoylation and depalmitoylation dynamics at a glance. **Journal of Cell Science.** 123:4007-4010.

Disponível em: <https://www.ncbi.nlm.nih.gov/pubmed/21084560 >

COURA, J.R. e VIÑAS, P.A. 2010. Chagas disease: a new worldwide challenge. **Nature.** 465: 56-57.
Disponível em: < https://www.ncbi.nlm.nih.gov/pubmed/20571554>

DAVDA, D. et al. 2013. Profiling targets of the irreversible palmitoylation inhibitor 2-bromopalmitate. **ACS Chemistry and Biology.** 8:1912-1917.
Disponível em: < https://www.ncbi.nlm.nih.gov/pubmed/23844586>

DE SOUZA, W. 1984. Cell biology of *Trypanosoma cruzi*. **International Review of Cytology.** 86:197-283.
Disponível em: < https://www.ncbi.nlm.nih.gov/pubmed/6368447>

DE SOUZA, W. 2002. Basic cell biology of *Trypanosoma cruzi.* **Current Pharmaceutical Design.** 8: 269-285.
Disponível em: < https://www.ncbi.nlm.nih.gov/pubmed/11860366>

DE SOUZA, W. et al. 2009. Electron microscopy and cytochemistry analysis of the endocytic pathway of pathogenic protozoa. **Progress on Histochemical Cytochemistry.** 44: 67-124.
Disponível em: < https://www.ncbi.nlm.nih.gov/pubmed/19410686>

DENNY, P.W. et al. 2000. Acylation-depedent protein export in *Leishmania*. **The Jounal of Biological Chemistry.** 275: 11017-11025.
Disponível em: < https://www.ncbi.nlm.nih.gov/pubmed/10753904>

DRISDEL, R.C. e GREEN, W.N. 2004. Labeling and quantifying sites of protein palmitoylation. **Biotechniques.** 36:276–285.
Disponível em: < https://www.ncbi.nlm.nih.gov/pubmed/14989092>

DOCAMPO, R. e MORENO, S.N. 1999. Acidocalcisome: A novel Ca 2+ storage compartment in trypanosomatids and apicomplexan parasites. **Parasitology Today.** 15: 443-448.
Disponível em: < https://www.ncbi.nlm.nih.gov/pubmed/10511686>

DOERRLER, W.T. et al. 1996. Acylation of Glycosaminyl Phosphatidylinositol Revisited. **The Journal of Biological Chemistry.** 271: 27031-27038.
Disponível em:< https://www.ncbi.nlm.nih.gov/pubmed/8900192>

EMMER, B.T. et al. 2011. Global analysis of protein palmitoylation in African trypanosomes. **Eukaryotic Cell.** 10: 455–463.
Disponível em: < https://www.ncbi.nlm.nih.gov/pubmed/21193548>

FANG, C. et al. 2016. Identification of palmitoylated transfitional endoplasmic reticulum ATPase by proteomic technique and Pan antipalmitoylation antibody. **Journal of Proteome Research.** 15: 956-962.
Disponível em: < https://www.ncbi.nlm.nih.gov/pubmed/26865113>

FERGUNSON, M.A. 1992. Site of palmitoylation of a phospholipase C-resistant glycosyl-phosphatidylinositol membrane anchor. **Biochemical Journal.** 284:297-300.
Disponível em: < https://www.ncbi.nlm.nih.gov/pubmed/1318027>

FIGUEIREDO, R.C. e SOARES, M.J. 1995. The Golgi complex of *Trypanosoma cruzi* epimastigote forms. **Journal of Submicroscopic Cytology and Pathology.** 27: 209-215.
Disponível em: < https://www.ncbi.nlm.nih.gov/pubmed/7757947>

FIGUEIREDO, R.C. et al. 1994. The reservosomes of epimastigote forms of *Trypanosoma cruzi*: occurrence during in vitro cultivation**. Parasitology Research.** 80: 517-522.
Disponível em: < https://www.ncbi.nlm.nih.gov/pubmed/7809003>

FIGUEIREDO, R.C. et al. 2004. Reservosome: an endocytic compartment in epimastigotes forms of the protozoan *Trypanosoma cruzi* (Kinetoplastida:

Trypanosomatidae). Correlation between endocytosis of nutrients and cell differentiation. **Parasitology**. 129: 431-438.
Disponível em: < https://www.ncbi.nlm.nih.gov/pubmed/15521631>

FILARDI, L.S. e BRENER, Z. 1987. Susceptibility and natural resistance of *Trypanosoma cruzi* strains to drugs used clinically in Chagas disease. **Transactions of the Royal Society of Tropical Medicine and Hygiene.** 81:755-759.
Disponível em: < https://www.ncbi.nlm.nih.gov/pubmed/3130683>

FOE, I.T. et al. 2015. Global analysis of palmitoylated proteins in *Toxoplasma gondii*. **Cell Host and Microbe.** 18: 501-511.
Disponível em: < https://www.ncbi.nlm.nih.gov/pubmed/26468752>

FRÉNAL, K. et al. 2013. Global analysis of apicomplexan protein S-acyl transferases reveals an enzyme essential for invasion. **Traffic.** 14:895-911.
Disponível em: < https://www.ncbi.nlm.nih.gov/pubmed/23638681>

FUKATA, Y. et al. 2016. Local palmitoylation cycles and specialized membrane domain organization. **Current Topics on Membranes.** 77: 97-141.
Disponível em: < https://www.ncbi.nlm.nih.gov/pubmed/26781831>

GAO, X. e HANNOUSH, R.M. 2014. Single-cell *in situ* imaging of palmitoylation in fatty-acylated proteins. **Nature Protocols.** 9: 2607-2623.
Disponível em: < https://www.ncbi.nlm.nih.gov/pubmed/25299157>

GIRARD-DIAS, W. et al 2012. On the ultrastructural organization of *Trypanosoma cruzi* using cryopreparation methods and electron tomography. **Histochemistry Cell Biology.** DOI: 10.1007/s00418-012-1002-8.
Disponível em: < https://www.ncbi.nlm.nih.gov/pubmed/22872316>

GOLDSTON, A.M. et al. 2014. Acylation in trypanosomatids: an essencial process and potential drug target. **Trends in Parasitol.** 30: 350-360.
Disponível em: < https://www.ncbi.nlm.nih.gov/pubmed/24954795>

GREAVES, J. e CHAMBERLAIN, L.H. 2011. DHHC palmitoyl transferases: substrate interactions and (patho)physiology. **Trends on Biochemistry Science.** 36:245-253.
Disponível em: < https://www.ncbi.nlm.nih.gov/pubmed/21388813>

HAMEL, L.D. et al. 2016. Identification of protein palmitoylation inhibitors from a scaffold ranking library. **Combinatorial Chemistry and High Throughput Screening.** 19: 262-274.
Disponível em: < https://www.ncbi.nlm.nih.gov/pubmed/?term=27009891>

JENNINGS, B.C. et al. 2009. 2-Bromopalmitate and 2-(2-hydroxy-5-nitro-benzylidene)-benzo[b]thiophen-3-one inhibit DHHC-mediated palmitoylation *in vitro*. **Journal of Lipid Research.** 50:233-242.
Disponível em: < https://www.ncbi.nlm.nih.gov/pubmed/18827284>

JONES M.L. et al. 2012. Analysis of protein palmitoylation reveals a pervasive role in Plasmodium development and Pathogenesis. **Cell Host and Microbe.** 12:246-258.
Disponível em: < https://www.ncbi.nlm.nih.gov/pubmed/22901544>

KESSLER, R.L. et al. 2017. Recently differentiated epimastigotes from *Trypanosoma cruzi* are infective to the mammalian host. **Molecular Microbiology.** 104:712-736
Disponível em: < https://www.ncbi.nlm.nih.gov/pubmed/28240790>

KIM, K.S. et al. 2013. DJ-1 Associates with lipid rafts by palmitoylation and regulates lipid rafts-dependent endocytosis in astrocytes. **Human Molecular Genetics.** 22: 4805–4817.
Disponível em: < https://www.ncbi.nlm.nih.gov/pubmed/23847046>

KUGERATSKI, F.G. et al 2015. pTcGW plasmid vectors 1.1 version: a versatile tool for *Trypanosoma cruzi* gene characterization. **Mem Inst Oswaldo Cruz.** 110: 687-690.
Disposível em: < https://www.ncbi.nlm.nih.gov/pubmed/26200713>

LIN, D.T. e CONIBEAR E. 2015. Enzymatic protein depalmitoylation by acyl protein thioesterases. **Biochemistry Society and Transactions.** 43:193-198.
Disponível em: < https://www.ncbi.nlm.nih.gov/pubmed/25849916>

LIN, M.J. et al. 2013. Massive palmitoylation-dependent endocytosis during reoxygenation of anoxic cardiac muscle. **eLife.** DOI: 10.7554/eLife.01295
Disponível em: < https://www.ncbi.nlm.nih.gov/pubmed/24282237>

LINDER, M.E. e DESCHENES, R.J. 2003. New insights into the mechanisms of protein palmitoylation. **Biochemistry.** 42: 4311–4320.
Disponível em: < https://www.ncbi.nlm.nih.gov/pubmed/12693927>

LINDER, M.E. et al. 2013. Massive endocytosis triggered by surface membrane palmitoylation under mitochondrial control in BHK fibroblasts. **eLife.** DOI: 10.7554/eLife.01293.
Disponível em: < https://www.ncbi.nlm.nih.gov/pubmed/24282236>

LIU, W. et al. 2010. Expression and cellular localization of calpain-like proteins in *Trypanosoma brucei*. **Molecular and Biochemical Parasitology.** 169: 20-26.
Disponível em: < https://www.ncbi.nlm.nih.gov/pubmed/19766148>

LONG, J.Z. et al. 2011. The metabolic serine hydrolases and their functions in mammalian physiology and disease. **Chemistry Reviews.** 111: 6022-6063.
Disponível em: < https://www.ncbi.nlm.nih.gov/pubmed/21696217>

MARIC, D. et al. 2011. Molecular determinants of ciliary membrane localization of *Trypanosoma cruzi* flagellar calcium-binding protein. **The Journal of Biological Chemistry.** 286:33109-33117.
Disponível em: < https://www.ncbi.nlm.nih.gov/pubmed/21784841>

MARTIN, B.R. 2013. Chemical approaches for profiling dynamic palmitoylation. **Biochemical Society Transactions.** 41: 43-49.
Disponível em: < https://www.ncbi.nlm.nih.gov/pubmed/23356256>

MARTIN, B.R. e CRAVATT B.F. 2009. Large-scale profiling of palmitoylation in mammalian cells. **Nature Methods.** 6:135-138.
Disponível em: < https://www.ncbi.nlm.nih.gov/pubmed/19137006>

MITCHELL, D.A. et al. 2006. Protein palmitoyation by a family of DHHC protein S-acyltransferases. **Journal of Lipid Research.** DOI: 10.1194\jlr.RG0007.JLR200.
Disponível em: < https://www.ncbi.nlm.nih.gov/pubmed/16582420>

DE PAULO MARTINS, V. et al. 2010. Acylation-dependent export of *Trypanosoma cruzi* phosphoinositide-specific phospholipase C to the outer surface of amastigotes. **The Journal of Biological Chemistry.** 285:30906-30917.
Disponível em: < https://www.ncbi.nlm.nih.gov/pubmed/20647312>

McCORMICK, P.J. et al. 2008. Palmitoylation controls recycling in lysomal sorting and traffincking. **Traffic.** 9:1984-1997.
Disponível em: < https://www.ncbi.nlm.nih.gov/pubmed/18817523>

MERINO, M.C. et al. 2014. Identification of *Giardia lamblia* DHHC proteins and the role of protein S-palmitoylation in the encystation process. **PLOS Neglected Tropical Disease.** DOI: 8: e2997.
Disponível em: < https://www.ncbi.nlm.nih.gov/pubmed/25058047>

MICHELS, P.A. e OPPERDOES, F.R. 1991. The evolutionary origin of glycosomes. **Parasitology Today.** 7: 1005-1009.
Disponível em: < https://www.ncbi.nlm.nih.gov/pubmed/15463459>

MILDER, R. e DEANE, M.P. 1969. The cytostome of *Trypanosoma cruzi* and *T. conorhini*. **The Journal of Protozoology.** 16:730-737.
Disponível em: < https://www.ncbi.nlm.nih.gov/pubmed/5362390>

MURTA, S.M. e ROMANHA, A.J. 1998. *In vivo* selection of a population of *Trypanosoma cruzi* and clones resistant to benznidazole. **Parasitology.** 116:165-171.
Disponível em: < https://www.ncbi.nlm.nih.gov/pubmed/9509026>

ODDI, S. et al. 2017. Palmitoylation of cysteine 415 of CB_1 receptor affects ligand-stimulated internalization and selective interaction with membrane cholesterol and caveolin 1. **Biochimica and Biophysica Acta.** 1862: 523-532.
Disponível em: < https://www.ncbi.nlm.nih.gov/pubmed/28215712>

OMS (Organização Mundial da Saúde). **Chagas disease (American tipanosomiasis).** Fact sheet. Março 2017. Disponível em:
< http://www.who.int/mediacentre/factsheets/fs340/en/ >. Acesso em 14 nov 17.

PEDRO, M.P. et al. 2013. 2-Bromopalmitate reduces protein deacylation by inhibition of acyl-protein thioesterase enzymatic activities. **PLOS ONE.** DOI:8:e75232.
Disponível em: < https://www.ncbi.nlm.nih.gov/pubmed/24098372>

PEREIRA, M.G. et al. 2011. *Trypanosoma cruzi* epimastigotes are able to store and mobilize high amounts of cholesterol in reservosome lipid inclusions. **PLOS ONE.** DOI: 10.1371/journal.pone.0022359.
Disponível em: < https://www.ncbi.nlm.nih.gov/pubmed/21818313>

PÉREZ-MOLINA, J.A. e MOLINA, I. 2017. Chagas disease. **Lancet.** DOI:10.1016\S0140-6736(17)31612-4.
Disponível em: < https://www.ncbi.nlm.nih.gov/pubmed/28673423>

PROTO, W.R. et al. 2011. *Trypanosoma brucei* metacaspase 4 is a pseudopeptidase and a virulence fator. **The Journal of Biological Chemistry.** 286: 39914-39925.
Disponível em:< https://www.ncbi.nlm.nih.gov/pubmed/21949125>

PUTILINA, T. et al. 1999. The DHHC domain: a new highly conserved cysteine-rich motif. **Molecular and Cellular Biochemistry.** 195: 219–226.
Disponível em: < https://www.ncbi.nlm.nih.gov/pubmed/10395086>

ROTH, A.F. et al. 2006. Global Analysis of Protein Palmitoylation in Yeast. **Cell.** 125:1003-1013.
Disponível em: < https://www.ncbi.nlm.nih.gov/pubmed/16751107>

ROTH, A.F. et al. 2002. The yeast DHHC cysteine-rich domain protein Akr1p is a palmitoyl transferase. **Journal of Cell Biology.** 159: 23-28.
Disponível em: < https://www.ncbi.nlm.nih.gov/pubmed/12370247>

SANT`ANNA, C. et al. 2008. New insights into the morphology of *Trypanosoma cruzi* reservosome. **Microscopic Research and Tecnique.** 71: 599-605.
Disponível em: < https://www.ncbi.nlm.nih.gov/pubmed/18452191>

SOARES, M.J. 1999. The reservosome of *Trypanosoma cruzi* epimastigotes: an organelle of the endocytic pathway with a role in metacyclogenesis. **Memórias do Instituto Oswaldo Cruz.** 94: 139-141.
Disponível em: < https://www.ncbi.nlm.nih.gov/pubmed/10677701>

SOARES, M.J. e DE SOUZA, W. 1988. Cytoplasmic organelles of trypanosomatids: a cytochemical and stereological study. **Journal of Submicroscopic Cytology and Pathology.** 20: 349-361.
Disponível em: < https://www.ncbi.nlm.nih.gov/pubmed/3135113>

SOARES, M.J. e DE SOUZA, W. 1991. Endocytosis of gold-labeled proteins and LDL by *Trypanosoma cruzi*. **Parasitology Research.** 77: 461-468.
Disponível em: < https://www.ncbi.nlm.nih.gov/pubmed/1656428>

SOARES, M.J. et al. 1992. Identification of a large pre-lysosomal compartment in the pathogenic protozoon *Trypanosoma cruzi*. **Journal of Cell Science.** 2: 157-167.
Disponível em: < https://www.ncbi.nlm.nih.gov/pubmed/1500438>

STEINDEL, M. et al. 2008. Characterization of *Trypanosoma cruzi* isolates from humans, vectors, and animal reservoirs following na outbreak of acute human Chagas disease in Santa Catarina State, Brazil. **Diagnostic Microbiolology and Infectious Disease.** 60: 25-32.
Disponível em: < https://www.ncbi.nlm.nih.gov/pubmed/17889480>

THANKAMONY, S.P. and KNUDSON, W. 2006. Acylation of CD44 and its association with lipid rafts are required for receptor and hyaluronan endocytosis. **The Journal of Biological Chemistry.** 45: 34601-34609.

Disponível em: < https://www.ncbi.nlm.nih.gov/pubmed/16945930>

URBINA, J.A. 2010. Specific chemotherapy of Chagas disease: Relevance current limitation and new approaches. **Acta Tropica.** 115:55-68.

Disponível em: < https://www.ncbi.nlm.nih.gov/pubmed/19900395>

VIEIRA, M. et al. 2005. Role for a P-type H+-ATPase in the acidification of the endocytic pathway of *Trypanosoma cruzi*. **Biochemical Journal.** 392: 467-474.

Disponível em: < https://www.ncbi.nlm.nih.gov/pubmed/16149915>

WAN, J. et al. 2007. Palmitoylated proteins: purification and identification. **Nature Methods.** 2: 1573-1584.

Disponível em: < https://www.ncbi.nlm.nih.gov/pubmed/17585299>

WEBB Y.et al. 2000. Inhibition of protein palmitoylation, raft localization, and T cell signaling by 2-bromopalmitate and polyunsaturated fatty acids. **The Journal of Biological Chemistry.**275:261-270.

Disponível em: < https://www.ncbi.nlm.nih.gov/pubmed/10617614>

WEDEGAERTNER, P.B. e BOURNE, I.I.R. 1994. Activation and depalmitoylation of Gs[alpha]. **Cell.** 77: 1063-1070.

Disponível em: < https://www.ncbi.nlm.nih.gov/pubmed/7912657>

YANG, W. et al. 2010. Proteome scale characterization of humam S-acylated proteins in lipid raft-enriched and non-raft membranes. **Molecular and Cellular Proteomics.** 9: 54-70.

Disponível em: < https://www.ncbi.nlm.nih.gov/pubmed/19801377>

YOUNG, F.B. et al. 2012. Putting proteins in their place: palmitoylation in Huntington disease and other neuropsychiatric diseases. **Progress on Neurobiology.** 97:220-238.

Disponível em: < https://www.ncbi.nlm.nih.gov/pubmed/22155432>

IV. Capítulo 1

Revelando as enzimas do ciclo da S-palmitoilação dinâmica de proteínas em *Trypanosoma cruzi*

A primeira parte desta tese teve como objetivo identificar as enzimas envolvidas no processo de palmitoilação, as PATs, e no processo de despalmitoilação, as PPTs em *T. cruzi*. Foi possível identificar 15 possíveis PATs e 2 PPTs no genoma do parasito. Todos esses genes foram amplificados, com exceção da TcPAT6 (negativo na PCR) e clonados na plataforma Gateway utilizando o vetor de expressão de proteínas em *T. cruzi* pTcGWFLAG, com excessão da TcPAT1 (TcHIP, já caracterizada pelo grupo). Foi possível obter epimastigotas transfectantes resistentes à G418, com excessão da TcPAT4. A localização da maioria das TcPATs foi na região anterior, próxima ao cinetoplasto, compatível com complexo de Golgi, bolsa flagelar e/ou vacúolo osmo-regulador do parasito. Já as PPTs tiveram localização dispersa pelo corpo do parasito. Estes dados estão compilados em um manuscrito submetido como Short Communication à revista indexada Memórias do Instituto Oswaldo Cruz, com fator de impacto 2,605 (Qualis CB-I: B1).

4.1. Objetivo

Identificar enzimas envolvidas na S-palmitoilação em *T. cruzi* e analisar sua localização subcelular.

4.2. Objetivos específicos

1. Realizar uma busca em banco de dados genômicos para identificar possíveis DHHC palmitoil transferases em *T. cruzi*;

2. Construir vetores plasmidiais episssomais para a expressão das enzimas candidatas fusionadas a etiquetas FLAG para determinação da localização subcelular em *T. cruzi*;

4.3. Artigo Submetido

Autores: Cassiano Martin Batista, Felipe Saad, Stephane Pini Costa Ceccoti, Iriane Eger, Maurilio José Soares

Título: Revealing the enzymes of the dynamic protein S-palmitoylation cycle in *Trypanosoma cruzi*

Revista: Memórias do Instituto Oswaldo Cruz

Fator de impacto (2016): 2,605 (Qualis CB-I: B1)

Submission Confirmation

Print

Thank you for your submission

Submitted to	Memórias do Instituto Oswaldo Cruz
Manuscript ID	MIOC-2018-0086
Title	Revealing the enzymes of the dynamic protein S-palmitoylation cycle in *Trypanosoma cruzi*
Authors	Batista, Cassiano Saad, Felipe Ceccoti, Stephane Eger, Iriane Soares, Maurilio
Date Submitted	16-Feb-2018

SHORT COMMUNICATION

Subcellular localization of FLAG tagged enzymes of the dynamic protein S-palmitoylation cycle of *Trypanosoma cruzi* epimastigotes

Running title: Dynamic Palmitoylation in *T. cruzi*

Cassiano Martin Batista[1], Felipe Saad[1], Stephane Pini Costa Ceccoti[1], Iriane Eger[2], Maurilio José Soares[1]

[1]Laboratory of Cell Biology, Carlos Chagas Institute/Fiocruz-PR, Curitiba, Paraná, Brazil

[2]Department of General Biology, State University of Ponta Grossa, Ponta Grossa, Paraná, Brazil

Corresponding Author:

Maurilio José Soares

Laboratório de Biologia Celular

Instituto Carlos Chagas / Fiocruz-PR

Rua Prof. Algacyr Munhoz Mader 3775

Cidade Industrial

81350-010 Curitiba – PR

Brasil

Email.: maurilio@fiocruz.br

Phone: (+55) (41) 3316-340

Summary

Dynamic S-palmitoylation of proteins is the addition of palmitic acid by zDHHC palmitoyl transferases (PATs) by thioester linkages and depalmitoylation by palmitoyl protein thioesterases (PPTs). A putative PAT (TcPAT1) has been previously identified in *Trypanosoma cruzi*, the etiological agent of Chagas disease. Here we demonstrate the presence of other 14 putative TcPATs and 2 PPTs in the parasite genome. *T. cruzi* cell lines expressing TcPATs and TcPPTs plus a FLAG tag at the C terminus were produced for most enzymes, with positive detection by indirect immunofluorescence. Our data indicate that a dynamic S-palmitoylation machinery is overexpressed in *T. cruzi* epimastigotes.

Key words: Dynamic S-palmitoylation, *Trypanosoma cruzi*, protein expression

Sponsorships: This work has been supported by CNPq, CAPES and Fiocruz.

Dynamic protein S-palmitoylation concern the addition of palmitate to cysteines of the modified protein by zDHHC palmitoyl transferases (PATs) thought thioester linkages and depalmitoylation by palmitoyl protein thioesterases (PPTs) (Conibear & Davis 2010). Protein S-palmitoylation cycles promote the insertion of target proteins into membranes, regulating their localization and function (Linder & Deschenes 2003).

PATs are key transmembrane enzymes, with cysteine rich domains in the DHHC motif (CRD-DHHC domain), in addition to DPG and TTxE structural domains (Greaves & Chamberlain 2011). PATs are involved in diverse biological processes in several organisms, such as *Homo sapiens* cancer (Ducker et al. 2004) and neurological diseases (Young et al. 2012; Cho & Park 2016), yeast endocytosis (Feng & Davis 2000), *Cryptococcus neoformans* virulence (Santiago-Tirado et al. 2015), *Giardia lamblia* encystation (Merino et al. 2014) and invasion in Apicomplexa (Frénal et al. 2013). TbPAT7 is responsible for flagellar localization of calflagin in the trypanosomatid protozoan *Trypanosoma brucei* (Emmer et al. 2009).

PPTs belong to the serine hydrolases family, are less abundant in number than PATs and are characterized by the presence of a serine active site for hydrolysis of the substrate, being able to cleave amide, ester and thioester bounds (Long & Cravatt 2011).

Goldston et al. (2014) identified, by *in silico* search, 15 PATs in the *Trypanosoma cruzi* genome, as opposed to 12 in *T. brucei* and 20 in *Leishmania major*. However, up to now only one PAT has been characterized in *T. cruzi*, the etiological agent of Chagas disease: TcHIP, or TcPAT1 (Batista et al. 2013). TcPAT1 is a 95.4 kDa Golgi protein expressed in different developmental stages of the parasite, with a modified DHYC motif (Batista et al. 2013). Such modified motif is functional in the homologue Akr1p enzyme of *Saccharomyces cerevisae* (Roth et al. 2002).

It has been recently shown that dynamic protein S-palmitoylation is involved in life cycle progression and virulence in some pathogenic protozoa (Brown et al. 2017). However, no evidence of global PATs or PPTs expression has been yet reported in *T. cruzi*. Thus, aim of this work was to verify the expression of dynamic protein S-palmitoylation enzymes in *T. cruzi* Dm28c (Contreras et al. 1988) epimastigote forms. An *in silico* search for PATs was made in the *T. cruzi* genomic data base (TritrypDB), in parallel with nucleotide BLAST alignment (nBlast-NCBI, Bethesda, MD, USA) of *T. cruzi* genes with the well characterized *S. cerevisiae* PAT genes that encode for Erf2 (with DHHC-CRD motif) (Lobo et al. 2002) and Akr1p (with DHYC-CRD motif) (Roth et al. 2002). As a result, 15 PATs genes were found, identical to that formerly identified by Goldston et al. (2014). Size of these genes varied from 768 (TcPAT7) to 2610 base pairs (TcPAT1) and the resulting protein products were between 30 and 95.4 kDa. Use of the software TMHMM Server v. 2.0 (*Center for Biological Sequence Analysis*, CBS, Lyngby, Denmark) and Phyre2 software (Kelly et al. 2015), which predicts transmembrane regions and do 3D protein models, allowed to determine that these proteins had three (TcPAT2 and 6) to seven (TcPAT5) transmembrane domains. By using pFAM software (Sanger Institute, Cambridge, UK) to predict protein domains, it was found that only TcPAT1 had the DHYC motif, while the number of cysteines close to the DHHC/DHYC motif varied from 5 to 9. Only TcPAT4, TcPAT10 and TcPAT14 had both DPG and TTxE structural motifs. On the other hand, TcPATs 5 and 9 had only the DPG motif, while TcPATs 1, 7 and 8 had only the TTxE motif (Fig. 1). Sequence identity between the TcPATs is very low, between 14.2% and 26.83%, as assessed using multiple alignment in Clustal Omega.

Using Phyre2 software, predicted 3D models were obtained for all TcPATs and TcPPTs. All predicted 3D models were similar for TcPATs, except for TcPAT1 (larger

and with ankyrin repeats). TcPPT1 and 2 were very different from each other. All 3D models had 100% confidence. (Fig. 2).

Aiming to produce transfectant cell lines of *T. cruzi* epimastigotes expressing TcPATs plus a FLAG tag at the C terminus (FLAGC tagged TcPAT), the genes were amplified using specific primers (Table 1) with recombination sites for the Gateway cloning platform (Thermo Fischer Scientific, Waltham, MA, USA) by using the entry plasmid vector pDONR 221 and the destination *T. cruzi* vector pTcGWFLAGC (Batista et al. 2010; Kugeratski et al. 2015). All genes were cloned, except TcPAT6 and TcPAT1 (that is already characterized). Three-day-old *T. cruzi* epimastigotes were transfected with a Gene Pulser XCell BIORAD electroporator (BIORAD Inc., Hercules, CA, USA), selected with 500 $\mu g.mL^{-1}$ G418 and maintained with 250 $\mu g.mL^{-1}$ of the same antibiotic, as previously described (Batista et al. 2010). Twelve resistant cell lines could be selected, with the exception of TcPAT4.

For subcellular localization by indirect immunofluorescence assays (IFA), *T. cruzi* transfectants were washed twice in PBS, fixed for 10 min with 4% paraformaldehyde, adhered to 0.1% poly-L-lysine coated coverslips, permeabilized with 0.5% triton/PBS, and incubated for one hour at 37ºC using a mouse anti-flag antibody (Sigma-Aldrich St. Louis, MO, USA) diluted 1:4000 in incubation buffer (PBS pH 7.4 containing 1.5% bovine serum albumin). After three washes in PBS, the samples were incubated in the same conditions with a secondary goat anti-mouse antibody coupled to AlexaFluor 594 (Thermo Fischer Scientific, Waltham, MA, USA) diluted at 1:600 in incubation buffer. The samples were washed three times with PBS, incubated for 5 min with 1.3 nM Hoechst 33342 (Sigma-Aldrich St. Louis, MO, USA) and the coverslips were mounted with Prolong Gold antifading agent (Thermo Fischer Scientific, Waltham, MA, USA). The slides were observed in a Nikon Eclipse E600 epifluorescence microscope. As a result,

TcPATs 3, 5, 8, 11, 12, 14 and 15 were located as single dots at the anterior region of the parasite, close to the kinetoplast and the flagellar pocket (Fig. 3). The positive reaction was frequently found lateral to the kinetoplast, which suggests Golgi, flagellar pocket or vacuole complex localizations. TcPAT2 labeling appeared as strong dots distributed throughout the cell body, suggestive of localization in some cytoplasmic organelle (Fig. 3). This was expected, since PATs are usually found at the endoplasmic reticulum, Golgi and plasma membranes (Ohno et al. 2006). Interestingly, most PATs with 4 transmembrane domains (5 out of 7) were at the anterior region located. Furthermore, 8 of 15 TcPATs have anterior region localization. TcPAT13 presents perinuclearlabelling (Fig 1), suggesting endoplasmic reticulum localization. No positive reaction was detected for TcPATs 7, 9, 10 (Fig. 3). Transcriptomic data from TritrypDB showed that TcPATs 7 and 9 are expressed in metacyclics trypomastigotes and not in epimastigotes, so epimastigotes maybe regulating these genes expression. Technique limitation could be an explanation for these negative results also, since transmembrane proteins could be of low expression level. These results indicated that at least eight TcPATs are overexpressed in *T. cruzi* epimastigotes.

In order to characterize TcPPTs, a genomic data search was performed as described above, and two genes were identified (Table 2). TcPPT1 is an 843 base pairs gene and the product (30.2 kDa) is homologue to *H. sapiens* acyl-protein thioesterase-1 (APT1) and lysophospholipase genes, which are involved in cytosolic and lysosomal protein depalmitoylation (Long & Cravatt 2011). TcPPT2 is a 951 base pairs gene and the product (35.5 kDa) is homologue to *H. sapiens* acyl-protein thioesterase-2 (APT2), involved in cytosolic depalmitoylation (Long & Cravatt 2011). Primers were then designed for isolation and amplification of these genes (Table 2).

The same steps described above for TcPATs were used to produce *T. cruzi* cell lines expressing TcPPTs plus a FLAG tag at the C terminus (FLAGC tagged TcPPTs). Resistant cell lines expressing TcPPT1 and TcPPT2 were selected with 500 $\mu g.mL^{-1}$ G418. After IFA in the same conditions as described above, both TcPPTs showed strong labeling dispersed through the cell body, suggesting a cytoplasmic localization (Fig. 4), indicating that *T. cruzi* epimastigotes overexpressed both TcPPTs, in the expected cytoplasmic localization.

In conclusion, our data indicate that a dynamic protein S-palmitoylation machinery with PATS and PPTs is present in *T. cruzi*. Future studies will be crucial to determine the importance of this machinery for the parasite survival. Palmitoylation and depalmitoylation of proteins can play an important role in this parasite, in events as diverse as nutrition, protein traffic, differentiation, host-cell interaction and infection establishment.

ACKNOWLEDGEMENTS

The authors thank the Program for Technological Development in Tools for Health-PDTIS-FIOCRUZ for use of its facility (Confocal and Electronic Microscopy Platform RPT07C) at the Instituto Carlos Chagas/Fiocruz-PR, Brazil.

AUTHORS CONTRIBUTIONS

CMB planned the experiments, designed the PATs primers, performed part of the cloning experiment, selected *T. cruzi* cell lines and wrote the first manuscript draft. FS performed cloning and IFAs. SC made PPTs primer design and cloning. IE helped to plan

the experiments and revised the manuscript. MJS conceived the study and edited the final form of the manuscript. All authors read and approved the final manuscript.

REFERENCES

Batista CM, Kalb LC, Moreira CM, Batista GT, Eger I, Soares MJ 2013. Identification and subcellular localization of TcHIP, a putative Golgi zDHHC palmitoyl transferase of *Trypanosoma cruzi*. *Exp Parasitol 134*: 52-60.

Batista M, Marchini FK, Celedon PA, Fragoso SP, Probst CM, Preti H, Ozaki LS, Buck GA, Goldenberg S, Krieger MA 2010. A high-throughput cloning system for reverse genetics in *Trypanosoma cruzi*. *BMC Microbiol 10*: 259.

Brown RW, Sharma AI, Engman DM 2017. Dynamic protein S-palmitoylation mediates parasites life cycle progression and diverse mechanisms of virulence. *Crit Rev Biochem Mol Biol 52*: 145-162.

Cho E, Park M 2016. Palmitoylation in Alzheimer's disease and other neurodegenerative diseases. *Pharmacol Res 111*: 133-151.

Conibear E, Davis NG 2010. Palmitoylation and depalmitoylation dynamics at a glance. *J Cell Sci 123*: 4007-4010.

Contreras VT, Araújo-Jorge TC, Bonaldo MC, Thomaz N, Barbosa HS, Meirelles MN, Goldenberg S 1988. Biological aspects of the DM28c clone of *Trypanosoma cruzi* after metaciclogenesis in chemically defined media. *Mem Inst Oswaldo Cruz 83*: 123-133.

Ducker CE, Stettler EM, French KJ, Upson JJ, Smith CD 2004. Huntingtin interacting protein 14 is an oncogenic human protein: palmitoyl acyltransferase. *Oncogene 23*: 9230-9237.

Emmer BT, Souther C, Toriello KM, Olson CL, Epting CL, Engman DM 2009. Identification of a palmiytoyl acyltransferase required for protein sorting to the flagellar membrane. *J Cell Sci 122*: 867-874.

Feng Y, Davis NG 2000. Akr1p and the type I casein kinases act prior to the ubiquitination step of yeast endocytosis: Akr1p is required for kinase localization to the plasma membrane. *Mol Cel Biol 20*: 5350-5359.

Frénal K, Tay CL, Mueller C, Bushell ES, Jia Y, Graindorge A, Billker O, Rayner JC, Soldati-Favre D. 2013. Global analysis of apliconplexan protein S-acyl transferases reveals an enzyme essential for evasion. *Traffic 14*: 895-911.

Goldston AM, Sharma AI, Paul KS, Engman DM 2014. Acylation in trypanosomatids: an essential process and potential drug target. *Trends Parasitol 30*: 350-360.

Greaves J, Chamberlain LH 2011. DHHC palmitoyl transferases: substrates interactions and (patho)physiology. *Trends Biochem Sci 36*: 245-253.

Kelly LA, Mazulin S, Yates CM, Was MN, Sternberg MJE 2015. The Phyre2 web portal for protein modeling, prediction and analysis. *Nature protocols 10*: 845-858.

Kugeratski FG, Batista M, Inoue AH, Ramos BD, Krieger MA, Marchini FK 2015. pTcGW plasmid vectors 1.1 version: a versatile tool for *Trypanosoma cruzi* gene characterization. *Mem Inst Oswaldo Cruz 110*: 687-690.

Linder ME, Deschenes RJ 2003. New insights into the mechanisms of protein palmitoylation. *Biochemistry 42*: 4311-4317.

Lobo S, Greentree WK, Linder ME, Deschenes RJ 2002. Identification of a Ras palmitoyltransferase in *Saccharomyces cerevisiae*. *J Biol Chem 277*: 41268-41273.

Long JZ, Cravatt BF 2011. The metabolic serine hydrolases and their functions in mammalian physiology and disease. *Chem Rev 111*: 6022-6063.

Merino MC, Zamponi N, Vranych CV, Touz MC, Rópolo AS 2014. Identification of *Giardia lamblia* DHHC proteins and the role of protein S-palmitoylation in the encystation process. *PloS Negl Trop Dis 8*: e2997.

Ohno Y, Kihara A, Sano T, Igarashi Y 2006. Intracellular localization and tissue-specific distribution of human and yeast DHHC cysteine-rich domain-containing proteins. *Biochim Biophys Acta 1761*: 474-483.

Roth AF, Feng Y, Chen L, Davis NG 2002. The yeast DHHC cysteine-rich domain protein Akr1p is a palmitoyl transferase. *J Cell Biol 159*: 23-28.

Santiago-Tirado FH, Peng T, Yang M, Hang HC, Doering TL 2015. A single protein S-acyl transferase acts through diverse substrates to determine Cryptococcal morphology, stress tolerance, and pathogenic outcome. *PLoS Pathog 11*: e1004908.

Young FB, Butland SL, Sanders SS, Sutton LM, Hayden MR 2012. Putting proteins in their place: palmitoylation in Huntington disease and other neuropsychiatric diseases. *Prog Neurobiol 97*: 220-238.

FIGURE LEGENDS

Figure 1. Identification and *in silico* analysis of *Trypanosoma cruzi* PATs. Fifteen TcPATs were identified, with predicted molecular mass from 30 to 95.4 kDa. All were transmembrane and contains DHHC motif, with the exception of TcPAT1 (DHYC). S1-SN: passages thought the membrane; kDa: molecular weight of the predicted protein; TTxE and DPG: structural motifs.

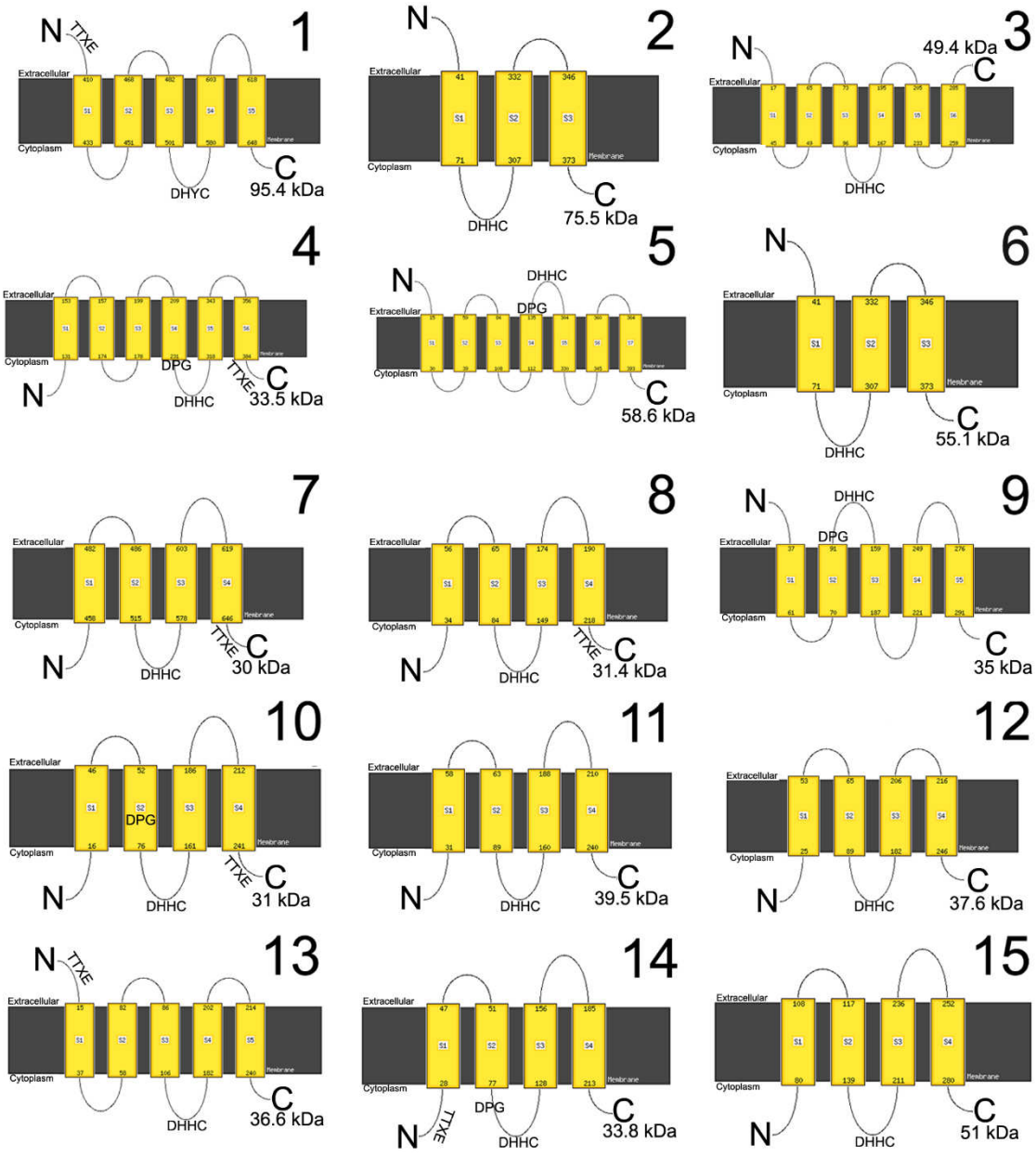

Figure 2. Predicted 3D models of *Trypanosoma cruzi* PATs and PPTs. Software Phyre2 was used. All 3D models were with 100% confidence.

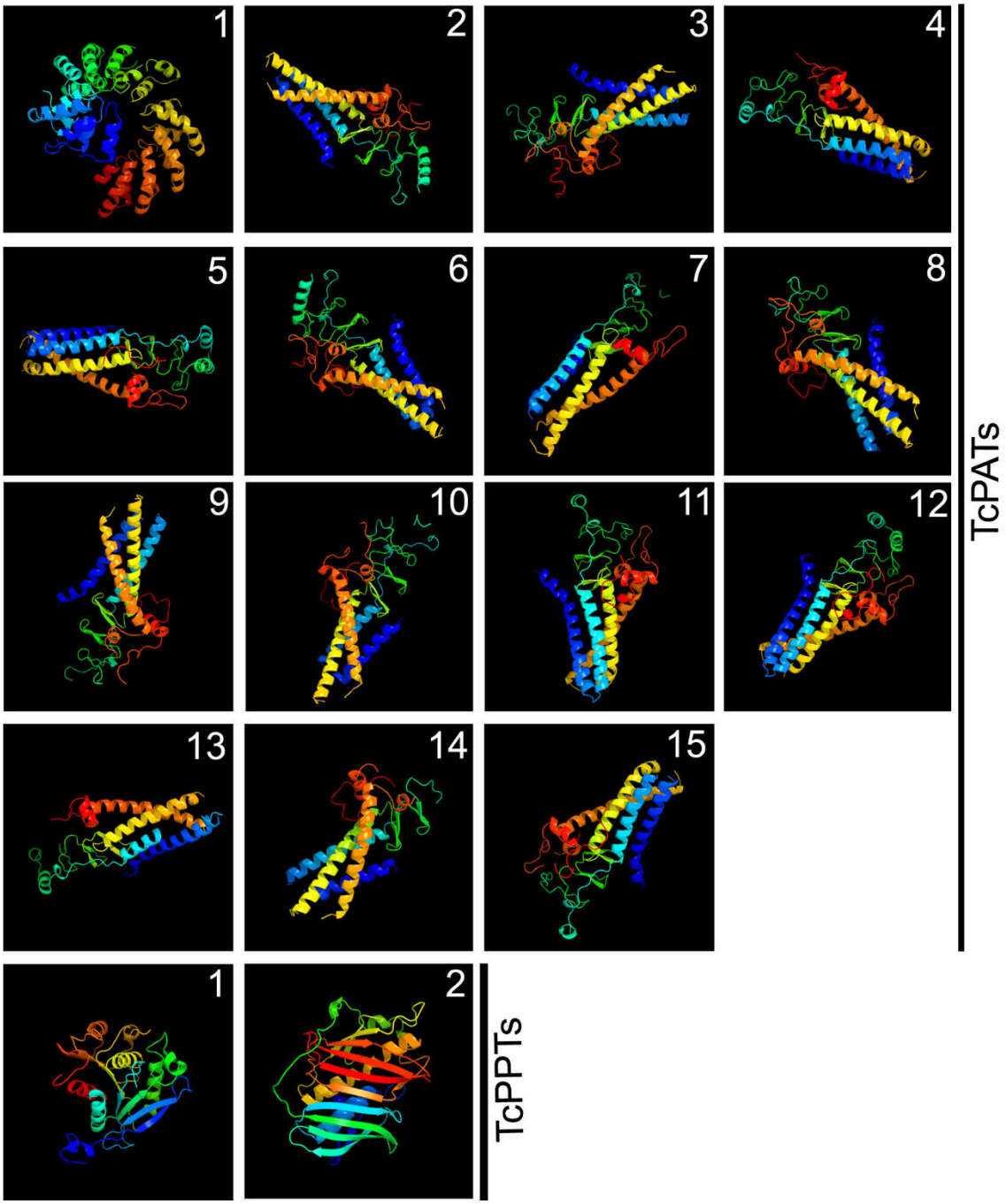

Figure 3. Localization of FLAG tagged PATs in *Trypanosoma cruzi* epimastigotes by immunofluorescence assay. Control: wild type epimastigote. Blue: Hoechst staining of nucleus (n) and kinetoplast (k) DNA. Red: PAT labeling (arrow) with AlexaFluor 594. Bars = 5 µm.

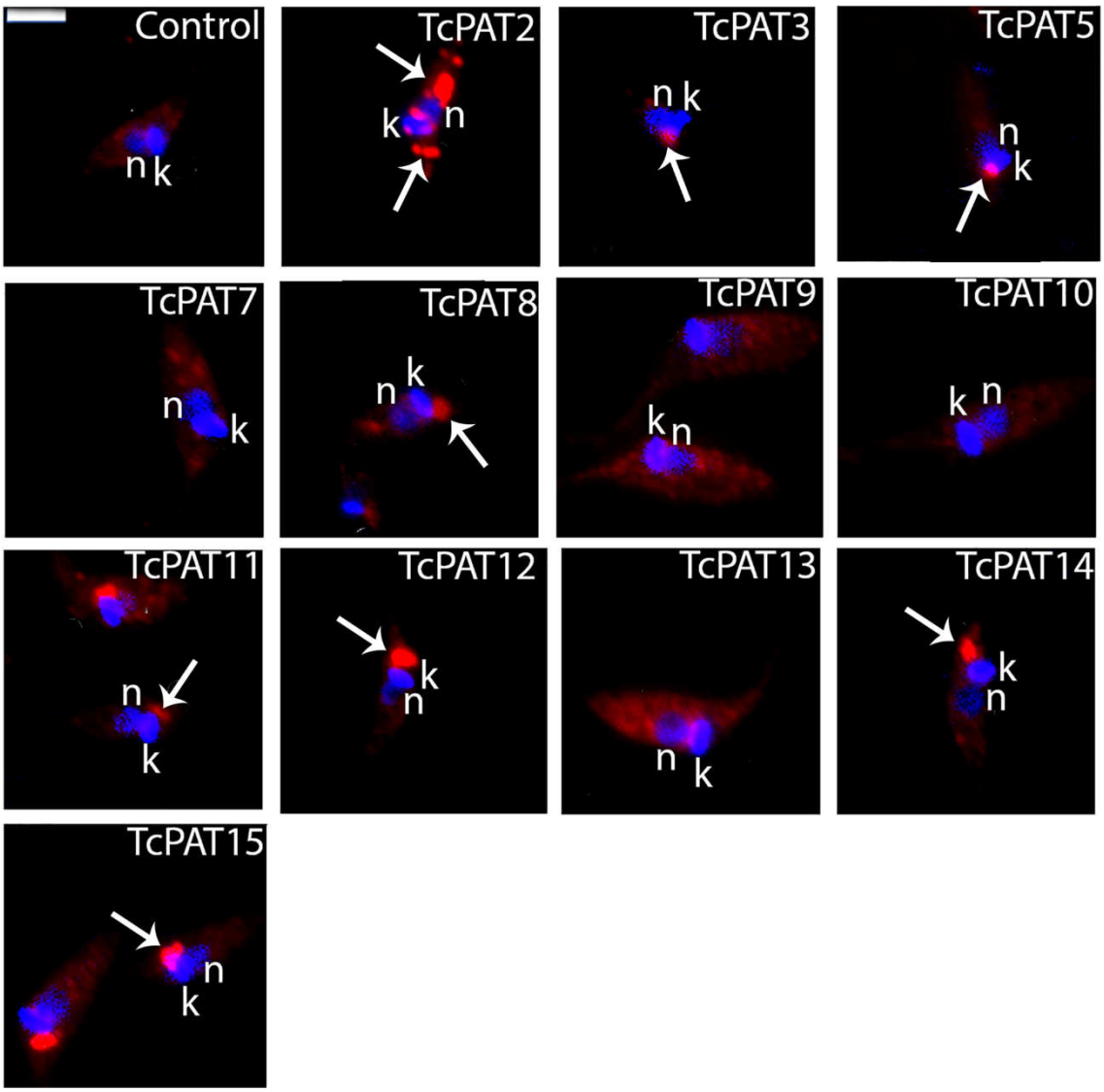

Figure 4. Localization of FLAG tagged PPTs in *Trypanosoma cruzi* epimastigotes by immunofluorescence assay. Control: wild type epimastigote. PPTs were labeled in red with AlexaFluor 594. Nucleus (n) and kinetoplast (k) DNA were labeled in blue with Hoechst. DIC: Differential Interference Contrast, showing the parasite morphology. Bars = 5 µm.

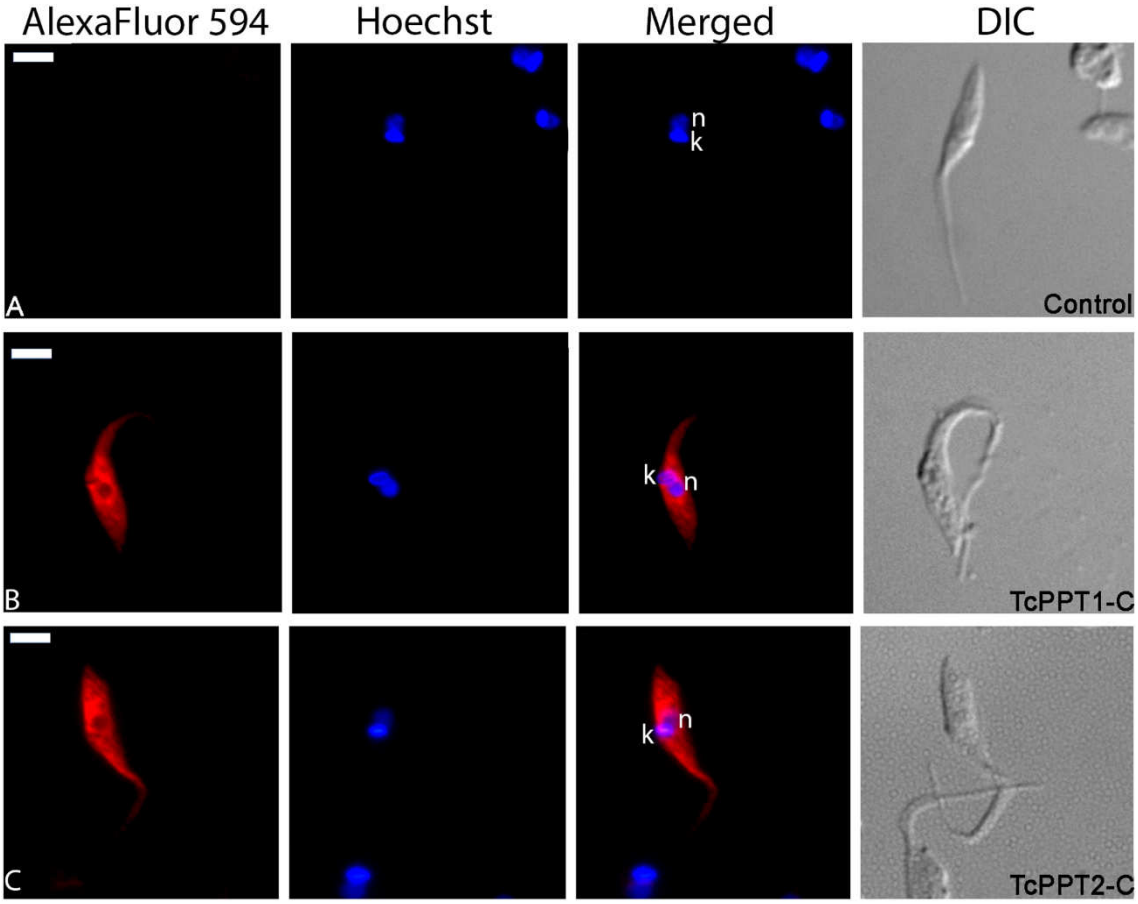

Table 1. Primers used for PAT isolation from gDNA of *Trypanosoma cruzi* (clone Dm28c) epimastigotes F'= forward primer; R'= reverse primer.

PAT/ Gene ID	F'/R' (5'-3')
TcPAT1/ *	ATGCAGGTGTTTGGCGCTCGGATG ACGGCGTTCATCTTTCACCT
TcPAT2/ TcCLB.506297.250	ATGCCACAGACTAACAGCACGGAATGG/ GGGTTCTCTGACTTCATGCGC
TcPAT3/ TcCLB.510899.50	ATGGGGCCCATACGCGTTGAAAGAG/ CACCTGCGTGGCACACAACT
TcPAT4/ TcCLB.508479.200	ATGTCAGGTTTCTGGTCTGTTCAGC/ CACCTCTGCTGTTTCAACGACAATAT

TcPAT5/ TcCLB.509029.170	ATGTCCGGAGAGACTTTTGCTTG/ CTCATATTTCATCCTCCGTTCTCCT
TcPAT6/ TcCLB.506177.40	ATGCGGTCATCTATGTTGCTGCTTTT/ TTCCTCCTTCATCTCCTCCTCGCT
TcPAT7/ TcCLB.510687.130	ATGGATGAATCAAACGACGCG/ CACGTCATTCTCAGCGTTTCG
TcPAT8/ TcCLB.511897.19	ATGGGTAAGATTTTTGAAATGGAGGT/ CCGTATCAAATCAACAAGAGTTCTCC
TcPAT9/ TcCLB.509769.33	ATGGATTGCGTGGTAGGTATGCGGAAT/ AACTAGAGCCTCAGTGTTCAACCAC
TcPAT10/ TcCLB.508239.40	ATGATGTCATTGTTATCACGATGGG/ CACAAGGTCGGCGTCATCG
TcPAT11/ TcCLB.511823.50	ATGTCGTTGCTTTGTTGTGATCC/ GTCATATTTGGGTGAAATGGGTG
TcPAT12/ TcCLB.506855.10	ATGGGGTCGTTGATTCCGC/ CACCGGCAACATCACCTCATC
TcPAT13/ TcCLB.510747.18	ATGAATGTACCCACTTCATCCAGTCCGAT/ CACATAAAACTCGGCGTTTTCC
TcPAT14/ TcCLB.511153.60	ATGGAGTCCGTGGAAGTGCTAGT/ TGCGATGATGGGGCTCTTATT
TcPAT15/ TcCLB.509105.20	ATGCGGTGCTGTGGGCG/ CATACCACCAGATCCGGGAAGCGAC

*(Batista et al. 2013).

Table 2. Identification, *in silico* analysis and primer design of *Trypanosoma cruzi* PPTs. PPT: Palmitoyl thioesterase; BP: Number of base pairs; kDa: molecular weight of the predicted protein; F': forward primer; R': reverse primer.

PPT/Gene ID	BP	kDa	F'/R' (5'-3')
TcCLB.506797.70 (TcPPT1)	843	30.2	ATGATCGGAACGCCGATAGAAAACT/ AGCCTTGGACTCAATCGCCGGCAATACCT
TcCLB.504149.55 (TcPPT2)	951	35.5	ATGCTTCTGCAGGACGTTATTGGAG/ GAGTCTCGATTTGTAGCCCTTTCCTG

4.4. Conclusão Capítulo 1

- Após buscas em bancos de dados genômicos, foram identificadas 15 possíveis DHHC palmitoil transferases (PATs) e duas palmitoil tioesterases (PPTs) em *T. cruzi*.
- Todas as TcPATs e TcPPTs, exceto TcPAT1 e TcPAT6, foram clonadas no vetor pTcGWFLAG.
- Foi possível obter parasitos transfectantes da maioria dos genes alvos, exceto para TcPAT4.
- A maioria das TcPATs concentrou-se na região anterior de formas epimastigotas, compatível com a localização de complexo de Golgi bolsa flagelar e/ou vacúolo contrátil;
- A localização das PPTs foi dispersa pelo citoplasma.

V. Capítulo 2

Obtenção de amastigotas intracelulares por cavitação

A segunda parte da tese foi a obtenção de formas amastigotas intracelulares isoladas por descompressão do nitrogênio (cavitação) para uso em ensaios biológicos, tais como endocitose, incubação com o inibidor de palmitoilação 2-BP e palmitoil proteômica. Foi possível obter uma população viável e purificada de amastigotas isoladas por esta técnica, com marcação positiva de Ssp4, uma proteína específica da superfície destas formas. Após realizar ensaios de endocitose, foi comprovada a atividade endocítica, com co-localização de transferrina e/ou albumina com cruzipaína nos reservossomos destas formas. Estes resultados foram publicados na revista PLOS ONE (Fator de impacto 2.806, Qualis CB1: B1).

O efeito do inibidor de palmitoilação 2-BP sobre os amastigotas isolados estão descritos no Capítulo 3 e os dados sobre a palmitoil proteômica no Capítulo 4.

5.1. Objetivo

Obter amastigotas intracelulares viáveis por cavitação para estudos de endocitose.

5.2. Objetivos específicos

1. Otimizar a pressão e o tempo necessário para lisar a célula hospedeira e isolar o parasito intacto;

2. Realizar imunofluorescência indireta com o marcador específico de superfície de amastigotas intracelulares Ssp4;

3. Realizar ensaios de endocitose.

5.3. Artigo publicado

Autores: Cassiano Martin Batista, Rafael Luis Kessler, Iriane Eger, Maurilio José Soares

Título: *Trypanosoma cruzi* intracellular amastigotes isolated by nitrogen decompression are capable of endocytosis and cargo storage in reservosomes

Revista: PLoS One. 2015 Jun 9;10(6):e0130165. doi: 10.1371/journal.pone.0130165.

Fator de impacto (2016): 2.806 (Qualis CB-I: B1)

PLOS | ONE

RESEARCH ARTICLE

Trypanosoma cruzi Intracellular Amastigotes Isolated by Nitrogen Decompression Are Capable of Endocytosis and Cargo Storage in Reservosomes

Cassiano Martin Batista[1☯*], Rafael Luis Kessler[2☯], Iriane Eger[1,3], Maurilio José Soares[1]

1 Laboratório de Biologia Celular, Instituto Carlos Chagas/Fiocruz-PR, Curitiba, Paraná, Brazil,
2 Laboratório de Genômica Funcional, Instituto Carlos Chagas/Fiocruz-PR, Curitiba, Paraná, Brazil,
3 Departamento de Biologia Geral, Universidade Estadual de Ponta Grossa, Ponta Grossa, Paraná, Brazil

☯ These authors contributed equally to this work.
* cassianombatista@gmail.com

Abstract

Epimastigote forms of *Trypanosoma cruzi* (the etiologic agent of Chagas disease) internalize and store extracellular macromolecules in lysosome-related organelles (LROs) called reservosomes, which are positive for the cysteine protease cruzipain. Despite the importance of endocytosis for cell proliferation, macromolecule internalization remains poorly understood in the most clinically relevant proliferative form, the intracellular amastigotes found in mammalian hosts. The main obstacle was the lack of a simple method to isolate viable intracellular amastigotes from host cells. In this work we describe the fast and efficient isolation of viable intracellular amastigotes by nitrogen decompression (cavitation), which allowed the analysis of amastigote endocytosis, with direct visualization of internalized cargo inside the cells. The method routinely yielded $5x10^7$ amastigotes—with typical shape and positive for the amastigote marker Ssp4—from $5x10^6$ infected Vero cells (48h post-infection). We could visualize the endocytosis of fluorescently-labeled transferrin and albumin by isolated intracellular amastigotes using immunofluorescence microscopy; however, only transferrin endocytosis was detected by flow cytometry (and was also analyzed by western blotting), suggesting that amastigotes internalized relatively low levels of albumin. Transferrin binding to the surface of amastigotes (at 4°C) and its uptake (at 37°C) were confirmed by binding dissociation assays using acetic acid. Importantly, both transferrin and albumin co-localized with cruzipain in amastigote LROs. Our data show that isolated *T. cruzi* intracellular amastigotes actively ingest macromolecules from the environment and store them in cruzipain-positive LROs functionally related to epimastigote reservosomes.

OPEN ACCESS

Citation: Batista CM, Kessler RL, Eger I, Soares MJ (2015) *Trypanosoma cruzi* Intracellular Amastigotes Isolated by Nitrogen Decompression Are Capable of Endocytosis and Cargo Storage in Reservosomes. PLoS ONE 10(6): e0130165. doi:10.1371/journal.pone.0130165

Academic Editor: Edecio Cunha-Neto, University of Sao Paulo, BRAZIL

Received: February 23, 2015

Accepted: May 18, 2015

Published: June 9, 2015

Data Availability Statement: All relevant data are within the paper and its Supporting Information files.

Funding: This work was supported by Coordenação de Aperfeiçoamento de Pessoal de Nível Superior (CAPES), Conselho Nacional de Desenvolvimento Científico e Tecnológico (CNPq) and Fundação Oswaldo Cruz (Fiocruz). The funders had no role in study design, data collection and analysis, decision to publish, or preparation of the manuscript.

Competing Interests: The authors have declared that no competing interests exist.

Introduction

The internalization of extracellular macromolecules by eukaryotic cells occurs by clathrin-mediated or clathrin-independent endocytosis [1–4]. In the protozoan parasite *Trypanosoma cruzi* (Euglenozoa: Kinetoplastea), a hemoflagellate that causes Chagas disease in humans [5–8], endocytic events are well characterized in epimastigotes, proliferative forms found in the insect vector.

T. cruzi epimastigotes ingest macromolecules via endocytic vesicles formed at two specialized cortical structures located at the anterior of the cell: the cytostome/cytopharynx complex and the flagellar pocket membrane [5, 6, 9]. After endocytosis, internalized macromolecules are directed to lysosome-related structures (LROs) called reservosomes, and co-localize with cruzipain, the major cysteine proteinase in *T. cruzi* [5, 10–12]. All *T. cruzi* developmental forms have LROs, as shown by the co-localization of serine carboxypeptidase, cruzipain and chagasin in axenic epimastigotes, intracellular and tissue culture-derived amastigotes, and trypomastigotes obtained from culture supernatants [13]. However, contrary to the role of reservosomes in epimastigotes, it is possible that the LROs of intracellular amastigotes may not be used for the storage of extracellular macromolecules internalized by the parasite [13].

The iron transporter transferrin [14] is a key molecule internalized by *T. cruzi* epimastigotes. In trypanosomatids, transferrin obtained by endocytosis is the main source of iron ions that are essential for DNA replication, antioxidant defense, mitochondrial respiration and also for the synthesis of the modified base 'J' [15]. Previous works indicate that transferrin uptake in epimastigotes occurs by receptor-mediated (but clathrin-independent) endocytosis, mainly through the cytostome/cytopharynx [6,16], while albumin internalization occurs by clathrin-dependent endocytosis at the flagellar pocket membrane [6–8].

While endocytosis by *T. cruzi* epimastigotes has been studied in detail, the endocytic activity of proliferative intracellular amastigotes—the most clinically relevant form of the parasite—is poorly understood. Morphologically, the presence of a cytostome [17] and of LROs with large electron-lucent rods [13] (similar to the reservosomes found in epimastigotes [8,18]) suggest that endocytosis is likely to occur in the amastigote form. However, endocytosis has rarely been detected in intracellular *T. cruzi* amastigotes.

A pioneering study in 1973 showed that intracellular *T. cruzi* "spheromastigotes" (i.e., amastigote-like forms) incorporated melanin granules from chick embryo pigmented epithelial cells, via the cytostome [19]. Also, *T. cruzi* amastigotes express receptors for human transferrin [20], and require iron for growth in axenic conditions [21], in peritoneal macrophages *in vitro*, and in mice [22]. Amastigotes internalize holo-transferrin (i.e., iron-loaded transferrin), as shown by the inability of acid treatment to dissociate amastigote-bound holo-transferrin at 37°C, when endocytosis is active, while dissociation occurs readily at 4°C, when endocytosis is blocked [20]. However, these authors could not demonstrate the intracellular localization of the internalized transferrin. More recently, Waghabi and co-workers (2005) showed that intracellular amastigotes internalize transforming growth factor-β (TGF-β) from host cardiomyocytes (by a poorly characterized process of receptor-mediated endocytosis), and that TGF-β uptake is important to regulate the intracellular life cycle of the parasite [23]. Nevertheless, the exact localization of the internalized TGF-β could not be determined. Finally, an ultrastructural study showed a few surface-bound transferrin-gold complexes in amastigotes collected from the supernatant of infected Vero cell cultures, but again no intracellular labeling was found [5].

The difficulty in detecting endocytosis in intracellular amastigotes is likely due to the fact that endocytic assays are technically challenging in this life cycle form. When assays are performed using infected cells, labeled tracers are first taken up by the host cells and, therefore, are mostly unavailable for uptake by intracellular amastigotes in the host cell cytoplasm [24]. Performing endocytosis assays with isolated amastigotes may represent an interesting alternative.

Intracellular amastigotes can be isolated directly from infected spleen and liver [25] or from infected tissue culture cells [26, 27] by density gradient centrifugation (using metrizamide and/or Percoll). Density gradient-based protocols are, however, very laborious and involve several medium changes, which can lead to a considerable loss of parasite viability. A different protocol, adapted from a method to purify *T. cruzi* metacyclic trypomastigotes [28, 29], used anion-exchange chromatography to separate *T. cruzi* intracellular amastigotes from cell debris and trypomastigotes, after needle-based disruption of infected cells [30]. Although this is a robust option to purify amastigotes in a larger scale, chromatography is also time consuming, and the positively-charged resin may induce changes in the parasite's surface glycoconjugates.

In the present work, we introduce a rapid cavitation procedure to isolate *T. cruzi* amastigotes from Vero cells. In this protocol, cavitation by nitrogen decompression is followed by a few centrifugation steps (but no density gradients), allowing the rapid purification of viable intracellular amastigotes that are competent for endocytosis. Flow cytometry, fluorescence microscopy and western blotting analyses demonstrated that the *T. cruzi* amastigotes isolated using this new methodology were capable of internalizing transferrin and albumin from the extracellular milieu, and that these molecules were directed efficiently to LROs. Importantly, we detected co-localization of ingested transferrin and albumin with cruzipain, in LROs. Our data also suggest that the LROs of *T. cruzi* intracellular amastigotes correspond to reservosomes.

Materials and Methods

Reagents

BCIP-NBT Color Development Substrate was purchased from Promega Corporation (Madison, WI, USA). Alkaline phophatase (AP)-conjugated rabbit anti-goat IgG and AP-conjugated rabbit anti-mouse IgG were purchased from Santa Cruz Biotechnology (Santa Cruz, CA, USA). Holo-transferrin, bovine serum albumin, Roswell Park Memorial Institute-1640 (RPMI-1640) medium, Dulbecco's modified Eagle medium (DMEM) and anti-transferrin goat IgG were purchased from Sigma-Aldrich (St. Louis, MO, USA). Bench Mark Protein Ladder, albumin-Alexa 488, transferrin-Alexa 633, Hoechst 33342, goat anti-mouse antibody coupled to AlexaFluor 488 or 594, and rabbit anti-goat antibody coupled to AlexaFluor 594 were purchased from Invitrogen-Life Technologies (Carlsbad, CA, USA). Prolong Gold antifade reagent was purchased from Molecular Probes-Life Technologies (Eugene, OR, USA). Fetal bovine serum (FBS) was purchased from Cultilab Ltda (Campinas, SP, Brazil). The anti-Ssp4 2C2 monoclonal antibody [30] was kindly provided by Dr. Renato Mortara (UNIFESP, Brazil).

Parasites

Culture epimastigote forms of *Trypanosoma cruzi* clone Dm28c [31] were maintained by weekly passages in liver infusion tryptose (LIT) medium [32] supplemented with 10% heat-inactivated fetal bovine serum (FBS), at 28°C.

In vitro-derived *T. cruzi* metacyclic trypomastigotes were obtained by incubating epimastigotes in TAU3AAG medium, according to a previously described metacyclogenesis (i.e., epimastigote-to-trypomastigote differentiation) protocol [33]. After 72 h of cultivation in this medium, ~80% of the cells in the supernatant were trypomastigotes.

Vero cells (ATCC CCL-81) were maintained in 75-cm^2 cell culture flasks (Corning Incorporated, Corning, NY, USA), in RPMI medium supplemented with 5% FBS, at 37°C (in a humidified 5% CO_2 atmosphere). Cells were infected with *in vitro*-derived metacyclic trypomastigotes (at a ratio of 10 parasites/cell), 24h after passage. After 4 h of interaction, host cell monolayers were washed with PBS (to remove non-adherent parasites) and then incubated in the same conditions with 7–10 ml DMEM medium supplemented with 10% FBS for four days, when

trypomastigote production peaked. Then, culture supernatants were collected, and cell-derived trypomastigotes that had been released into the supernatant were harvested by centrifugation at 3,000g, for 15 min.

Axenic amastigotes were obtained by *in vitro* amastigogenesis [34]. Briefly, trypomastigotes were collected from the supernatant of infected Vero cell cultures (4-days post-infection), washed with PBS and incubated in high glucose DMEM medium, at pH 5, and 37°C (in a humidified 5% CO_2 atmosphere). After 24 hours, almost 100% of the cells had an amastigote shape.

Isolation of *T. cruzi* intracellular amastigotes by nitrogen cavitation

To isolate intracellular amastigotes from host cells, five culture flasks with $1x10^6$ infected Vero cells each were washed three times with PBS (under gentle agitation), 48 hours post-infection (i.e., at the peak of intracellular amastigote replication), to eliminate contamination with extracellular amastigotes. Then, cultures were trypsinized for 10 min at 37°C, and the trypsinization was halted by the addition of cold FBS 1:1 (v/v). The infected cells in suspension were lysed by nitrogen decompression (cavitation), in a 4639 cell disruption vessel (Parr Instrument Company, Moline, IL, USA), using 180 psi pressure, for 5 min. Intact Vero cells were removed by centrifugation at low speed (10 min, 800*g*), and intracellular amastigotes were recovered from the supernatant. Cell debris were removed from the amastigote fraction by three centrifugation steps at 2,000*g* for 5 minutes, to produce a supernatant of isolated intracellular amastigotes.

Endocytosis assay

Isolated intracellular amastigotes, axenic amastigotes and culture epimastigotes (positive control) were subjected to a previously described endocytosis assay [5], using $2x10^6$ parasites for flow cytometry analyzes, $5x10^6$ for fluorescence microscopy studies and 10^7 for western blotting. Briefly, after 15 min under stress in PBS at 25°C, parasites were incubated with 50 μg/ml transferrin-AlexaFluor 633 or albumin-AlexaFluor 488, for 30 min, at 37°C (amastigotes) or 28°C (epimastigotes). Alternatively, parasites were incubated at 4°C to allow transferrin binding without internalization [6], or the retention of albumin in the flagellar pocket [10]. Negative control cells were incubated in the absence of labeled transferrin or albumin.

Transferrin dissociation assay

Membrane-bound transferrin was dissociated using a previously described method [17], with modifications. Parasites were subjected to endocytosis assays as described above (using 50 μg/ml transferrin-AlexaFluor 633) and then incubated for 5s at 4°C with 0.25 M acetic acid/0.5 M sodium chloride, pH 3.5, after which the pH was quickly neutralized with 1 M sodium acetate. Transferrin dissociation from the parasite's surface was analyzed by western blotting and flow cytometry, as described below.

Western blotting. For western blotting, 10^7 epimastigotes or isolated intracellular amastigotes that had been subjected to endocytosis and transferrin dissociation assays (using 125 μg/ml transferrin-AlexaFluor 633) were washed, ressuspended in 15 μL PBS + 5 μL denaturing buffer (final concentration: 40 mM Tris-HCl pH 6.8, 1% SDS, 2.5% β-mercaptoethanol, 6% glycerol and 0.005% bromophenol blue), boiled for 5 min and then vortexed. Samples were run on 10% SDS-PAGE gels, and then transferred (by wet transfer) onto nitrocellulose membranes (Hybond C, Amersham Biosciences, Buckinghamshire, United Kingdom) according to standard protocols [35]. Membranes were blocked in blocking buffer (5% non-fat milk/0.05% Tween-20 in PBS), which was also used for all antibody incubations. After blocking, membranes were incubated for 2 h with an anti-transferrin goat antiserum (1:200, dilution), and then for 1 h with a mouse antiserum against TcGAPDH (1:5000 dilution) [36]. After 3

washes with 0.05% Tween-20/PBS, membranes were incubated for 1h with AP-conjugated rabbit anti-goat (1:7000 dilution) and AP-conjugated rabbit anti-mouse (1:500 dilution) IgG antibodies, washed 3 times with 0.05% Tween 20/PBS, and reactive bands were visualized using the BCIP-NBT solution, according to the manufacturer's instructions. The Bench Mark Protein Ladder (10–220 kDa) was used to determine molecular weights.

Transferrin band densitometry was performed using the ImageJ 1.45s software (National Institute of Mental Health-NIMH, Bethesda, Maryland, USA). Integrated band densities estimated by ImageJ were used to calculate the ratios between the signal at 28°C (epimastigotes) or 37°C (amastigotes) and that at 4°C, for both untreated and acetic acid-treated parasites.

Flow cytometry

Live parasites that had internalized transferrin-AlexaFluor 633 or albumin-AlexaFluor 488 were analyzed in a FACSAria II flow cytometer (Becton-Dickinson, San Jose, USA), using 660/20 and 530/30 nm band-pass filters, respectively. A total of 20,000 events were acquired in the regions of the FSC x SSC plot previously shown to correspond to parasites [37]. Data analysis was performed using the FlowJo software (FlowJo, Ashland, OR, USA), and the normalized median fluorescence intensities of transferrin and albumin were calculated as the ratios between the median fluorescence intensities of treated and untreated cells. Statistical analysis was performed using the software GraphPad Instat (GraphPad Software Inc, La Jolla, CA, USA), by ANOVA followed by Tukey-Kramer multiple comparisons test.

To detect the amastigote-specific surface protein Ssp4 [38], *in vitro*-derived metacyclic trypomatigotes and amastigotes (intracellular and axenic) were washed twice in PBS and fixed for 15 min in 4% formaldehyde. Cells were then incubated for 30 min at 28°C with an anti-Ssp4 monoclonal antibody [38] diluted to 1:3200, in PBS (pH 7.2). Samples were washed with PBS and incubated for 30 min at 28°C with a goat anti-mouse secondary antibody coupled to AlexaFluor 488 (1:1000 in PBS). Cells were washed with PBS and immediately analyzed by flow cytometry (as described above), using a 530/30 nm band pass filter. In parallel, anti-Ssp4 stained cells were adhered to poly-L-lysine coated slides and observed under a Nikon E600 epifluorescence microscope (Nikon Instruments, Tokyo, Japan).

Immunofluorescence microscopy

To detect native cruzipain, isolated amastigotes and culture epimastigotes were washed twice in PBS, fixed for 30 min with 4% paraformaldehyde, permeabilized for 5 min in 0.5% Triton in PBS, and incubated for 2 h at 37°C with 50 µg/ml anti-cruzipain monoclonal antibody (CZP-315.D9; [39]), in PBS. Samples were then washed three times in PBS and incubated, for 2 h at 37°C, with a goat anti-mouse secondary antibody coupled to AlexaFluor 488 diluted to 1:600 in 'incubation buffer' (PBS with 1.5% BSA).

To co-localize transferrin-AlexaFluor 633 or albumin-AlexaFluor 488 with cruzipain, parasites that had been subjected to endocytosis assays were fixed for 30 min in 4% paraformaldehyde and permeabilized for 5 min with 0.5% Triton in PBS. For co-localization with transferrin-AlexaFluor 633, samples were incubated with both CZP-315.D9 (50 µg/ml) and the anti-transferrin goat antiserum (to enhance the AlexaFluor 633 signal; diluted to 1:150 in incubation buffer), washed three times in PBS and then incubated with goat anti-mouse-AlexaFluor 488 (to detect cruzipain) and rabbit anti-goat—AlexaFluor 594 (to detect transferrin) secondary antibodies (diluted to 1:600 in incubation buffer). For co-localization with albumin-AlexaFluor 488, samples were incubated with CZP-315.D9 and then with a goat anti-mouse-AlexaFluor 594 secondary antibody (using the same dilution conditions mentioned above).

After antibody incubations, all samples were washed three times in PBS, incubated for 5 min with 1.3 nM Hoechst 33342, mounted with Prolong Gold antifade reagent and examined under a Nikon Eclipse E600 epifluorescence microscope.

Results and Discussion

Rapid and efficient isolation of viable *T. cruzi* intracellular amastigotes by nitrogen decompression

T. cruzi epimastigote forms internalize albumin and transferrin and store these molecules in reservosomes, the late endocytic organelles in this parasite stage [5,8]. In contrast, little is known about the endocytic activity of the proliferative intracellular amastigote form, which prevails in chronic chagasic patients and represents the most clinically relevant form of this parasite [40]. Thus, the aim of our study was to analyze the endocytic activity of amastigotes by using transferrin and albumin as probes.

Given that the study of endocytosis by intracellular amastigotes is hindered by the concomitant endocytic activity of host cells, we first attempted to make fluorescent-labeled endocytic tracers available to amastigotes directly in the host cell's cytoplasm, using mild detergent treatments (with saponin and lysolecithin) of infected cells; however, host cells were killed by the lowest detergent concentrations required for transferrin entry into the cytoplasm (data not shown).

Therefore, we developed a protocol to isolate viable, endocytosis-competent intracellular amastigotes from infected host cells, using nitrogen decompression (also known as nitrogen cavitation). Nitrogen decompression is an effective method for lysis and homogenization of cell suspensions [41], and is based on oxygen-free nitrogen dissolution under high pressure. After a sudden release of the pressure, nitrogen 'bubbles out' from the solution, including the cell interior, culminating in plasma membrane disruption. Depending on the cell type, higher pressures (leading to higher nitrogen dissolution) are needed for effective lysis. Mammalian cells are successfully disrupted after the release of 250–500 psi of pressure, while smaller cells with a resistant cell wall, such as bacteria, need around 1,500 psi [41]. Trypanosomatids have a sub-pellicular corset of microtubules that maintains parasite shape and provides resistance to mechanical pressure [42]. Hence, higher pressures are required to disrupt *T. cruzi* cells by cavitation, when compared with those needed to lyse mammalian cells, and we explored this difference efficiently to release intracellular amastigotes from infected cells.

Cell disruption by nitrogen decompression allowed the release of ~$5x10^7$ amastigotes per $5x10^6$ infected Vero cells (NIH 3T3 fibroblasts and H9C2 myoblasts were also used successfully for intracellular amastigote isolation; data not shown). Morphological analysis by light microscopy showed that the parasites obtained by nitrogen cavitation had the typical amastigote shape (Fig 1A). Flow cytometry analysis of parasites labeled for the amastigote-specific surface protein Ssp4 showed that isolated intracellular amastigotes had strong Ssp4 expression, similar to that observed in axenic amastigotes (Fig 1B), while trypomastigotes and epimastigotes did not express Ssp4. These data confirmed that the isolated parasites were indeed amastigotes. Interestingly, isolated intracellular amastigotes had a narrower profile of Ssp4 expression than axenic amastigotes, indicating that axenic amastigotes constitute a more heterogeneous population formed by parasites in a variety of differentiation stages.

Infected Vero cells containing intracellular amastigotes were more susceptible to cavitation than uninfected ones, and could be lysed effectively with as little as 180 psi, a condition that did not affect intracellular amastigotes (S1 Fig). Flow cytometry using a GFP-fluorescent *T. cruzi* clone [43] showed that, after cavitation, almost all infected Vero cells were disrupted, releasing GFP-positive viable intracellular amastigotes (S1 Fig). In contrast, uninfected Vero cells could only be lysed efficiently after the release of 350–400 psi, which also disrupted ~25% of

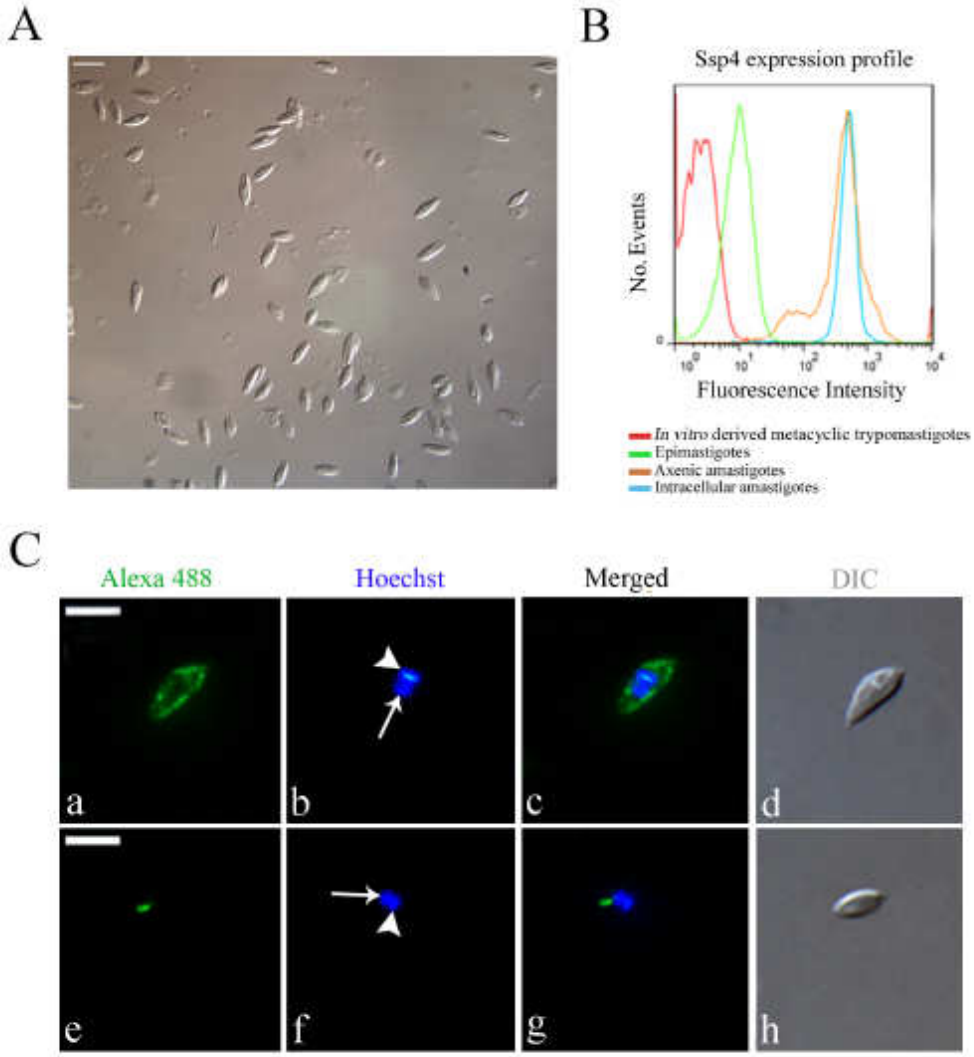

Fig 1. *Trypanosoma cruzi* intracellular amastigotes isolated by nitrogen decompression have normal shape, high levels of Ssp4, and cruzipain labeling in posterior organelles. (A) Differential interference contrast (DIC) image of the fraction of isolated intracellular amastigotes obtained after nitrogen decompression and differential centrifugation. Note that most cells have the typical amastigote shape. Scale bar, 10 μm. (B) Flow cytometry analysis of axenic and isolated intracellular amastigotes, culture epimastigotes and *in vitro*-derived trypomastigotes labeled with an antibody against Ssp4, a specific amastigote marker. Trypomastigotes and epimastigotes had low levels of fluorescence signal (possibly due to auto-fluorescence), while axenic and intracellular amastigotes showed higher fluorescence intensity. (C) Immunofluorescence microscopy of isolated intracellular amastigotes labeled with an anti-Ssp4 antiserum (green, in a-d), or with the anti-cruzipain monoclonal antibody CZP-315.D9 (green, in e-h). The nucleus (arrow) and the kinetoplast (arrowhead) are stained blue with Hoechst 33342, and parasite morphology was visualized by DIC. While Ssp4 localizes to the cell surface, the cruzipain signal is found specifically in lysosome related organelles posterior to the nucleus. Scale bars, 5 μm.

doi:10.1371/journal.pone.0130165.g001

intracellular amastigotes (not shown). Hence, by performing nitrogen cavitation at 180 psi, only infected cells were disrupted, resulting in increased recovery of intact amastigotes and a reduction in the amount of cell debris, which could be removed easily by successive washes

(Fig 1A). We used a 5-min cavitation period routinely, and longer cavitation periods (10 min) did not increase parasite yield (data not shown).

We confirmed the expression of Ssp4 by indirect immunofluorescence, and also to analyzed the localization of the reservosome/LRO marker cruzipain in intracellular amastigotes (Fig 1C). We observed a strong Ssp4 signal on the cell surface of isolated intracellular amastigotes (Fig 1C), as previously described for extracellular amastigotes obtained from the transformation of blood or cell culture trypomastigotes [38]. The anti-cruzipain monoclonal antibody CZP-315.D9 recognized an LRO-like structure posterior to the nucleus (Fig 1C), a localization compatible with that of LROs [13].

Previously described methods for the isolation of *T. cruzi* amastigotes are laborious and involve several medium changes and/or anion-exchange chromatography [25–29], with considerable loss of parasite viability and likely changes in the amastigote surface glycoconjugates (due to the interaction with the positively-charged resin). The nitrogen decompression method for intracellular amastigote isolation described here is easier and faster than previously described protocols, and yields viable amastigotes efficiently, and is likely to represent an excellent tool for studies on different aspects of amastigote biology.

Isolated intracellular amastigotes internalize fluorescently-labeled transferrin

Most data suggestive of endocytosis by amastigotes is indirect [19–23]. Soares and De Souza (1991) showed direct evidence of transferrin binding to the surface of cell-derived amastigotes, but not of transferrin internalization, suggesting a low level of endocytic activity by amastigotes [5]. In our work we have also tried to visualize transferrin endocytosis directly by transmission electron microscopy (TEM) in isolated intracellular amastigotes, but no intracellular transferrin-gold complexes were observed (data not shown). These results were likely due to the relatively low endocytic activity of amastigotes, compared with that of epimastigotes, where cargo-gold complexes can be readily detected by TEM. Thus, we attempted to detect endocytosis in isolated intracellular amastigotes by more sensitive techniques than TEM, such as western blotting and flow cytometry.

Using western blotting, we confirmed the presence of holo-transferrin (MW 76–81 kDa) in protein extracts of amastigotes and epimastigotes (positive control cells) subjected to a transferrin uptake assay (Fig 2). The anti-TcGAPDH antiserum used as a loading control recognized a polypeptide of the correct molecular weight (~40 kDa) in all *T. cruzi* developmental forms (Fig 2A).

Whole cell extracts of isolated intracellular amastigotes incubated at the endocytosis-permissive temperature of 37°C (likely to include both surface bound and internalized transferrin) contained more transferrin than extracts of parasites incubated at 4°C, when endocytosis does not occur and, thus, only surface-bound transferrin should be detected (Fig 2A). After a rapid (5s) acetic acid treatment, which leads to the dissociation of surface-bound transferrin [20], holo-transferrin levels in amastigotes incubated at 37°C remained similar to those observed without acetic acid treatment. In epimastigotes, transferrin localizes inside the flagellar pocket and the cytostome/cytopharynx complex, and then accumulates in the reservosomes [5,8]. While the intracellular pool of labeled transferrin is not accessible to acetic acid treatment, this treatment is expected to remove most surface-bound transferrin, in parasites incubated at 4°C. In this study, we observed a residual signal after acetic acid treatment in parasites incubated at 4°C (Fig 2A), probably due to surface-bound transferrin that could not be readily removed from to the interior of the cytostome/cytopharynx or from the flagellar pocket (Fig 2A). Densitometry analysis showed that the ratio between the transferrin signal at 28°C and that at 4°C was higher for parasites treated with acetic acid compared with untreated parasites (Fig 2B), in

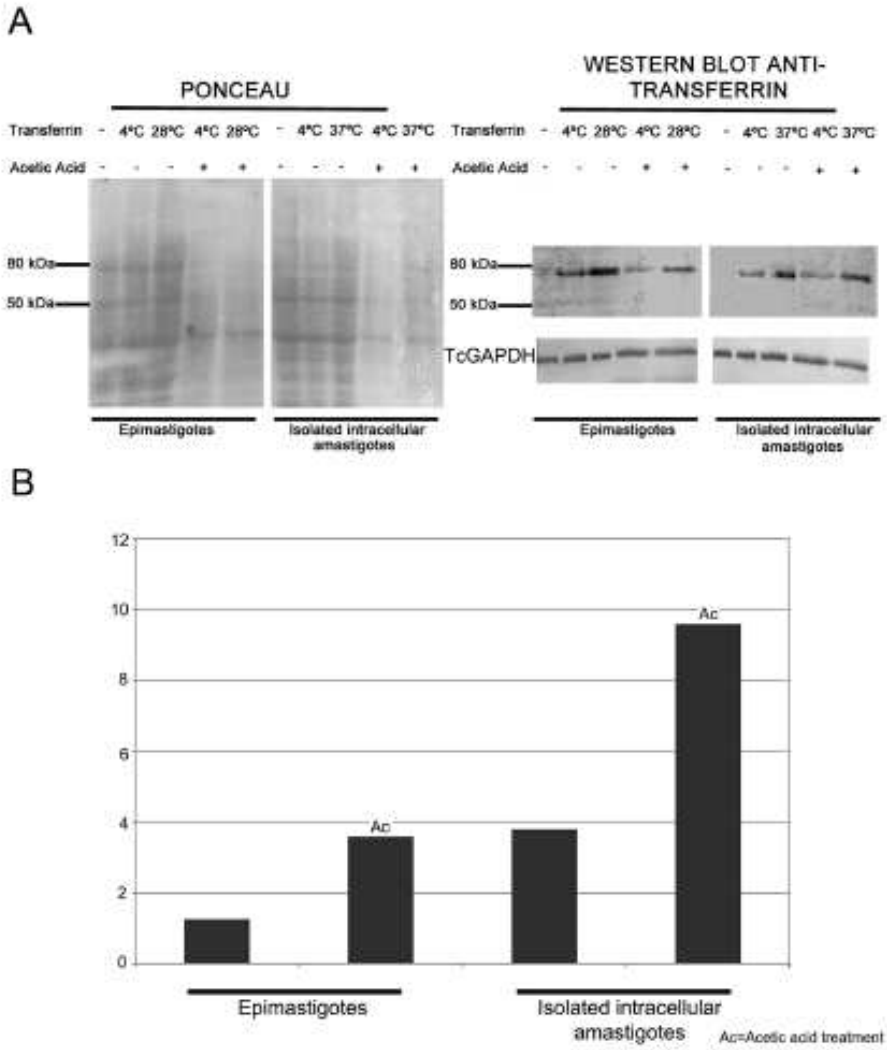

Fig 2. Western blotting analysis of transferrin-AlexaFluor 633 uptake in isolated *Trypanosoma cruzi* intracellular amastigotes. (A) Detection of holo-transferrin (using anti-transferrin goat antiserum) in total protein extracts of isolated intracellular amastigotes and epimastigotes (positive control for endocytosis) endocytosis assays at different temperatures. The panel on the left shows the Ponceau-stained membrane used for transferrin immuno-blotting analysis (on the right). The protein band with approximately 80 kDa corresponds to transferrin. Protein extract from isolated intracellular amastigotes incubated with transferrin at 37°C showed a strong band, indicating transferrin internalization. TcGAPDH (~40 kDa) was used as a loading control. (B) Ratios between the integrated densities of the transferrin band at 28 or 37°C and 4°C (Y-axis), based on measurements performed using ImageJ.

doi:10.1371/journal.pone.0130165.g002

agreement with the hypothesis that acid treatment removed the predominantly surface-bound transferrin at 4°C, while the internalized transferrin prevalent in parasites incubated at 37°C was resistant to acid treatment.

Overall, the western blotting data suggest that transferrin binds to the surface of amastigotes (at 4 and 37°C) and is internalized by parasites (at 37°C). A positive control for endocytosis using epimastigotes (at an endocytosis-permissive temperature of 28°C, instead of 37°C)

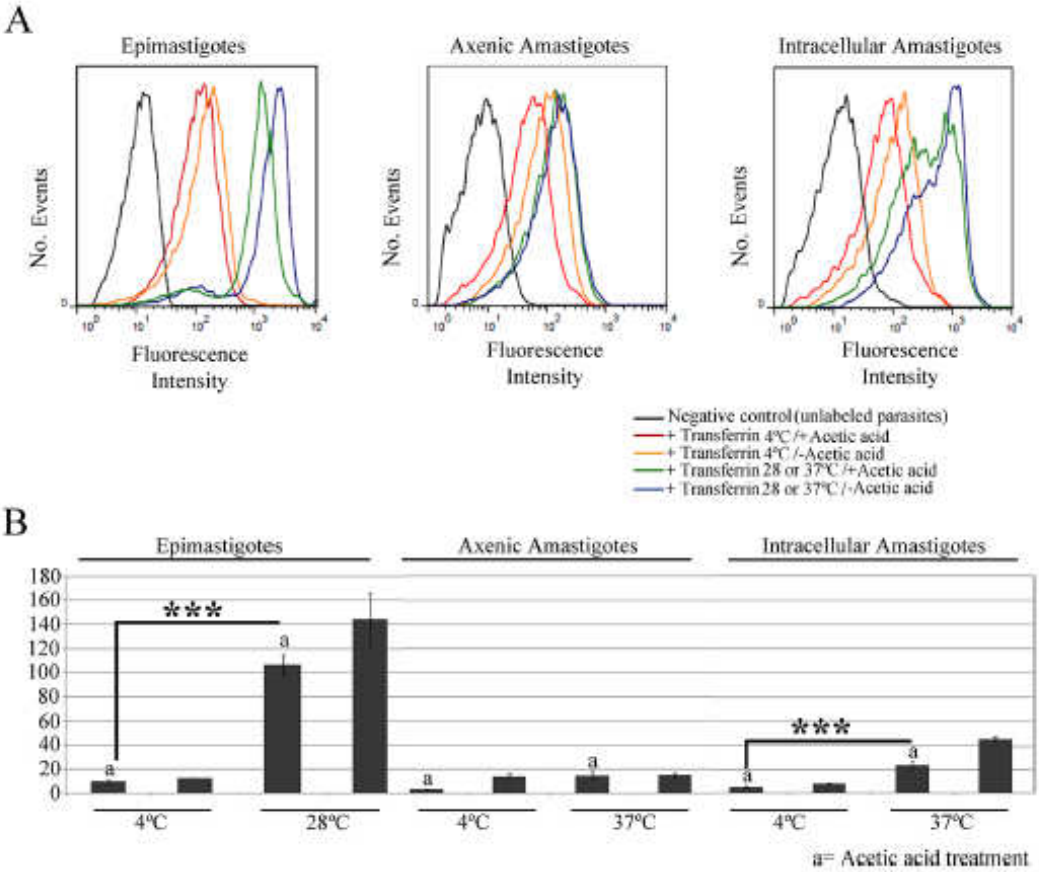

Fig 3. Flow cytometry analysis of transferrin-AlexaFluor 633 endocytosis by amastigotes and epimastigotes of *Trypanosoma cruzi*. (A) Flow cytometry histograms of parasites incubated with transferrin at different temperatures, and then treated with acetic acid, or left untreated. Epimastigotes were used as positive control, and negative control parasites (black) were incubated in medium without labeled transferrin. These data show that isolated intracellular amastigotes internalize transferrin at 37°C. (B) Normalized medians (stained/unstained control) of the fluorescence peaks. Note the low endocytosis levels in axenic amastigotes (N = 3). ***p<0.001. a, acetic acid treatment.

doi:10.1371/journal.pone.0130165.g003

showed a very similar pattern to that observed for amastigotes, supporting our interpretation of the amastigote data.

Isolated intracellular amastigotes have higher intracellular levels of labeled transferrin than axenic amastigotes

Flow cytometry analysis provided further support to the notion that transferrin is internalized by isolated intracellular amastigotes, since the transferrin-AlexaFluor 633 signal in these parasites increased significantly ($p<0.001$) when endocytic assays were performed at the endocytosis-permissive temperature 37°C, compared with samples incubated at 4°C (Fig 3A). The fluorescence signal increased in cells incubated at 4°C, compared with controls without transferrin, in line with the western blotting data that suggest that binding of transferrin to the surface of isolated intracellular amastigotes occurs at this temperature. The transferrin-AlexaFluor 633 signal decreased after acetic acid treatment in isolated intracellular amastigotes incubated

at 4°C, and also in those incubated at 37°C. However, the fluorescence intensity of cells incubated at 37°C and treated with acetic acid remained higher than that of cells incubated at 4°C, but not subjected to acid treatment (Fig 3A). These results suggest that a considerable proportion of the labeled transferrin in cells incubated at 37°C was found in internal organelles and, thus, was resistant to acid treatment (Fig 3A).

Similar results were obtained for a positive control for endocytosis using epimastigotes (at an endocytosis-permissive temperature of 28°C, instead of 37°C): the fluorescence signal was higher in cells incubated at 28°C, when compared with those incubated at 4°C (Fig 3A). Also, acetic acid treatment decreased the fluorescence intensity in both cases, although a higher signal remained in cells incubated at 37°C, indicating transferrin internalization.

Interestingly, we observed a relatively low fluorescence signal in axenic amastigotes incubated at 37°C, similar to that seen in cells incubated at 4°C (Fig 3A). These data indicate that axenic amastigotes ingest only a limited amount of transferrin and, therefore, do not represent a reliable model for studies on *T. cruzi* endocytosis. Normalized medians of the fluorescence peaks showed that the endocytic activity is higher in epimastigotes than in isolated intracellular amastigotes, while axenic amastigotes showed only minimal endocytic activity (Fig 3B).

Labeled transferrin co-localizes with cruzipain in lysosomal-related organelles (LROs) of isolated intracellular amastigotes

To examine the destination of the internalized transferrin, isolated intracellular amastigotes were subjected to endocytosis assays and then processed for immunofluorescence for the detection of transferrin and also of cruzipain, a marker of LROs (i.e., the reservosomes), the final destination of internalized transferrin in epimastigotes. In positive control cells (epimastigotes) incubated at 4°C, only cruzipain was detected in the reservosomes, located at the posterior end of the cell (Fig 4A and 4D), while transferrin was found at the anterior end of the cell (likely

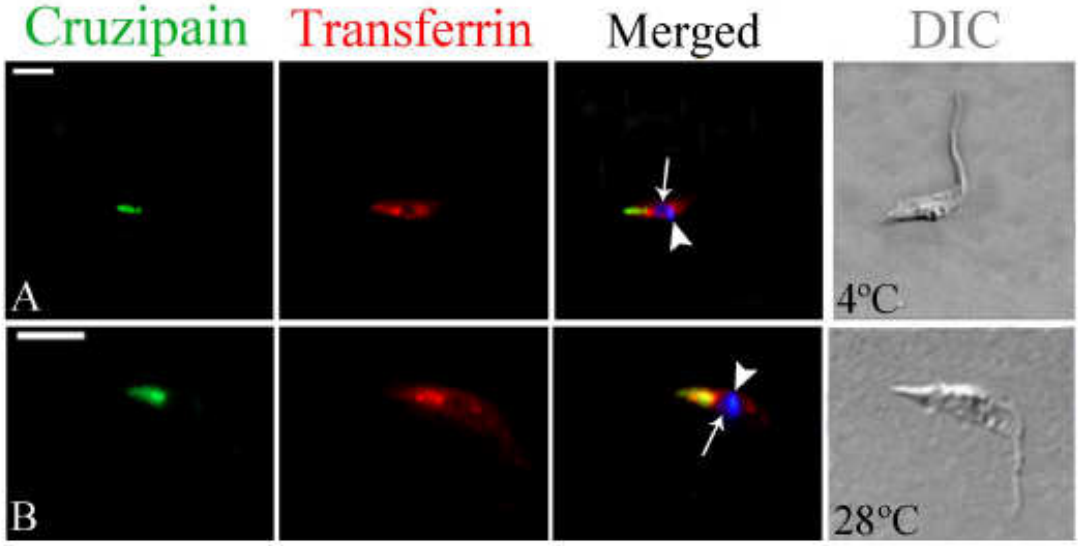

Fig 4. Fluorescence microscopy analysis of transferrin-AlexaFluor 633 endocytosis by *Trypanosoma cruzi* epimastigotes. Cells were allowed to ingest transferrin and were then labeled with an anti-transferrin antibody (in red) and with the anti-cruzipain mAb CZP-315.D9 (CZP; in green). At 4°C no co-localization was observed (A), while transferrin and cruzipain co-localized at the posterior region of the cell after incubation at 28°C (B), resulting in yellow staining of the reservosomes. The nucleus (arrow) and kinetoplast (arrowhead) are stained with Hoechst 33342 (in blue). DIC, differential interference contrast. Scale bars, 5 μm.

doi:10.1371/journal.pone.0130165.g004

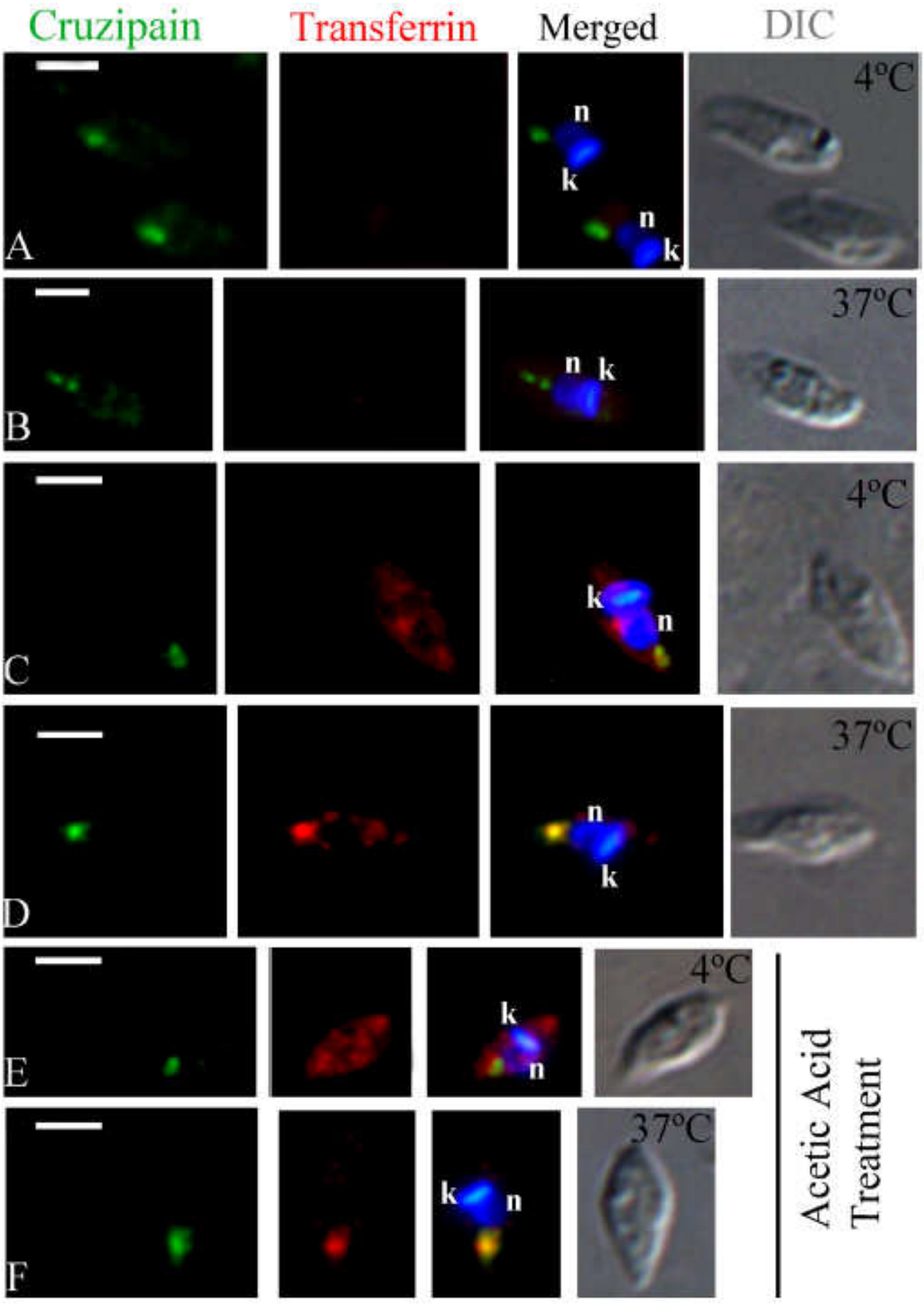
Cruzipain
Transferrin
Merged
DIC
4°C
37°C
4°C
37°C
4°C
37°C
A
B
C
D
E
F
n
k
Acetic Acid Treatment

Fig 5. Fluorescence microscopy analysis of transferrin-AlexaFluor 633 endocytosis by isolated intracellular amastigotes of *Trypanosoma cruzi*. Cells were allowed to ingest transferrin-AlexaFluor 633 and were then incubated with anti-transferrin antibody (in red) and anti-cruzipain mAb (CZP-315.D9; in green). (A-B) Isolated intracellular amastigotes incubated without transferrin at 4°C or 37°C, showed no transferrin labeling (negative control), while cruzipain was located at the posterior region of the cell. (C) Isolated intracellular amastigotes incubated with transferrin at 4°C. No co-localization with cruzipain was observed. (D) Isolated intracellular amastigotes incubated with transferrin at 37°C. Co-localization with cruzipain was observed at the posterior region of the cell. (E-F) Isolated intracellular amastigotes incubated with transferrin at 4°C and 37°C and then subjected to acetic acid treatment. No co-localization of transferrin with cruzipain was observed at 4°C (E), while co-localization with cruzipain occurred at the posterior region at 37°C (F). The nucleus (n) and the kinetoplast (k) were stained with Hoechst 33342 (in blue). DIC, differential interference contrast. Scale bars, 2.5 μm.

doi:10.1371/journal.pone.0130165.g005

corresponding to the cytostome) and in dense spots close to the nucleus, likely corresponding to the bottom of the cytopharynx [9,17,44]. In epimastigotes incubated at 28°C there was co-localization of transferrin with cruzipain at the reservosomes (Fig 4E and 4H), as previously shown [11,12,39].

As expected, transferrin labeling in isolated intracellular amastigotes (4 or 37°C) was not intense, but was clearly detectable in most cells. No co-localization with cruzipain occurred at 4°C: transferrin labeling was prominent at a discrete spot close to the nucleus and the kinetoplast (corresponding to the location of the bottom of the cytopharynx), while cruzipain localized to the posterior region of the cell (Fig 5A and 5B). In contrast, we detected co-localization of transferrin and cruzipain in LROs at the posterior region of the cell, in amastigotes incubated at 37°C, although co-localization was not clear in all cells (Fig 5C and 5D). A similar result was obtained when amastigotes were subjected to endocytosis assays and then treated with acetic acid (Fig 5E and 5F).These data indicate a low level of protein uptake; nevertheless, internalized transferrin was delivered to (and stored in) cruzipain-positive LROs at the posterior of the cell.

Ingested albumin co-localizes with cruzipain in isolated intracellular amastigotes, confirming a storage function for amastigote LROs

To examine the internalization of a different endocytic marker, we analyzed the uptake of albumin-AlexaFluor 488 complexes by isolated intracellular amastigotes, using flow cytometry. As expected, we observed an intense fluorescence signal indicative of albumin internalization in epimastigotes (i.e., positive control cells) incubated with Albumin-AlexaFluor 488 at 28°C; this signal was significantly higher ($p<0.001$) than that observed in controls cells incubated at 4°C or not given the labeled tracer (Fig 6). However, only a weak albumin-AlexaFluor 488 fluorescence signal was detected in isolated intracellular amastigotes, regardless the experimental condition (Fig 6), indicating minimal endocytosis of albumin by this developmental form.

Despite the failure to detect albumin-AlexaFluor 488 internalization by flow cytometry, we could detect endocytosis of this labeled tracer by isolated intracellular amastigotes using fluorescence microscopy (Fig 7); however, labeling was relatively weak and not observed in all cells. Control experiments with epimastigotes showed that, at 4°C, albumin-AlexaFluor 488 complexes were occasionally found at the flagellar pocket region, but did not co-localize with cruzipain in the reservosomes (Fig 7A). However, at 28°C albumin and cruzipain co-localized in reservosomes, as shown here for the first time (Fig 7B). Similar results were obtained with isolated intracellular amastigotes: at 4°C no co-localization was observed (Fig 7C), while at 37°C albumin and cruzipain occasionally co-localized at LROs (Fig 7D). At both temperatures cruzipain was also detected in the anterior region of cell, maybe *en route* to LROs and/or to the secretory pathway. These results, combined with the flow cytometry data, indicate that amastigotes are capable of albumin uptake, albeit only at low levels.

Thus, contrary to the suggestion that amastigote LROs are not *bona fide* components of the endocytic pathway [13], our findings show that *T. cruzi* amastigote forms internalize

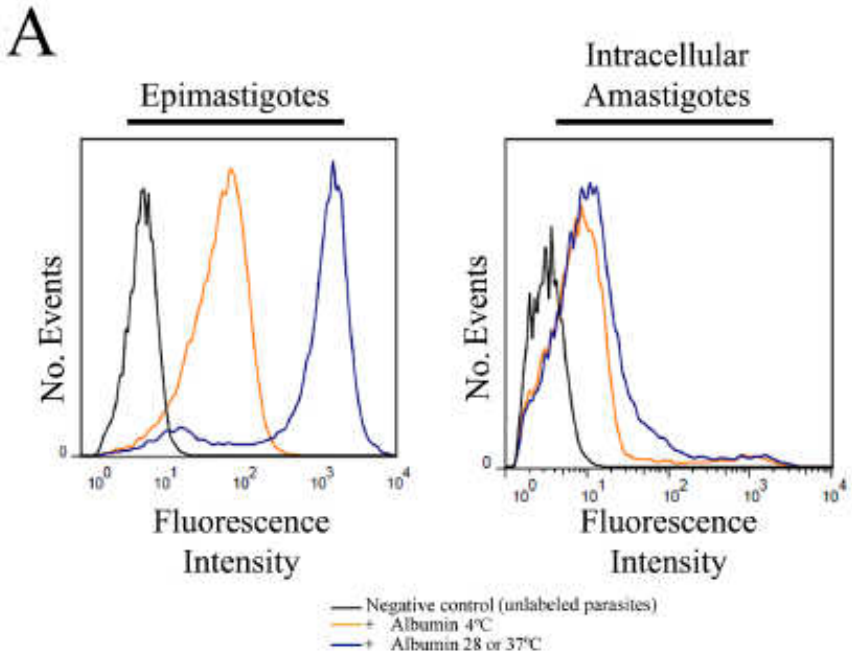

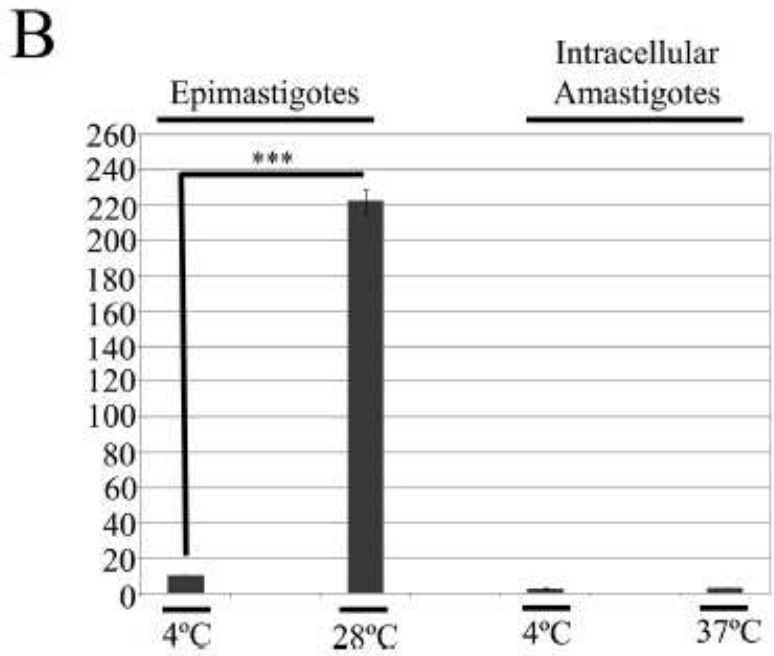

Fig 6. Flow cytometry analysis of albumin-AlexaFluor 488 endocytosis in *T. cruzi* by isolated intracellular amastigotes. (A) Flow cytometry histograms of cells incubated with labeled albumin at different temperatures. Epimastigotes were used as positive control, and negative control parasites (black) were incubated in medium without labeled albumin. These data show that isolated intracellular amastigotes internalize low amounts of albumin at 37°C. (B) Normalized medians of the fluorescence peaks, relative to the negative control (N = 3). ***p<0.001.

doi:10.1371/journal.pone.0130165.g006

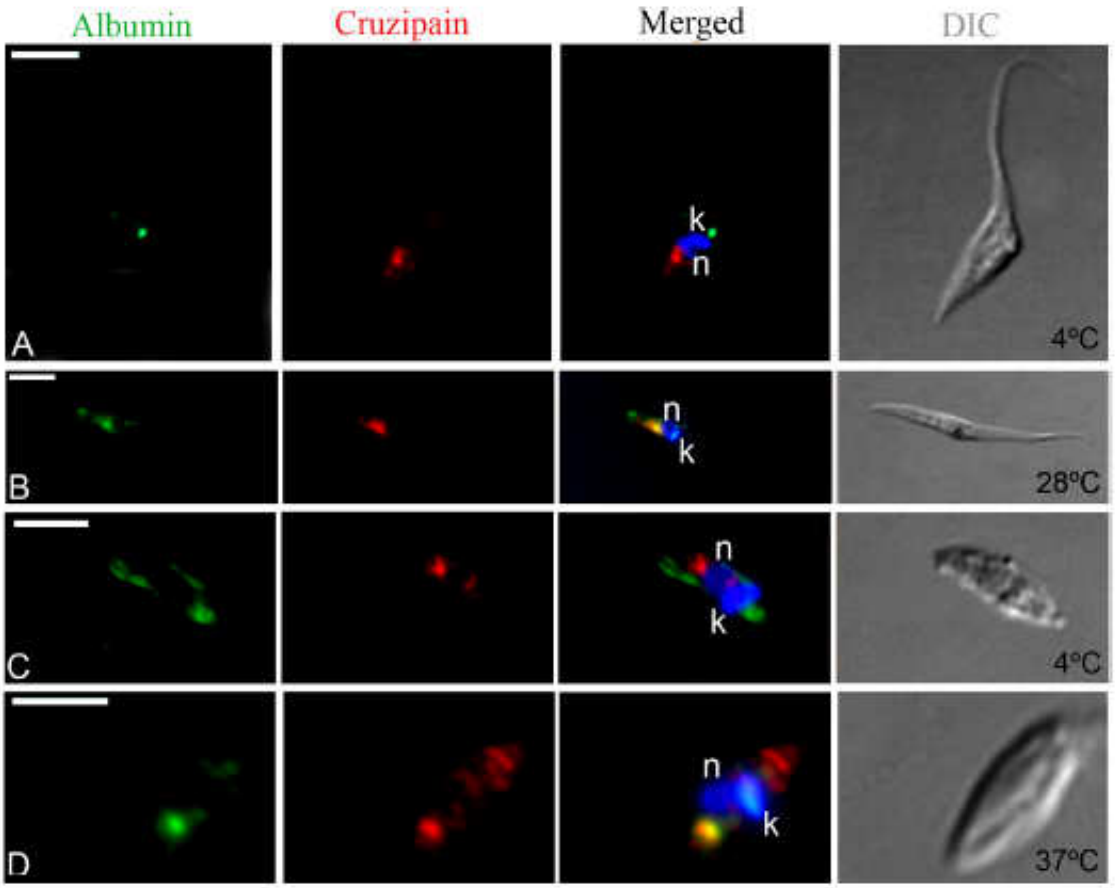

Fig 7. Fluorescence microscopy analysis of albumin-AlexaFluor 488 endocytosis by isolated intracellular amastigotes of *T. cruzi*. Cells were allowed to ingest albumin-AlexaFluor 488 (in green) and were then labeled with the anti-cruzipain mAb CZP-315.D9 (in red). In epimastigotes (A) and isolated intracellular amastigotes (C) incubated at 4°C, we did not observe co-localization of albumin (at the anterior end of the cell, nearest to the kinetoplast—k) and cruzipain (at the posterior end of the cell, nearest to the nucleus—n). In contrast, in epimastigotes (B) and isolated intracellular amastigotes (D) incubated at endocytosis-permissive temperatures (28°C or 37°C, respectively), we detected co-localization of albumin and cruzipain at the posterior region of the cell. The nucleus (n) and kinetoplast (k) are stained with Hoechst 33342 (in blue). DIC, differential interference contrast. Scale bars, 5 μm.

doi:10.1371/journal.pone.0130165.g007

macromolecules and target ingested cargo to cruzipain-positive LROs. To our knowledge, these data represent the first direct evidence that amastigote LROs correspond to the reservosomes observed in epimastigote forms (Fig 8).

Conclusions

Host cell lysis by nitrogen decompression (cavitation) allows rapid and efficient isolation of viable *T. cruzi* intracellular amastigotes that have the typical amastigote shape and are positive for the amastigote-specific antigen Ssp4. Our data show that isolated intracellular amastigotes of *T. cruzi* display endocytic activity, although at lower levels than epimastigotes. Also, we show that internalized cargo (transferrin and albumin) accumulates in amastigote LROs, a clear indication that these organelles are functionally related to the reservosomes observed in epimastigotes.

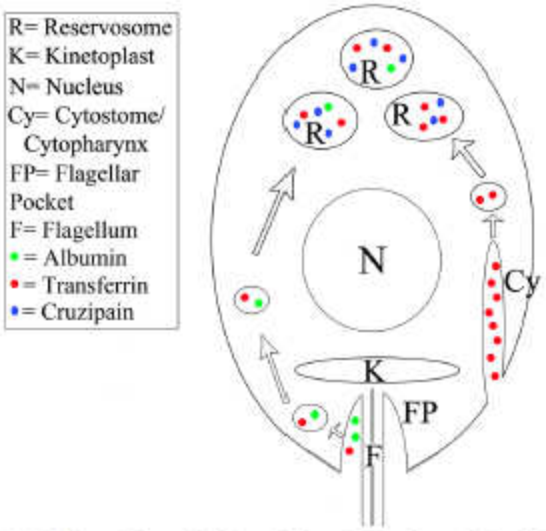

Fig 8. Schematic model of transferrin and albumin uptake by isolated *Trypanosoma cruzi* intracellular amastigotes. As in epimastigotes, transferrin uptake by amastigotes occurs mainly through the cytostome/cytopharynx complex (Cy). After internalization, transferrin is directed to the reservosomes (R), where it is stored together with lysosomal proteases such as cruzipain (Cz), the major cysteine protease of this parasite. Albumin (A) is internalized via the flagellar pocket region, but albumin endocytic activity is low. The destination of ingested macromolecules is the reservosomes.

doi:10.1371/journal.pone.0130165.g008

Supporting Information

S1 Fig. Flow cytometry analysis of intracellular amastigotes release by nitrogen cavitation. Density plots showing the distribution of cell populations before and after Vero cell lysis by nitrogen decompression at 180 psi, compared with the profile obtained after trypsinization, but before nitrogen decompression. Vero cell cultures were infected with a GFP-expressing (GFP+) *T. cruzi* cell line, to verify host cell disruption and amastigote (Ama) release. Almost all infected Vero cells were disrupted after cavitation, releasing GFP+ amastigotes. Cell gates are marked in the plot on the right.
(TIF)

Acknowledgments

The authors thank the Program for Technological Development in Tools for Health-PDTIS-FIOCRUZ for use of its facilities (Flow Cytometry Platform RPT08L and Confocal and Deconvolution Platform RPT07C at the Instituto Carlos Chagas/Fiocruz-PR, Brazil). The authors also thank Dr. Alexandre Dias Tavares Costa for critical reading of the manuscript.

Author Contributions

Conceived and designed the experiments: IE MJS. Performed the experiments: CMB RLK. Analyzed the data: CMB RLK IE MJS. Contributed reagents/materials/analysis tools: MJS. Wrote the paper: CMB RLK IE MJS.

References

1. Mayor S, Pagano RE. Pathways of clathrin-independent endocytosis. Nat Rev Mol Cell Biol. 2007; 8: 603–612. PMID: 17609668
2. Lundmark R, Carlsson SR. Driving membrane curvature in clathrin-dependent and clathrin-independent endocytosis. Sem Cell Develop Biol. 2010; 21: 363–370.
3. Mayor S, Parton RG, Donaldson JG. Clathrin-independent pathways of endocytosis. Cold Spring Harb Perspect Biol. 2014; 6: a016758. doi: 10.1101/cshperspect.a016758 PMID: 24890511
4. Kirchhausen T, Owen D, Harrison SC. Molecular structure, function, and dynamics of clathrin-mediated membrane traffic. Cold Spring Harb Perspect Biol. 2014; 6: a016725. doi: 10.1101/cshperspect.a016725 PMID: 24789820
5. Soares MJ, De Souza W. Endocytosis of gold-labeled proteins and LDL by *Trypanosoma cruzi*. Parasitol Res. 1991; 77: 461–468. PMID: 1656428
6. Figueiredo RC, Soares MJ. Low temperature blocks fluid-phase pinocytosis and receptor-mediated endocytosis in *Trypanosoma cruzi* epimastigotes. Parasitol Res. 2000; 86: 413–418. PMID: 10836515
7. Kalb LC, Frederico YCA, Batista CM, Eger I, Fragoso SP, Soares MJ. Clathrin expression in *Trypanosoma cruzi*. BMC Cell Biol. 2014; 15: 23. doi: 10.1186/1471-2121-15-23 PMID: 24947310
8. De Souza W, Sant'Anna C, Cunha-e-Silva NL. Electron microscopy and cytochemistry analysis of the endocytic pathway of pathogenic protozoa. Prog Histochem Cytochem. 2009; 44: 67–124. doi: 10.1016/j.proghi.2009.01.001 PMID: 19410686
9. Alcantara CL, Vidal JC, de Souza W, Cunha-e-Silva NL. The three-dimensional structure of the cytostome-cytopharynx of *Trypanosoma cruzi* epimastigotes. J Cell Sci. 2014; 127: 2227–2237. doi: 10.1242/jcs.135491 PMID: 24610945
10. Porto-Carreiro I, Attias M, Miranda K, De Souza W, Cunha-e-Silva NL. *Trypanosoma cruzi* epimastigote endocytic pathway: cargo enters the cytostome and passes through an early endosomal network before storage in reservosomes. Eur J Cell. 2000; Biol 79: 858–69. PMID: 11139150
11. Soares MJ, Souto-Padrón T, De Souza W. Identification of a large pre-lysosomal compartment in the pathogenic protozoon *Trypanosoma cruzi*. J Cell Sci. 1992; 2: 157–167.
12. Cazzulo JJ, Cazzulo Franke MC, Martinez J, Franke de Cazzulo BM. Some kinetic properties of a cysteine proteinase (cruzipain) from *Trypanosoma cruzi*. Biochem Biophys Acta. 1990; 1037: 186–191. PMID: 2407295
13. Sant'Anna C, Parussini F, Lourenço D, De Souza W, Cazzulo JJ, Cunha-e-Silva NL. All *Trypanosoma cruzi* developmental forms present lysosome-related organelles. Histochem Cell Biol. 2008; 130: 1187–1198. doi: 10.1007/s00418-008-0486-8 PMID: 18696100
14. Bothwell H, Charlton RW, Cook JD, Finch CH. Iron metabolism in man. Oxford: Blackwell; 1979.
15. Taylor MC, Kelly JM. Iron metabolism in trypanosomatids, and its crucial role in infection. Parasitol. 2010; 6: 899–917.
16. Corrêa JR, Atella GC, Batista MM, Soares MJ. Transferrin uptake in *Trypanosoma cruzi* is impaired by interference on cytostome-associated cytoskeleton elements and stability of membrane cholesterol, but not by obstruction of clathrin-dependent endocytosis. Exp Parasitol. 2008; 119: 58–66. doi: 10.1016/j.exppara.2007.12.010 PMID: 18234197
17. Milder R, Deane MP. The cytostome of *Trypanosoma cruzi* and *T. conorhini*. J Protozool. 1969; 16: 730–737. PMID: 5362390
18. Sant'Anna C, Pereira MG, Lemgruber L, De Souza W, Cunha-e-Silva NL. New insights into the morphology of *Trypanosoma cruzi* reservosome. Microsc Res Tech. 2008; 71: 599–605. doi: 10.1002/jemt.20592 PMID: 18452191
19. Meyer H, De Souza W. On the fine structure of *Trypanosoma cruzi* in tissue culture of pigment epithelium from the chick embryo. Uptake of melanin granules by the parasite. J Protozool. 1973; 20: 590–593. PMID: 4128532
20. Lima MF, Villalta F. *Trypanosoma cruzi* receptors for human transferrin and their role. Mol Biochem Parasitol. 1990; 38: 245–252. PMID: 2183049
21. Loo VG, Lalonde RG. Role of iron in intracellular growth of *Trypanosoma cruzi*. Infect Immun. 1984; 45: 726–730. PMID: 6381312
22. Lalonde RG, Holbein BE. Role of iron in *Trypanosoma cruzi* infection in mice. J Clin Invest. 1984; 73: 470–476. PMID: 6421677
23. Waghabi MC, Keramidas M, Bailly S, Degrave W, Mendonça-Lima L, Soeiro MN, et al. Uptake of host cell transforming growth factor-β by *Trypanosoma cruzi* amastigotes in cardiomyocytes: potential role in parasite cycle completion. Am J Pathol. 2005; 167: 993–1003. PMID: 16192635

24. Mayle KM, Le AM, Kamei D. The intracellular trafficking pathway of transferrin. Biochim Biophis Acta. 2012; 1820: 264–281. doi: 10.1016/j.bbagen.2011.09.009 PMID: 21968002

25. Abrahamsohn IA, Katzin AM, Milder RV. A method for isolating *Trypanosoma cruzi* amastigotes from spleen and liver using two-step discontinuous gradient centrifugation. J Parasitol. 1983; 69: 437–439. PMID: 6343578

26. Villalta F, Kierszenbaum F. Growth of isolated amastigotes of *Trypanosoma cruzi* in cell-free medium. J Protozool. 1982; 29: 570–576. PMID: 6816925

27. de Carvalho TU, De Souza W. Separation of amastigotes and trypomastigotes of *Trypanosoma cruzi* from cultured cells. Z Parasitenkd. 1983; 69: 571–575. PMID: 6356671

28. Marques AF, Nakayasu ES, Almeida IC. Purification of extracellular and intracellular amastigotes of *Trypanosoma cruzi* from mammalian host-infected cells. Protocol Exchange. 2011; doi: 10.1038/protex.2011.265

29. de Sousa MA. A simple method to purify biologically and antigenically preserved bloodstream trypomastigotes of *Trypanosoma cruzi* using DEAE-cellulose columns. Mem Inst Oswaldo Cruz. 1983; 78: 317–333. PMID: 6361445

30. Contreras VT, Araque W, Delgado VS. *Trypanosoma cruzi*: metacyclogenesis *in vitro*—I. Changes in the properties of metacyclic trypomastigotes maintained in the laboratory by different methods. Mem Inst Oswaldo Cruz. 1994; 89: 253–259. PMID: 7885254

31. Contreras VT, Araújo-Jorge TC, Bonaldo MC, Thomaz N, Barbosa HS, Goldenberg S. Biological aspects of the DM28c clone of *Trypanosoma cruzi* after metacyclogenesis in chemically defined media. Mem Inst Oswaldo Cruz. 1988; 83: 123–133. PMID: 3074237

32. Camargo EP. Growth and differentiation in *Trypanosoma cruzi*. I. Origin of metacyclic trypanosomes in liquid media. Rev Inst Med Trop São Paulo. 1964; 6: 93–100.

33. Contreras VT, Salles JM, Thomas N, Morel CM, Goldenberg S. *In vitro* differentiation of *Trypanosoma cruzi* under chemically defined conditions. Mol Biochem Parasitol. 1985; 16: 315–327. PMID: 3903496

34. Hernández-Osorio LA, Marquez-Duñas C, Florencio-Martínez LE, Ballesteros-Rodea G, Martínez-Calvillo S, Manning-Cela RG. Improved method for *in vitro* secondary amastigogenesis of *Trypanosoma cruzi*: morphometrical and molecular analysis of intermediate developmental forms. J Biomed Biotech. 2010: Article ID 283842, 10 pages.

35. Sambrook J, Fritsch EF, Maniatis T. Detection and analysis of proteins expressed from cloned genes. In Molecular cloning: A laboratory manual. Vol. 3, 2nd edition. Woodbury: Cold Spring Harbor Laboratory Press; 1989. pp. 60–74.

36. Gradia DF, Rau K, Umaki AC, de Souza FS, Probst CM, Correa A, et al. Characterization of a novel Obg-like ATPase in the protozoan *Trypanosoma cruzi*. Int J Parasitol. 2009; 39: 49–58. doi: 10.1016/j.ijpara.2008.05.019 PMID: 18713637

37. Kessler RL, Soares MJ, Probst CM, Krieger MA. *Trypanosoma cruzi* response to sterol biosynthesis inhibitors: morphophysiological alterations leading to cell death. PLOS ONE. 2013; 8(1): e55497. doi: 10.1371/journal.pone.0055497 PMID: 23383204

38. Andrews NW, Hong KS, Robbins ES, Nussenzweig V. Stage-specific surface antigens expressed during the morphogenesis of vertebrate forms of *Trypanosoma cruzi*. Exp Parasitol. 1987; 64: 474–484. PMID: 3315736

39. Batista CM, Medeiros LC, Eger I, Soares MJ. mAb CZP-315.D9: an anti-recombinant cruzipain monoclonal antibody that specifically labels the reservosomes of *Trypanosoma cruzi* epimastigotes. Biomed Res Int. 2014; Article ID 714749, 9 pages.

40. Urbina JA. Specific chemotherapy of Chagas disease: relevance, current limitations and new approaches. Acta Tropica. 2010; 115: 55–68. doi: 10.1016/j.actatropica.2009.10.023 PMID: 19900395

41. Simpson RJ. Disruption of cultured cells by nitrogen cavitation. Cold Spring Harb Protoc. 2010; doi: 10.1101/pdb.prot5513

42. De Souza W. Electron microscopy of trypanosome- A historical view. Mem Inst Oswaldo Cruz. 2008; 103: 313–325. PMID: 18660983

43. Kessler RL, Gradia DF, Pontello Rampazzo R de C, Lourenço ÊE, Fidêncio NJ, Manhaes L, et al. Stage-regulated GFP Expression in *Trypanosoma cruzi*: applications from host-parasite interactions to drug screening. PLOS ONE. 2013; 8: e67441. doi: 10.1371/journal.pone.0067441 PMID: 23840703

44. Ramos TC, Freymüller-Haapalainen E, Schenkman S. Three-dimensional reconstruction of *Trypanosoma cruzi* epimastigotes and organelle distribution along the cell division cycle. Cytometry A. 2011; 79: 538–544. doi: 10.1002/cyto.a.21077 PMID: 21567937

5.4. Conclusão Capítulo 2

- Foi padronizado o isolamento de amastigotas intracelulares de *T. cruzi* por cavitação.
- Amastigotas isolados foram positivos para o marcador específico de amastigotas Ssp4.
- A atividade endocítica foi comprovada em amastigotas intracelulares isolados por cavitação, com co-localização de cruzipaína, transferrina e albumina nos reservossomos.

VI. Capítulo 3

Tratamento de *Trypanosoma cruzi* com 2-bromopalmitato altera morfologia, endocitose, diferenciação e infectividade

Após a padronização do isolamento de amastigotas intracelulares, a próxima parte da tese teve como objetivo analisar os efeitos do inibidor de S-palmitoilação 2-bromopalmitato (2-BP) sobre *T. cruzi*. Como resultados: 1) o valor de CI_{50} de 2-bromopalmitato foi estimado em 130 µM em formas epimastigotas (48h), 216 nM em tripomastigotas metacíclicos (24h), 242 µM em amastigotas intracelulares isolados por cavitação (24h) e 262 µM em tripomastigotas de cultura (4h); 2) a incubação de epimastigotas com 2-BP na concentração estimada pelo CI_{50} por 48h alterou (a) a localização de TcFCaBP, uma proteína de flagelo sabidamente palmitoilada; (b) a morfologia: presença de grandes vacúolos translúcidos na região posterior e alterações na ultraestrutura do complexo de Golgi; 3) a endocitose de transferrina e albumina foi inibida em aproximadamente 90%; 4) a metaciclogênese foi inibida em até 90%; 5) a infectividade foi reduzida em até 75% dos tripomastigotas metacíclicos obtidos do experimento de diferenciação e 45,5% para tripomastigotas de cultura tratados. Estes dados estão compilados em um manuscrito submetido à revista BMC Cell Biology (Fator de 2,405 (Qualis CB-I: B1).

6.1. Objetivo

Analisar os efeitos do inibidor de S-palmitoilação 2-bromopalmitato (2-BP) sobre *T. cruzi*.

6.2. Objetivos específicos

1. Determinar o valor de CI_{50} (concentração que inibe 50% da proliferação) de 2-BP em *T. cruzi*;

2. Avaliar alterações na morfologia, endocitose, na proliferação, na diferenciação e na infectividade de *T. cruzi* após o tratamento com 2-BP*;*

3. Verificar alterações na localização de proteínas palmitoiladas após tratamento com 2-BP.

6.3. Artigo Submetido

Autores: Cassiano Martin Batista, Rafael Luis Kessler, Iriane Eger, Maurilio José Soares

Título: Treatment of *Trypanosoma cruzi* with 2-bromopalmitate alters morphology, endocytosis, differentiation and infectivity

Revista: BMC Cell Biology

Fator de impacto (2016): 2,405 (Qualis CB-I: B1)

De: "BMC Cell Biology Editorial Office" <em@editorialmanager.com>

Data: 12/01/2018 10:34

Assunto: Confirmation of your submission to BMC Cell Biology - CEBI-D-18-00003

Para: "Maurilio José Soares" <mauriliojsoares@gmail.com>

CEBI-D-18-00003

Treatment of Trypanosoma cruzi with 2-bromopalmitate alters morphology, endocytosis, differentiation and infectivity

Cassiano Martin Batista; Rafael Luis Kessler; Iriane Eger; Maurilio José Soares, Ph.D.

BMC Cell Biology

Dear Dr Soares,

Thank you for submitting your manuscript 'Treatment of Trypanosoma cruzi with 2-bromopalmitate alters morphology, endocytosis, differentiation and infectivity' to BMC Cell Biology.

The submission id is: CEBI-D-18-00003. Please refer to this number in any future correspondence.

During the review process, you can keep track of the status of your manuscript by accessing the following website: https://cebi.editorialmanager.com/

If you have forgotten your password, please use the 'Send Login Details' link on the login page at https://cebi.editorialmanager.com/. For security reasons, your password will be reset.

Best wishes,

Editorial Office

BMC Cell Biology

https://bmccellbiol.biomedcentral.com/

Treatment of *Trypanosoma cruzi* with 2-bromopalmitate alters morphology, endocytosis, differentiation and infectivity

Short title: Effect of 2-BP on *Trypanosoma cruzi*

Cassiano Martin Batista[1], Rafael Luis Kessler[2,3], Iriane Eger[4], Maurilio José Soares[1*]

[1]Laboratory of Cell Biology, Carlos Chagas Institute/Fiocruz-PR, 81310-020 Curitiba, Paraná, Brazil

[2]Laboratory of Functional Genomics, Carlos Chagas Institute/Fiocruz-PR, 81310-020 Curitiba, Paraná, Brazil

[3]Mammalian Cell Biotechnology Laboratory, Molecular Biology Institute of Paraná (IBMP), 81310-020 Curitiba, Paraná, Brazil

[4]Department of General Biology, State University of Ponta Grossa, 84010-290 Ponta Grossa, Paraná, Brazil

Cassiano Martin Batista: cassianombatista@gmail.com

Rafael Luis Kessler: kessler@ibmp.org.br

Iriane Eger: iriane.eger@gmail.com

Maurilio José Soares: maurilio@fiocruz.br

[*]Corresponding Author

Abstract

Background. Palmitoylation is a post-translational protein modification that adds palmitic acid to a cysteine residue through a thioester linkage, promoting membrane localization, protein stability, regulation of enzymatic activity, and the epigenetic regulation of gene expression. Little is known on such important process in the pathogenic protozoan *Trypanosoma cruzi*, the etiological agent of Chagas disease.

Results. The effect of 2-bromopalmitate (2-BP, a palmitoylation inhibitor) was analyzed on different developmental forms of *Trypanosoma cruzi*. The IC_{50}/48h value for culture epimastigotes was estimated as 130 µM. The IC_{50}/24h value for metacyclic trypomastigotes was 216 nM, while for intracellular amastigotes it was 242 µM. Our data showed that 2-BP alters *T. cruzi*: 1) morphology, as assessed by bright field, scanning and transmission electron microscopy; 2) mitochondrial membrane potential, as shown by flow cytometry after incubation with rhodamine-123; 3) endocytosis, as seen after incubation with transferrin or albumin and analysis by flow cytometry/fluorescence microscopy; 4) *in vitro* metacyclogenesis; and 5) infectivity, as shown by host cell infection assays.

Conclusion. Our results indicate that 2-BP inhibits key cellular processes of *T. cruzi* that may be regulated by palmitoylation of vital proteins.

Key words: 2-Bromopalmitate, 2-BP inhibition, differentiation, endocytosis, palmitoylation, *Trypanosoma cruzi*

Background

Palmitoylation is a post-translational protein modification that consists in addition of palmitic acid to a cysteine residue through a thioester linkage. This modification promotes membrane localization, regulation of enzymatic activity, regulation of gene expression and protein stability [1-3]. Palmitoylation is a reversible, dynamic modification regulated by enzymes that either transfer palmitic acid to a target protein (palmitoyl acyltransferases: PATs) or cleave the thioester linkages between palmitic acid and the modified proteins (palmitoyl protein thioesterases: PPTs) [4]. Palmitoylation represents an important modification in cells of a variety of organisms, such as mammals [5-7], yeasts [8,9], fishes [10], plants [11,12] and nematodes [13]. This modification is well characterized in humans, as it is strongly involved in Huntington's disease and other neuropsychiatric diseases [14,15] and cancer [16]. Palmitoylation was also recorded in pathogenic protozoa, including *Toxoplasma gondii* [17], *Plasmodium falciparum* [18] and *Trypanosoma brucei* [19].

2-bromopalmitate (2-BP), a palmitate analogue, is a well-known inhibitor of palmitoylation [20]. There are two proposed mechanisms for the 2-BP action: direct inhibition of PATs or blockage of palmitic acid incorporation by direct covalent competition with palmitate [21]. It has been suggested that 2-BP also inhibits PPTs, disturbing the acylation cycle of the protein GAP-43 at the depalmitoylation level and consequently affecting its kinetics of membrane association [22]. Incubation of the apicomplexan *T. gondii* with 50 µM 2-BP efficiently altered parasite morphology, gliding and host cell invasion [23]. In the African trypanosome *T. brucei*, the calculated IC_{50} values were 197 µM for the procyclic form and 226 µM for the bloodstream life form [19]. However, no 2-BP or global palmitoylation studies have been reported yet for *Trypanosoma cruzi*, a protozoan parasite that causes Chagas disease in Latin America.

Two *T. cruzi* proteins are known to be palmitoylated: TcFCaBP [24], which is involved in parasite motility, and TcPI-PLC [25], which is involved in evading the host immune system. Only one putative PAT has been identified in this protozoan (TcHIP/TcPAT1), localized in the Golgi complex of different life stages [26]. However, other still unidentified proteins should be also palmitoylated in *T. cruzi*, and palmitoylation is probably involved in diverse biological functions. A recent review on protein acylation in trypanosomatids with a focus on myristoylation and palmitoylation suggested that protein acylation represents an interesting target for the development of new trypanocidal drugs [27]. Indeed, *T. cruzi* N-myristoyltransferase (TcNMT), an enzyme that catalyzes the attachment of myristic acid to an N-terminal glycine residue of proteins, has been validated as a potential chemotherapeutic target in *T. cruzi* mammal stages [28].

The aim of this study was to assess the *in vitro* effect of 2-BP on *T. cruzi*. The data presented here show that this inhibitor alters the parasite morphology, endocytosis, differentiation and infectivity and suggest the importance of palmitoylation for parasite survival and its involvement in crucial biological processes.

Methods

Reagents

Trypan Blue, Dulbecco's Modified Eagle Medium (DMEM), penicillin (10,000 units), streptomycin (10 mg/mL), trypsin from porcine pancreas, 2-bromopalmitate (2-BP), dimethyl sulfoxide (DMSO), potassium chloride, propidium iodide, RNase A, carbonyl cyanide 3-chlorophenylhydrazone (CCCP), acridine orange, Giemsa stain, formaldehyde, paraformaldehyde, glutaraldehyde, Hoechst staining solution and poly-L-lysine were purchased from Sigma-Aldrich (St. Louis, MO, USA). Transferrin-

AlexaFluor 633, Albumin-AlexaFluor 488, rhodamine-123, goat anti-mouse IgG AlexaFluor 488 conjugate, goat anti-mouse IgG AlexaFluor 594 conjugate and Prolong Gold were purchased from Molecular Probes/Life Technologies (Eugene, OR, USA). Potassium ferrocyanide, Permount, sodium cacodylate, osmium tetroxide and PolyBed-812 resin were purchased from Electron Microscopy Sciences (Hatfield, PA, USA). Sodium dodecyl sulfate (SDS) was purchased from Ludwig Biotecnologia (Alvorada, RS, Brazil). Fetal bovine serum (FBS) was purchased from Gibco/Invitrogen/Life Technologies (Eugene, OR, USA). Nonidet 40 (NP-40) was purchased from Anresco Laboratories (San Francisco, CA, USA).

Vero cells

Vero cells (ATCC CCL-81) were maintained at 37°C in 75-cm^2 cell culture flasks (Corning Incorporated, Corning, NY, USA) in DMEM medium supplemented with 10% FBS in a humidified 5% CO_2 atmosphere. For weekly seeding, the cell monolayers were washed twice with PBS, trypsinized and the detached cells were collected by centrifugation for 5 minutes at 800 ×*g*. The cells were then inoculated at 10^6 cells/flask in fresh DMEM medium and kept as described above.

Trypanosoma cruzi

Culture epimastigote forms of *T. cruzi* clone Dm28c [29] were maintained at 28°C by weekly passages in Liver Infusion Tryptose (LIT) medium [30] supplemented with 10% heat-inactivated fetal bovine serum (FBS).

In vitro-derived metacyclic trypomastigotes were obtained by incubating epimastigotes in Triatomine Artificial Urine (TAU/TAU3AAG) medium, according to a previously described metacyclogenesis (i.e., epimastigote-to-trypomastigote

differentiation) protocol [31], with a yield of approximately 50%. Metacyclic trypomastigotes were purified with a DEAE-cellulose column as previously described [31].

Cell-derived trypomastigotes were obtained from Vero cell cultures infected with *in vitro*-derived metacyclic trypomastigotes, at a ratio of 100 parasites/cell. After 4 h of interaction the host cell monolayers were washed with PBS to remove the non-adherent parasites. Infected cells were then incubated for six days in 10 mL of DMEM medium supplemented with 10% FBS, when trypomastigote production peaked. The culture supernatant was collected, and the cell-derived trypomastigotes released into the supernatant were harvested by centrifugation for 15 min at 3,000*g*. The parasites were then used for the experiments and to maintain the infection cycle.

Determination of IC_{50} value for 2-BP

A 100 mM 2-BP stock solution was prepared in DMSO. The solution was filtered through a 0.22-µm Millipore filter (Merck Millipore Co, Tullagreen, CO, Ireland) and stored at 4°C. After dilution in culture medium, the DMSO concentration in the experiments never exceeded 1%, and it did not affect parasite growth.

To calculate the concentration of 2-BP that inhibited 50% growth of the epimastigote cultures (IC_{50}/48h), the parasites (10^6/mL) were incubated at 28°C with different concentrations of 2-BP (25 to 400 µM) in biological triplicates. Cell counts were made after 48 h with a Neubauer chamber. The population density was calculated and the death percentage was estimated relative to the untreated control (LIT medium with 1% DMSO), generating dose-effect curves. The CompuSyn software [33] was then used to calculate the IC_{50}/48h value by using the death percentage for each 2-BP concentration.

For morphological analysis, the parasites were processed for bright field, scanning and transmission electron microscopy as described below.

To calculate the IC_{50}/24h for metacyclic and cell-derived trypomastigotes, the parasites (10^6 cells/mL) were incubated with different concentrations of 2-BP (0.1 to 175 µM for metacyclic trypomastigotes; 0.1 to 400 µM for cell-derived trypomastigotes) in biological triplicates. After 24 h at 28°C (or 4 h at 37°C for culture trypomastigotes, to avoid differentiation into extracellular amastigote-like forms) the parasite number was counted in a Neubauer chamber and the death percentage was calculated relative to the untreated control (culture medium with 1% DMSO). The CompuSyn software was used to calculate the IC_{50} value.

To calculate the IC_{50} value for intracellular amastigotes, 24-hour-old infected Vero cell cultures (10^6 cells/mL) were incubated with 2-BP (0.4 to 125 µM) in biological triplicates in a humidified 5% CO_2 atmosphere. After 24 and 48 h of treatment, the infected host cells were lysed by nitrogen decompression [34] and the number of released amastigotes was counted in a Neubauer chamber. Population density was then compared to the untreated control (medium with 0.125% DMSO). The CompuSyn software was used to calculate the IC_{50} value. The number of released trypomastigotes was then evaluated after 72 h of treatment (96 h of infection).

The IC_{50}/24h for intracellular amastigotes was calculated with purified amastigotes obtained from 48-hour-old infected cells cultures, by lysing the host cells with nitrogen decompression [34]. After three steps of centrifugation at low speed to remove the Vero cells, the purified intracellular amastigotes were incubated at 37°C with DMEM medium in 6-well plates (approximately 10^7 parasites/well) in a humidified 5% CO_2 atmosphere. This cell suspension was centrifuged after 30 min to remove remaining intact Vero cells and new DMEM medium (containing additional 1000 units penicillin

and 100 µg/mL streptomycin) was added. The purified isolated intracellular amastigotes were then incubated for 24 h with 2-BP (0.4 to 500 µM) in biological triplicates. The CompuSyn software was used to calculate the IC_{50} value.

Cytotoxicity to Vero cells

To calculate the cytotoxicity for Vero cells (CC_{50}/24h), 10^5 cells/mL were cultivated in 6-well plates in biological triplicates. After 24 h, the cultures were washed twice with PBS and incubated at 37°C with different concentrations of 2-BP (75 to 300 µM) in a humidified 5% CO_2 atmosphere. After 24 h of treatment, cell cultures were washed twice with PBS, trypsinized, washed in DMEM medium, stained with Trypan blue (0.02% final concentration) for cell viability analysis and counted in Neubauer chamber. The percentage of dead cells was estimated relative to the untreated control (culture medium with 0.3% DMSO). The CompuSyn software was used to calculate the CC_{50}/24h value.

Flow cytometry of *T. cruzi* epimastigotes treated with IC_{50}/48h 2-BP

Flow cytometry experiments were performed with a FACS Aria-II (Becton-Dickinson, San Jose, CA, USA). A total of 20,000 events were acquired in the region previously identified as corresponding to *T. cruzi* epimastigotes [35]. The data were analyzed using the FlowJo software package (FlowJo, Ashland, OR, USA).

For cell cycle assays, parasite DNA was stained with propidium iodide (PI). The 2-BP treated epimastigotes ($2x10^6$ cells) were washed twice in PBS, incubated with cell cycle buffer (3.4 mM Tris-HCl, 30 µg/mL PI, 0.1% NP-40, 10 mM sodium chloride,

700U/L RNAse, pH 7.6) and immediately analyzed using a 610/20 nm bandpass filter. Cell debris and doublets were excluded using a width × area gate. The Dean-Jett-Fox algorithm of FlowJo was used to estimate the percentage of cells in the G1, S and G2/M phases of the cell cycle.

For mitochondrial membrane potential analysis, 2-BP treated epimastigotes ($2x10^6$ cells) were washed twice in PBS and then incubated for 15 min at room temperature with 10 µg/mL rhodamine-123. After two washes with PBS, the parasites were analyzed using a 530/30 nm bandpass filter. CCCP at 100 µM for 5 min was used as a positive control of the mitochondrial membrane potential destabilization [36]. The relative mitochondrial membrane potential was determined by considering normalized median ratios (treated/control) of the fluorescence level. The normalized fluorescence medians were used for statistical analysis.

For cell viability assay, 2-BP treated epimastigotes were washed twice in PBS, incubated for 5 min at room temperature with PI (5 µg/mL) and then analyzed without washing. Positively stained cells (610/20 nm bandpass filter) were considered dead.

For acid compartment analysis, the 2-BP treated epimastigotes ($2x10^6$ cells) were washed twice in PBS, incubated for 15 min at room temperature with 5 µg/mL acridine orange, washed twice with PBS and then analyzed using a 695/20 nm bandpass filter. The normalized fluorescence medians were analyzed as described above [35]. In parallel, parasites were adhered to glass slides and visualized with epifluorescence microscopy using a B-2A (long pass emission) filter (Nikon, Chiyoda, Japan).

Endocytosis assays

Epimastigotes were incubated for 4 h with IC_{50}/48h 2-BP, washed twice in PBS and subjected to a previously described endocytosis assay [34,37] using $2x10^6$ parasites

for flow cytometry analysis or $5x10^6$ cells for fluorescence microscopy studies. After 15 min under stress in PBS at 25°C, the parasites were incubated for 30 min at 28°C with 50 µg/ml transferrin-AlexaFluor 633 or albumin-AlexaFluor 488. Negative control cells were incubated in the absence of labeled transferrin or albumin. For flow cytometry, living epimastigotes were analyzed using 660/20 and 530/30 nm bandpass filters for transferrin-AlexaFluor 633 or albumin-AlexaFluor 488 acquisition, respectively. The normalized median fluorescence intensity of transferrin and albumin was calculated as the ratio between the median fluorescence intensity of the treated and untreated cells. Data acquisition and analysis was performed as described above [34].

2-BP treatment during *in vitro* metacyclogenesis

Mid log-phase epimastigotes were collected and submitted to various treatments with 130 µM 2-BP during metacyclogenesis: (a) Control: five days in LIT/0.13% DMSO and then incubation for 2 h in TAU and 72 h in TAU3AAG media without 2-BP; (b) Pre-stress: five days in LIT medium with IC_{50}/48h 2-BP followed by incubation for 2h in TAU without 2-BP; (c) Stress: five days in LIT medium and then 2 h in TAU medium containing with IC_{50}/48h 2-BP; and (d) Post-stress: five days in LIT medium, stress for 2 h in TAU medium and incubation for 15 min in TAU3AAG with IC_{50}/48h 2-BP.

After 2-BP treatments the cells were washed twice with PBS to remove 2-BP and incubated for 72 h in TAU3AAG medium. The parasites in the supernatants were then collected and counted in Neubauer chamber to obtain the ratio of metacyclic trypomastigotes / epimastigotes per mL. For morphological analysis, the parasites were processed for light microscopy.

Infection assays

Metacyclic trypomastigotes obtained from 2-BP treatments during metacyclogenesis (see above) were used to infect Vero cells. Briefly, 10^7 metacyclic trypomastigotes were incubated with 10^6 Vero cells and after 24 h noninvasive trypomastigotes were removed by PBS whashes. After 6 days, the infected cultures were washed with PBS and the released trypomastigotes were collected from the PBS by centrifugation. The trypomastigotes were then counted and processed for light and fluorescence microscopy analysis.

In other experiment, cell-derived trypomastigotes that were previously treated with IC_{50} 2-BP were used to infect Vero cells. Briefly, the parasites ($2x10^7$ cells/mL) were pre-incubated for 4 h with IC_{50} 2-BP (262 µM), washed twice with PBS, counted in Neubauer chamber and then incubated for 2 h with 10^6 adhered Vero cells. Non-adherent parasites were then washed out with PBS. Four days after infection the released trypomastigotes were collected, counted in Neubauer chamber and processed for light and fluorescence microscopy. Vero cell cultures infected with untreated trypomastigotes were used as a control.

Light microscopy

The parasites were adhered for 10 min to 0.1% poly-L-lysine coated slides, fixed for 2 min at room temperature with methanol, air dried and then incubated for 30 min at room temperature with Giemsa stain. The samples were then washed with MilliQ water and mounted with Permount. After 24 h the slides were observed with a Nikon E600 microscope (100x objective) in bright field mode for image acquisition.

Fluorescence microscopy

To detect the native TcFCaBP, epimastigotes and metacyclic trypomastigotes were incubated with the respective IC_{50} value of 2-BP, washed twice in PBS, fixed for 20 min with 4% formaldehyde and incubated for 1 h at room temperature with incubation buffer (1.5% BSA/PBS). This step was followed by incubation for 1 h at 37°C with a primary mAb 25 monoclonal antibody against TcFCaBP [38], which was diluted to 1:1000 in incubation buffer. The samples were then washed three times in PBS and incubated for 1 h at 37°C with a secondary goat anti-mouse antibody coupled to AlexaFluor-488 or AlexaFluor-594 (1:600) in incubation buffer.

To co-localize transferrin-AlexaFluor-633 or albumin-AlexaFluor-488 with cruzipain (CZP), the epimastigotes subjected to the endocytosis assays were fixed for 30 min in 4% paraformaldehyde and permeabilized for 5 min with 0.5% Triton in PBS. For co-localization of CZP/transferrin-AlexaFluor-633, the samples incubated with CZP-315.D9 mAb (at 50 µg/ml)[39], were washed three times in PBS and then incubated with a secondary goat anti-mouse-AlexaFluor-488 antibody (1:600 in incubation buffer). For the co-localization with CZP/albumin-AlexaFluor-488, the samples were incubated with CZP-315.D9 mAb and then incubated with a secondary goat anti-mouse-AlexaFluor-594 antibody.

After antibody incubations, all samples were washed three times in PBS, incubated for 5 min with 1.3 nM Hoechst 33342, washed twice in PBS and twice in MilliQ Water, mounted with Prolong Gold anti-fading reagent and then examined under a Nikon Eclipse E600 epifluorescence microscope.

Scanning electron microscopy

Parasites were washed twice in PBS and fixed for 1 h at room temperature in 2.5% glutaraldehyde in 0.1 M phosphate buffer, pH 7.2. The fixed parasites were washed

twice in 0.1 M cacodylate buffer and then adhered for 15 min at room temperature to 0.1% poly-L-lysine coated coverslips. The non-adhered cells were washed out twice with 0.1 M cacodylate buffer and the adhered cells were then incubated for 15 min at room temperature with 1% osmium tetroxide diluted in 0.1 M cacodylate buffer. The samples were washed three times with 0.1 M cacodylate buffer and dehydrated in a graded acetone series (30%, 50%, 70%, 90% and 100% acetone, 5 min each). This step was followed by critical point drying in a Leica EM CPD300 and gold sputtering in a Leica EM ACE200. The samples were visualized in a JEOL JSM-6010 PLUS/LA scanning electron microscope at 20 kV.

Transmission electron microscopy

Parasites were washed twice in PBS and fixed for 1 h in 2.5% glutaraldehyde in 0.1 M phosphate buffer at room temperature. The fixed parasites were washed twice in 0.1 M cacodylate buffer and then post-fixed with 1% osmium tetroxide / 1.6% potassium ferrocyanide / 5 mM $CaCl_2$ diluted in 0.1 M cacodylate buffer for 30 min at room temperature. The samples were washed three times with 0.1 M cacodylate buffer, dehydrated in a graded acetone series (5 min in 30, 50, 70, 90 and 100%) and then embedded in PolyBed812 resin. Ultrathin sections were obtained in a Leica EM UC6 ultramicrotome, collected on copper grids, contrasted with uranyl acetate and lead citrate and then visualized in a JEOL 1400Plus transmission electron microscope at 90 kV.

Statistical Analysis

All experiments were performed in independent biological triplicates. Statistical analysis was performed using the software GraphPad Instat (GraphPad Software Inc, La Jolla, CA, USA) for ANOVA followed by a Bonferroni’s multiple comparisons test.

Results

Effect of 2-BP on different *T. cruzi* developmental forms

The IC_{50}/48 h value of 2-BP for culture epimastigotes was estimated as 130 µM (Fig 1A). The estimated IC_{50} value (IC_{50}/24h) of 2-BP for metacyclic trypomastigotes was 216 nM (Fig 1B), while for cell-derived trypomastigotes it was 262 µM (Fig. 1C).

The cytotoxic effect (CC_{50}/24h) of 2-BP on Vero cells was calculated before the assays with intracellular amastigotes, and its estimated value was 138 µM. Concentrations higher than 200 µM killed 100% of the host cells. No effect on number and morphology of intracellular amastigotes was observed after 24 or 48 h of treatment of infected Vero cells with up to 125 µM 2-BP (data not shown). However, 125 µM 2-BP enhanced the intracellular differentiation into trypomastigote forms. Isolation of intracellular forms by nitrogen decompression after 24 h of treatment showed several trypomastigote-like stages, characterized by the presence of a bar kinetoplast close to the nucleus (Additional file 1: Figure S1). There was an increase of approximately 40% in the number of released trypomastigotes after four days of infection (72 h of treatment) when compared to untreated cultures.

Finally, intracellular amastigotes were isolated from the host cells by nitrogen decompression and were then incubated with different concentrations of 2-BP. In this case, the estimated IC_{50}/24h value was 242 µM (Fig. 1D). This high concentration could

explain why we failed to calculate the IC_{50} value for intracellular amastigotes (no effect up to 125 µM).

Mislocalization of TcFCaBP after incubation with 2-BP

Epimastigotes and metacyclic trypomastigotes were treated respectively for 48 or 24 h with their 2-BP IC_{50} values and then incubated with a monoclonal antibody against TcFCaBP, a flagellar calcium-binding protein known to be palmitoylated [24, 37]. While untreated epimastigotes (Fig. 2A) and metacyclic trypomastigotes (Fig. 2C), showed prominent flagellar labeling, the 2-BP-treated cells lost their flagellar labeling and showed a disperse reaction throughout the cell body (Figs. 2B and 2D).

Morphology, viability and physiology of *T. cruzi* epimastigotes were altered by treatment with IC_{50}/48h 2-BP

2-BP treated epimastigotes had translucent vacuoles at the posterior region and were occasionally linked by the flagella (insets in Figs. 3A and 3B). Scanning electron microscopy showed a leakage of intracellular material at the flagellar pocket region (Figs 3A and 3B). Transmission electron microscopy showed large electron lucent vacuoles at the posterior cell region and Golgi alterations (Figs. 3C and 3D).

To certify that the large vacuoles observed by light and transmission electron microscopy were reservosomes (acidic pre-lysosomal organelles found at the posterior end of *T. cruzi* epimastigotes), 2-BP-treated epimastigotes were incubated with acridine orange. Analysis by flow cytometry showed a 2-fold increase in the median red fluorescence intensity peak (Additional file 2: Figure S2, left panel). Using fluorescence microscopy, a strong red labeling was found in structures at the posterior region of the

treated cells (Additional file 2: Figure S2, right panel), thus indicating that these large vacuoles corresponded to reservosomes.

The size (FSC) and granularity (SSC) of 2-BP-treated epimastigotes were analyzed by flow cytometry, and they showed statistically significant increases of approximately 13% and 11% ($p \leq 0.0012$ and $p \leq 0.007$), respectively, compared to the control (Figs 4A and 4B). There was no significant difference in the distribution of cells in the different cell division cycle stages (G1, S and G2-M) between the treated and the control parasites (Fig. 4C).

In mitochondrial viability assays with rhodamine-123, the normalized median of the fluorescence peaks in the stained cells decreased 47% ($p \leq 0.001$) in the 2-BP-treated epimastigotes (Fig. 4D), showing that the mitochondrial potential was altered by the palmitoylation inhibition although only 1.5% of the population was dead after 48 h of incubation with 2-BP (Fig. 4E), thus indicating that most parasites were viable.

Endocytosis in *T. cruzi* epimastigotes is hindered by 2-BP

Epimastigotes were treated for 4 h with 130 µM 2-BP, washed and then incubated for 30 min in LIT medium containing endocytic markers. Two different tracers were used: transferrin (mostly internalized via the cytostome) and albumin [40].

Incubation with transferrin-Alexa 633 and analysis by flow cytometry showed that 2-BP treated parasites had low endocytic activity, with an approximately 90% reduction in the normalized 633 fluorescence median (Fig. 5A). Fluorescence microscopy showed that untreated cells internalized transferrin partially in co-localization with the reservosomal marker cruzipain (Fig. 5B). On the other hand, transferrin fluorescence was reduced in 2-BP parasites and no co-localization with cruzipain was observed (Fig. 5C).

Treated epimastigotes incubated with albumin-Alexa 488 showed an approximately 90% reduction in normalized 488 fluorescence (Fig 6A). Fluorescence microscopy showed no co-localization with cruzipain and little albumin was ingested (Figs. 6B and 6D).

Trypanosoma cruzi metacyclogenesis is altered by 2-BP

The metacyclic trypomastigotes/epimastigotes ratio was evaluated after 72 h in the supernatant of the TAU3AAG differentiation medium (Fig. 7A). While in the control this ratio was approximately 5:1, for 2-BP-treated parasites the ratio ranged from 0.5:1 (2-BP in pre-stress medium) to 2.5:1 (2-BP in post-stress medium) (Fig. 7B). Incubation with TcFCaBP mAb showed that all treatments (2-BP in pre-stress, stress or post-stress media) led to mislocalization of this flagellar protein, which was found at the parasite surface, but not at the flagellum.

Morphology of parasites from the culture supernatants was analyzed by light microscopy. Metacyclic trypomastigotes were abundant in the untreated control (Fig. 7C). When 2-BP was added to pre-stress assays, then epimastigotes prevailed (Fig. 7C) and the few detected metacyclic trypomastigotes were smaller, with their nucleus and kinetoplast closely located. When 2-BP was added to the stress and post-stress assays, round cells prevailed and the few detected metacyclic trypomastigotes were morphologically similar to those of the control (Fig. 7C).

Infectivity of *T. cruzi* trypomastigotes is altered by 2-BP

Trypomastigotes obtained from the TAU3AAG supernatants of the 2-BP metacyclogenesis assay were used to infect Vero cells. Six days after infection, the released trypomastigotes were counted and the parasite number was compared to that of

trypomastigotes collected from Vero cell cultures that were infected with untreated parasites. There was a significant inhibition in the number of released trypomastigotes for all 2-BP treatments, ranging from 48.5% to 75% (Fig. 8A).

Light microscopy showed round-shaped, smaller and thicker parasites with a round nucleus in all treated groups when compared to the control trypomastigotes (Fig. 8A). Released trypomastigotes from the control and pre-stress assays were incubated with TcFCaBP mAb and were visualized by fluorescence microscopy (Fig. 8B). In the control parasites protein localization was enriched in their flagella (Fig. 8B), while in the trypomastigotes from the 2-BP experiments the localization was diffuse on the cell surface or was partially located at the flagellar membrane (Fig. 8B).

In another experiment, cell-derived trypomastigotes were treated with IC_{50} 2-BP (262 µM) and then used to infect Vero cells. At this experimental point (before infection), aliquots of the treated and untreated (control) trypomastigotes were incubated with the TcFCaBP mAb. In untreated trypomastigotes the labeling was in the flagellum, while in treated parasites the labeling was diffuse in the cytoplasm, with a few trypomastigotes presenting flagellar labeling (Fig. 9A, “before infection”). After four days of infection the released trypomastigotes were collected and incubated with the TcFCaBP mAb. The same result was obtained: while in trypomastigotes from the control experiment the labeling was in the flagellum (Fig.9A, “after infection”), in trypomastigotes obtained from the the 2-BP treatment assay the labeling was diffuse in the cytoplasm, with a few trypomastigotes presenting flagellar labeling (Fig. 9A, “after infection”). The released trypomastigotes were counted and their numbers were compared. There was a 45.5% inhibition in the number of released parasites in the treatment assay (Fig. 9B). The morphology of the released parasites from the treatment assay was analyzed by light

microscopy, showing round-shaped, smaller, thicker cells with a rounded nucleus, when compared to the control trypomastigotes (Fig. 9C).

Discussion

Protein palmitoylation promotes membrane localization, regulation of enzymatic activity, regulation of gene expression and protein stability [1-3]. Many palmitoylated proteins are important for diverse aspects of pathogenesis in eukaryotic parasites, including differentiation into infective life cycle stages, biogenesis and tethering of secretory organelles, assembling the machinery powering motility and targeting virulence factors to the plasma membrane [41]. Here we analyzed the effect 2-BP, a palmitate analogue that inhibits palmitoylation, on the different life stages of the pathogenic protozoan *T. cruzi*.

T. cruzi culture epimastigotes incubated with 130 µM 2-BP (IC_{50}/48h) did not show flagellar localization of TcFCaBP (a flagellar protein that is known to be palmitoylated), which is in agreement with the data obtained with *T. cruzi* TcFCaBP palmitoylation-deficient mutants (C4A and ΔN) [24], thus indicating that 2-BP also inhibits palmitoylation in *T. cruzi* epimastigotes. TcFCaBP was also mislocated in metacyclic and culture trypomastigotes that were incubated with an IC_{50} value of 2-BP (216 nM and 262 µM, respectively), thus demonstrating that palmitoylation is an important modification for protein localization in *T. cruzi*.

Incubation of infected Vero cells for 72 hours with 2-BP resulted in a 40% increase in the number of released trypomastigotes. It is possible that 2-BP treatment led to deregulation of metabolic pathways (e.g., energy production, nucleotide metabolism, pteridine biosynthesis and/or fatty acid oxidation) in the host cells or in the intracellular parasites, which are key processes for the parasite intracellular development [42],

accelerating the parasite intracellular differentiation cycle. Indeed, several enzymes and transporters for the above mentioned metabolic pathways were already identified in the *T. brucei* palmitoylome [19].

2-BP-treated epimastigotes showed marked morphological alterations. The large vesicles close to the Golgi complex that were observed by transmission electron microscopy could be a result of inhibition of palmitoylation, leading to accumulation of depalmitoylated proteins in vesicles at the trans-Golgi network, since it is known that the Golgi compartment acts as a hub for palmitoylation [43]. It is possible that the vesicles observed close to the Golgi could leave the flagellar pocket by exocytosis, thus forming the extracellular material observed by scanning electron microscopy.

Internalization of transferrin and albumin was inhibited in the 2-BP-treated epimastigotes. Our data on transferrin inhibition are in agreement with a former work on the inhibition of diferric transferrin receptor-mediated endocytosis that is associated with palmitoylation of the transferrin receptor [44], thus suggesting that the transferrin receptor of *T. cruzi* is palmitoylated. Indeed, the existence of a transferrin receptor in *T. cruzi* has been proposed [45], but this receptor has been not yet identified. Our data indicate that the two endocytic portals of *T. cruzi* epimastigotes, the cytostome and the flagellar pocket [37,46], are deficient for transferrin/albumin internalization when palmitoylation is inhibited. Accordingly, the pellet of 2-BP-treated epimastigotes was paler than that of the control parasites (data not shown), indicating that treated parasites were deficient in incorporating hemin from the LIT medium.

The translucent vacuoles observed by light microscopy at the posterior end of epimastigotes corresponded to the large, electron-lucent vacuoles found by transmission electron microscopy. Incubation with acridine orange showed an approximately 99% increase of the fluorescence signal by flow cytometry and a stronger red labeling by

fluorescence microscopy at the posterior cell end, indicating that these large vacuoles correspond to the reservosomes, acidic organelles that accumulate ingested proteins [46]. The lower endocytic capacity of 2-BP-treated epimastigotes resulted in the appearance of these less dense reservosomes.

It has been proposed that the content of reservosomes is metabolized during the metacyclogenesis process [47]. Considering that the 2-BP-treated epimastigotes had poor endocytic activity, we analyzed the effect of incubating epimastigotes with 2-BP before metacyclogenesis (pre-stress assay). As a result, treated epimastigotes had a decreased ability to differentiate (up to 75%). Light microscopy showed that some resulting metacyclic forms had a nucleus close to the kinetoplast, indicating that the development of the differentiation process was affected. Therefore, it seems that epimastigotes bearing reservosomes with low protein content have decreased aptitude for the differentiation process.

All morphological alterations found in 2-BP stressed epimastigotes indicate that inhibition of palmitoylation was highly detrimental for differentiation and infectivity. When the resulting metacyclic trypomastigote forms were submitted to an infection assay, the percentage of released trypomastigotes decreased from 48.5% to 25%, demonstrating that the inhibition of palmitoylation interfered with parasite infectivity, possibly due to loss of surface proteins involved in host cell interactions. Metacyclic trypomastigotes obtained from the pre-stress metacyclogenesis assays were used to infect Vero cell cultures. As a result, released trypomastigotes (i.e., after 10 days without treatment with 2-BP) still showed TcFCaBP mislocalization and nuclear/kinetoplast morphological alterations, which could contribute to reduce the number of released parasites.

We submitted cell-derived trypomastigotes treated with IC_{50} 2-BP to a host cell interaction assay to determine whether the inhibition of palmitoylation could result in

reduced infectivity. The number of released trypomastigotes decreased 45.5% in the treated group, demonstrating that the inhibition of palmitoylation interfered with host cell interactions. Compared to the control trypomastigotes, the treated trypomastigotes had round-shaped, smaller, thicker cell bodies with a round nucleus, together with mislocalization of TcFCaBP. These results further indicate that palmitoylation was altered in the treated trypomastigotes.

Our data on global palmitoylation inhibition by 2-bromopalmitate show that such inhibition deregulates *T. cruzi* growth, viability, morphology, endocytosis, differentiation and host cell interaction/infectivity *in vitro*, which are crucial biological processes for the parasite survival. The next step is to identify and validate the biochemical pathways involved with palmitoylation that lead to these alterations by proteomic and reverse genetic approaches. Future studies focusing on the characterization of these pathways are also paramount to understand the role of palmitoylation-dependent protein localization in parasite survival.

Some palmitoylation inhibitor compounds have been already described [48], and one of them, Compound V (CV) behaved similarly to 2-BP, in that it inhibited all four of the DHHC proteins tested. 2-BP and CV inhibited autoacylation of the PAT enzyme, which is tightly correlated with the ability to transfer palmitate to substrate [49]. Future works with these specific palmitoylation inhibitors against *T. cruzi* could elucidate the role played by palmitoylation in the parasite life cycle.

Conclusions

2-bromopalmitate treatment in *Trypanosoma cruzi* alters morphology, endocytosis, differentiation and infectivity**,** which suggests that palmitoylation is an

important cellular process that may be a good target for further cellular/molecular biology studies.

Declarations

Ethics approval and consent to participate

Not applicable.

Consent for publication

Not applicable.

Availability of data and materials

All data generated or analyzed during this study are included in this published article and its supplementary information files.

Competing interests

The authors declare that they have no competing interests.

Funding

This work was supported by CNPq, CAPES and Fiocruz.

Authors' contributions

CMB planned and performed the experiments, analyzed the data and wrote the manuscript. RLK acquired, analyzed the flow cytometry data and help to write the paper. IE also planned experiments, analyzed the data and revised the manuscript. MJS conceived the study and edited the final version of the manuscript. All authors read and approved the final manuscript.

Acknowledgements

The authors thank the Program for Technological Development in Tools for Health-PDTIS-FIOCRUZ for use of its facilities (Flow Cytometry Platform RPT08L and Confocal and Electronic Microscopy Platform RPT07C at the Instituto Carlos Chagas/Fiocruz-PR, Brazil). The authors also thank Dr. Robert Brown for critically reading this manuscript.

References

1. Fukata Y, Murakami T, Yokoi N, Fukata M. Local palmitoylation cycles and specialized membrane domain organization. Curr Top Membr. 2016;77:97-141.

2. Blaskovic S, Adibekian A, Blanc M, van der Goot GF. Mechanistic effects of protein palmitoylation and the cellular consequences thereof. Chem Phys Lipids 2014;180:44-52.

3. Corvi MM, Berthiaume LG, De Napoli MG. Protein palmitoylation in protozoan parasites. Front Biosci. 2011;3:1067-79.

4. Conibear E, Davis NG. Palmitoylation and depalmitoylation dynamics at a glance. J Cell Sci. 2010;123:4007-10.

5. Martin BR, Cravatt BF. Large-scale profiling of palmitoylation in mammalian cells. Nat Methods 2009;6:135-8.

6. Sanders SS, Martin DD, Butland SL, Lavallée-Adam M, Calzolari D, Kay C, et al. Curation of the mammalian palmitoylome indicates a pivotal role for palmitoylation in diseases and disorders of the nervous system and cancers. PLoS Comput Biol. 2015;11:e1004405.

7. Martin BR, Wang C, Adibekian A, Tully SE, Cravatt BF. Global profiling of dynamic protein palmitoylation. Nat Methods 2012;9:84-9.

8. Roth AF, Wan J, Bailey AO, Sun B, Kuchar JA, Green WN, et al. Global analysis of protein palmitoylation in yeast. Cell 2006;125:1003-1013.

9. Nichols CB, Ost KS, Grogan DP, Pianalto K, Hasan S, Alspaugh JA. Impact of protein palmitoylation on the virulence potential of *Cryptococcus neoformans*. Eukaryot Cell 2015;14:626-35.

10. Wang C, Chen X, Shi W, Wang F, Du Z, Li X, et al. 2-Bromopalmitate impairs neural stem/progenitor cell proliferation, promotes cell apoptosis and induces malformation in zebrafish embryonic brain. Neurotoxicol Teratol. 2015;50: 53-63.

11. Hemsley PA, Weimar T, Lilley K, Dupree P, Grierson C. Palmitoylation in plants: new insights through proteomics. Plant Signal Behav. 2013;8:e25209.

12. Zhang YL, Li E, Feng QN, Zhao XY, Ge FR, Zhang Y et al. Protein palmitoylation is critical for the polar growth of root hairs in Arabidopsis. BMC Plant Biol. 2015;15:50.

13. Edmonds MJ, Morgan A. A systematic analysis of protein palmitoylation in *Caenorhabditis elegans*. BMC Genomics 2014;15:841.

14. Cho E, Park M. Palmitoylation in Alzheimer's disease and other neurodegenerative diseases. Pharmacol Res. 2016;111:133-51.

15. Young FB, Butland SL, Sanders SS, Sutton LM, Hayden MR. Putting proteins in their place: palmitoylation in Huntington disease and other neuropsychiatric diseases. Prog Neurobiol. 2012;97:220-38.

16. Ducker CE, Stettler EM, French KJ, Upson JJ, Smith CD. Huntingtin interacting protein 14 is an oncogenic human protein: palmitoyl acyltransferase. Oncogene 2004;23:9230-7.

17. Caballero MC, Alonso AM, Deng B, Attias M, De Souza W, Corvi MM. Identification of new palmitoylated proteins in *Toxoplasma gondii*. Biochim Biophys Acta 2016;1864:400-8.

18. Jones ML, Collins MO, Goulding D, Choudhary JS, Rayner JC. Analysis of protein palmitoylation reveals a pervasive role in Plasmodium development and Pathogenesis. Cell Host Microbe 2012;12:246-58.

19. Emmer BT, Nakayasu ES, Souther C, Choi H, Sobreira TJ, Epting CL et al. Global analysis of protein palmitoylation in African trypanosomes. Eukaryot Cell 2011;10:455-63.

20. Webb Y, Hermida-Matsumoto L, Resh MD. Inhibition of protein palmitoylation, raft localization, and T cell signaling by 2-bromopalmitate and polyunsaturated fatty acids. J Biol Chem. 2000;275:261-70.

21. Davda D, El Azzouny MA, Tom CT, Hernandez JL, Majmudar JD, Kennedy RT et al. Profiling targets of the irreversible palmitoylation inhibitor 2-bromopalmitate. ACS Chem Biol. 2013;8:1912-7.

22. Pedro MP, Vilcaes AA, Tomatis VM, Oliveira RG, Gomez GA, Daniotti JL. 2-Bromopalmitate reduces protein deacylation by inhibition of acyl-protein thioesterase enzymatic activities. PLoS One, 2013;8:e75232.

23. Alonso AM, Coceres VM, De Napoli MG, Nieto Guil AF, Angel SO, Corvi MM. Protein palmitoylation inhibition by 2-bromopalmitate alters gliding, host cell invasion and parasite morphology in *Toxoplasma gondii*. Mol Biochem Parasitol. 2012;184:39-43.

24. Maric D, McGwire BS, Buchanan KT, Olson CL, Emmer BT, Epting CL, Engman DM. Molecular determinants of ciliary membrane localization of *Trypanosoma cruzi* flagellar calcium-binding protein. J Biol Chem. 2011;286:33109-17.

25. Martins VP, Okura M, Maric D, Engman DM, Vieira M, Docampo R, et al. Acylation-dependent export of *Trypanosoma cruzi* phosphoinositide-specific phospholipase C to the outer surface of amastigotes. J Biol Chem. 2010;285:30906-17.

26. Batista CM, Kalb LC, Moreira CM, Batista GT, Eger I, Soares MJ. Identification and subcellular localization of TcHIP, a putative Golgi zDHHC palmitoyl transferase of *Trypanosoma cruzi*. Exp Parasitol. 2013;134:52-60.

27. Goldston AM, Sharma AI, Paul KS, Engman DM. Acylation in trypanosomatids: an essential process and potential drug target. Trends Parasitol. 2014;30:350-60.

28. Herrera LJ, Brand S, Santos A, Nohara LL, Harrison J, Norcross NR, et al. Validation of n-myristoyltransferase as potential chemotherapeutic target in mammal-dwelling stages of *Trypanosoma cruzi*. PLoS Negl Trop Dis. 2016;10:e0004540.

29. Contreras VT, Salles JM, Thomas N, Morel CM, Goldenberg S. *In vitro* differentiation of *Trypanosoma cruzi* under chemically defined conditions. Mol Biochem Parasitol. 1985;16:315-27.

30. Camargo EP. Growth and differentiation in *Trypanosoma cruzi*. I. Origin of metacyclic trypanosomes in liquid media. Rev Inst Med Trop São Paulo 1964;6:93-100.

31. Contreras VT, Araújo-Jorge TC, Bonaldo MC, Thomaz N, Barbosa HS, Meirelles MN, et al. Biological aspects of the DM28c clone of *Trypanosoma cruzi* after

metacyclogenesis in chemically defined media. Mem Inst Oswaldo Cruz 1998;83:123-33.

32. Sambrook J, Fritsch EF, Maniatis T. Molecular cloning - A laboratory manual. 2nd ed. New York: Cold Spring Harbor Laboratory Press. 1989.

33. Chou TC, Martin N. Compusyn for drug combinations: PC software and user's guide. ComboSyn Inc., Paramus, NJ, USA. 2005 (available at www.combosyn.com).

34. Batista CM, Kessler RL, Eger I, Soares MJ. *Trypanosoma cruzi* intracellular amastigotes isolated by nitrogen decompression are capable of endocytosis and cargo storage in reservosomes. PLoS One 2015;10:e0130165

35. Kessler RL, Soares MJ, Probst CM, Krieger MA. *Trypanosoma cruzi* response to sterol biosynthesis inhibitors: morphophysiological alterations leading to cell death. PLoS One 2013;8:e55497.

36. Heytler PG. Uncoupling of oxidative phosphorylation by carbonyl cyanide phenylhydrazones. I. Some characteristics of m-CI-CCP action on mitochondria and chloroplasts. Biochemistry 1963;2:357-61.

37. Soares MJ, De Souza W. Endocytosis of gold-labeled proteins and LDL by *Trypanosoma cruzi*. Parasitol Res. 1991;77:461-68.

38. Schenkman S, Diaz C, Nussenzweig V. Attachment of *Trypanosoma cruzi* trypomastigotes to receptors at restricted cell surface domains. Exp Parasitol. 1991;72:76-86.

39. Batista CM, Medeiros LC, Eger I, Soares MJ. mAb CZP-315.D9: an antirecombinant cruzipain monoclonal antibody that specifically labels the reservosomes of *Trypanosoma cruzi* epimastigotes. Biomed Res Int. 2014;2014:714-49.

40. Kalb LC, Frederico YC, Batista CM, Eger I, Fragoso SP, Soares MJ. Clathrin expression in *Trypanosoma cruzi*. BMC Cell Biol. 2014;15: 23.

41. Brown RW, Sharma AI, Engman DM. Dynamic protein S-palmitoylation mediates parasite life cycle progression and diverse mechanisms of virulence. Crit Rev Biochem Mol Biol. 2017;52:145-62.

42. Caradonna KL, Engel JC, Jacobi D, Lee CH, Burleigh BA. Host metabolism regulates intracellular growth of *Trypanosoma cruzi*. Cell Host Microbe 2013;13:108-17.

43. Michaelson D, Ahearn I, Bergo M, Young S, Philips M. Membrane trafficking of heterotrimeric G proteins via the endoplasmic reticulum and Golgi. Mol Biol Cell 2002;13:3294-302.

44. Alvarez E, Girones N, Davis RJ. Inhibition of the receptor-mediated endocytosis of diferric transferrin is associated with the covalent modification of the transferrin receptor with palmitic acid. J Biol Chem. 1990;265:16644-55.

45. Lima MF, Villalta F. *Trypanosoma cruzi* receptors for human transferrin and their role. Mol Biochem Parasitol. 1990;38:245-52.

46. Porto-Carreiro I, Attias M, Miranda K, De Souza W, Cunha-e-Silva N. *Trypanosoma cruzi* epimastigote endocytic pathway: cargo enters the cytostome and passes through an early endosomal network before storage in reservosomes. Eur J Cell Biol. 2000;79:858-69.

47. Soares MJ. The reservosome of *Trypanosoma cruzi* epimastigotes: an organelle of the endocytic pathway with a role on metacyclogenesis. Mem Inst Oswaldo Cruz 1999;94: 139-41.

48. Ducker CE, *Griffel LK, Smith RA, Keller SN, Zhuang Y, Xia Z, Diller JD, Smith CD. Discovery and characterization of inhibitors of human palmitoyl acyltransferases.* Mol Cancer Ther.2006;5**:**1647-*59.*

49. Jennings BC, Nadolski MJ, Ling Y, Baker MB, Harrison ML, Deschenes RJ, Linder ME. 2-Bromopalmitate and 2-(2-hydroxy-5-nitro-benzylidene)-benzo[b]thiophen-3-one inhibit DHHC-mediated palmitoylation in vitro. J Lipid Res. 2009;50:233-42.

Figure legends

Figure 1. Effect of 2-BP on different *Trypanosoma cruzi* developmental forms.

(A) Effect on epimastigotes. IC_{50} value was estimated as 130 µM. n=3, p<0.001. (B) Effect on metacyclic trypomastigotes. IC_{50}/24h value was estimated as 216 nM. n=3, p<0.001. (C) Effect on culture trypomastigotes. IC_{50}/4h value was estimated as 262 µM. n=3, p<0.001. (D) Effect on isolated intracellular amastigotes. IC_{50}=242 µM. n=3, p<0.001.

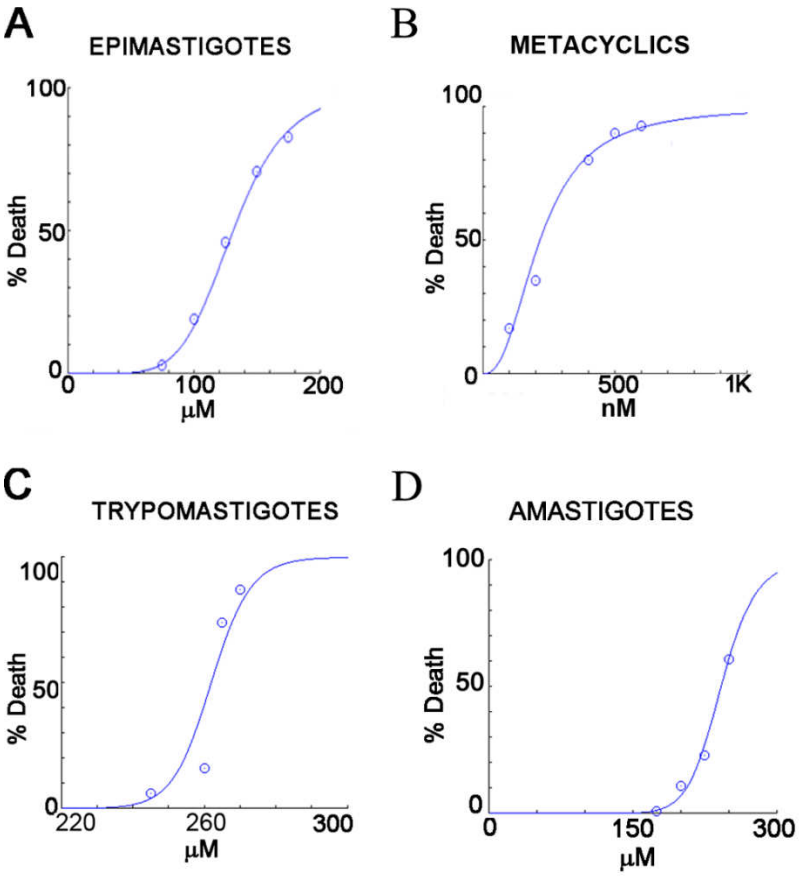

Figure 2. Localization of TcFCaBP in *Trypanosoma cruzi* epimastigotes and metacyclic trypomastigotes after 2-BP treatment.

(A-C) Negative control (CTL), showing flagellar localization (in red) of TcFCaBP in epimastigotes (A) and trypomastigotes (C). Nucleus and kinetoplast are stained with DAPI (blue). (B-D) Incubation with 130 µM 2-BP hindered flagellar localization of TcFCaBP. n: nucleus; k: kinetoplast; f: flagellum. Bars=5 µm.

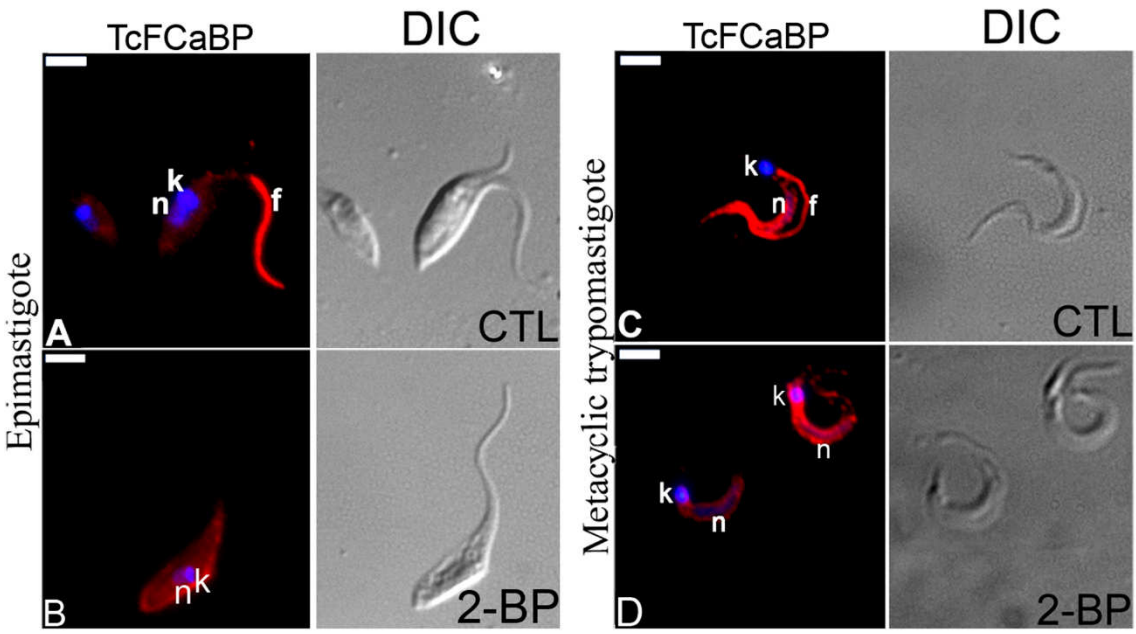

Figure 3. M**orphological alterations of *Trypanosoma cruzi* epimastigotes treated with IC_{50}/48h 2-BP.**

(A-B) Scanning electron microscopy of control (A) and 2-BP-treated (B) parasites. Note the extracellular leakage at the flagellar pocket region of treated epimastigotes (arrows). Insets (bar=5 µm): bright field microscopy of Giemsa-stained parasites. Control parasite (in A) showing the characteristic elongated shape; treated parasites (in B) were larger, with large vacuoles and were adhered by their flagella. (C-D) Transmission electron microscopy. Control epimastigote (C) showing the typical elongated morphology. A representative Golgi complex is shown in the inset. 2-BP-treated parasites (D) presented large electron lucent vacuoles at the anterior tip (arrows) and Golgi complex alterations (arrow in inset). N: nucleus; K: kinetoplast; FP: flagellar pocket; G: Golgi complex; R: reservosome; M: mitochondrion. Bars=5 µm.

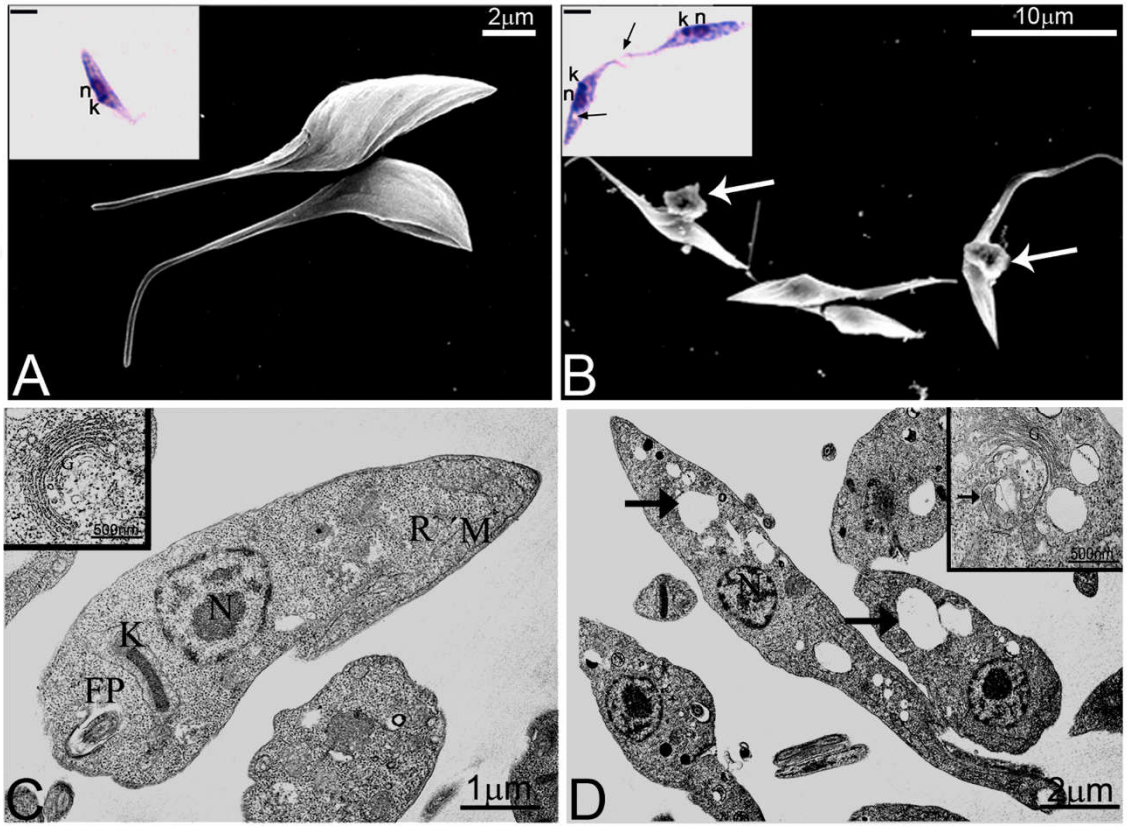

Figure 4. IC_{50}/48h 2-BP treatment Effect on *Trypanosoma cruzi* epimastigotes as assessed by flow cytometry.

(A) Forward scatter (FSC) analysis of control (CTL) and treated parasites, showing the larger size of the treated epimastigotes. (B) Side scatter (SSC) analysis of CTL and 2-BP parasites, showing an increase in granulosity. (C) Cell cycle analysis, showing no difference between CTL and 2-BP treated parasites in the different cell cycle stages. (D) Mitochondrial potential analysis by rhodamine-123, showing a decrease in the membrane potential for 2-BP-treated epimastigotes; 100 µM CCCP: positive control. (E) Cell viability analysis of CTL and 2-BP parasites by propidium iodide, showing a few dead cells in 2-BP-treated cultures.

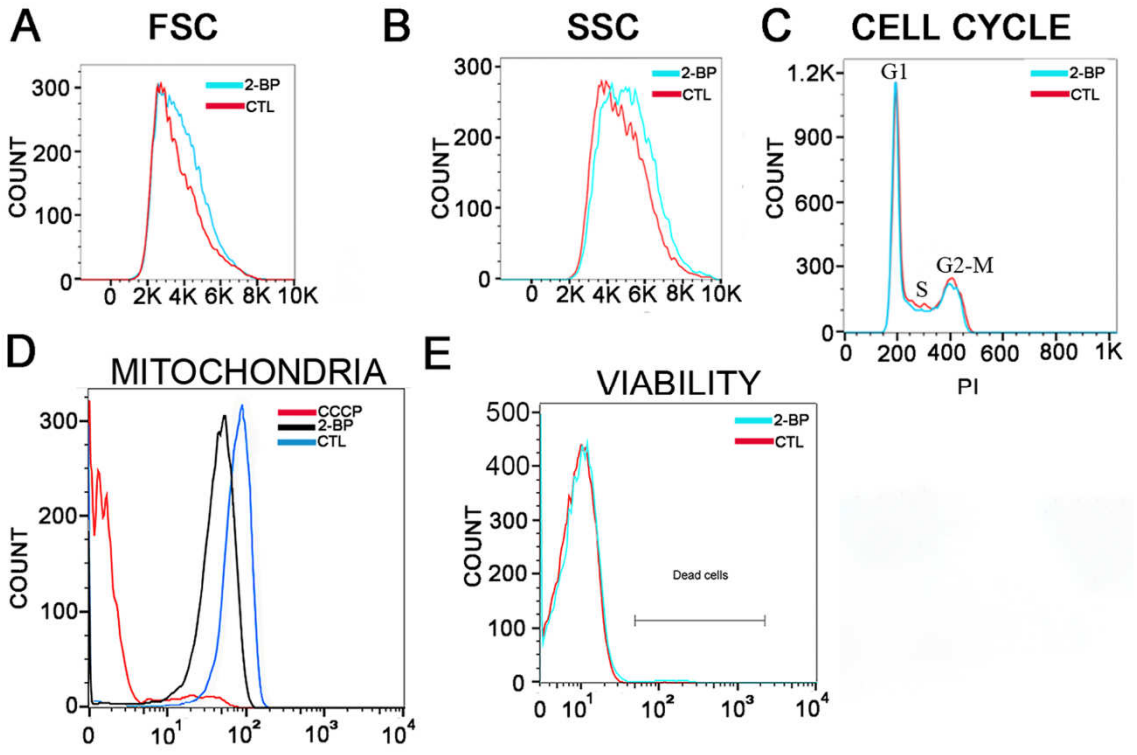

Figure 5. Transferrin-AlexaFluor 633 endocytosis is altered in *Trypanosoma cruzi* epimastigotes by 2-BP treatment.

(A) Flow cytometry analysis showing that transferrin internalization was inhibited after 4 h of treatment with 2-BP. ***: $p<0.001$. (B) Control cell: co-localization of internalized transferrin (TF-633) with cruzipain (CZP) in reservosomes by fluorescence microscopy. (C) Parasites treated for 4 h with 2-BP showing no fluorescence signal for transferrin. n: nucleus; k: kinetoplast. Bars=5 µm.

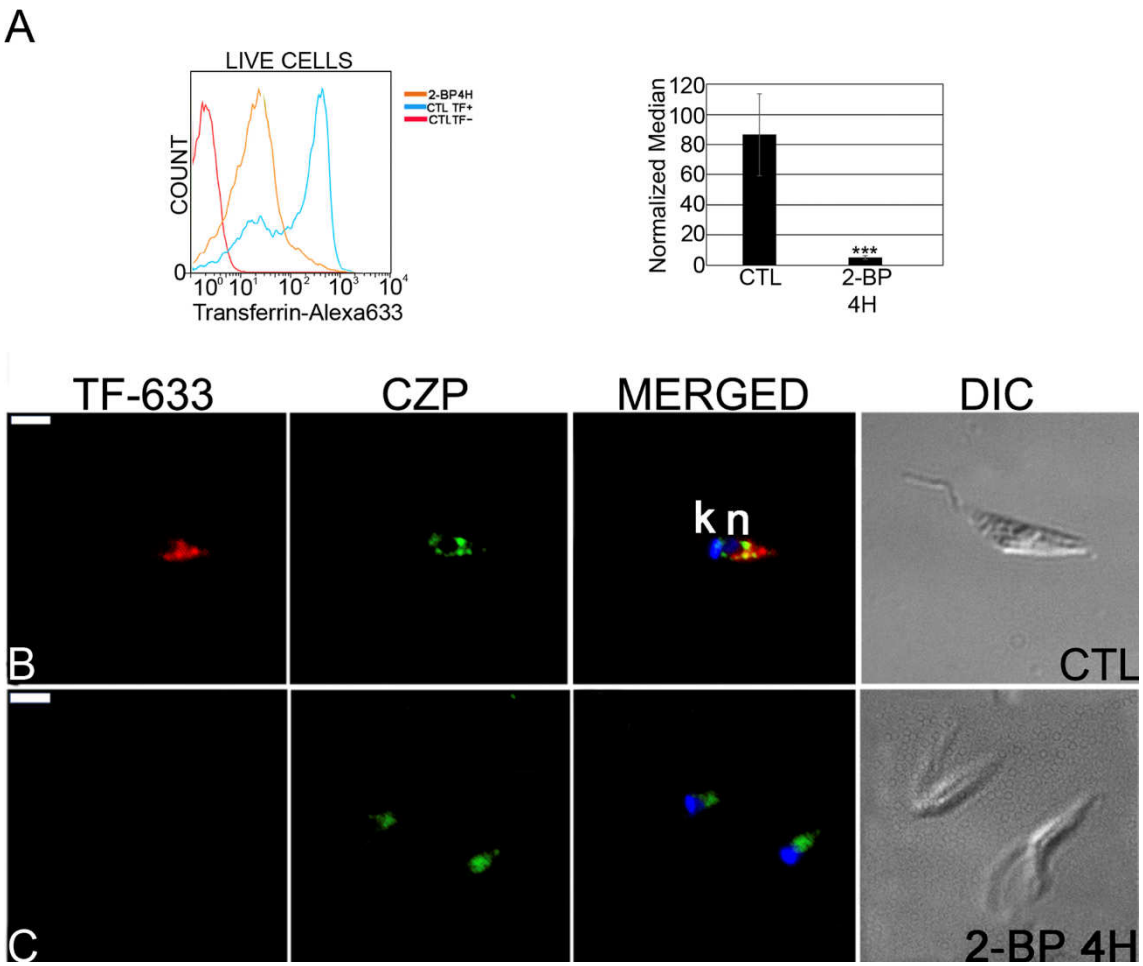

Figure 6. Albumin-Alexa 488 endocytosis is altered in *Trypanosoma cruzi* epimastigotes by 2-BP treatment.

(A) Flow cytometry analysis showing that albumin internalization was inhibited after treatment for 4 h with 2-BP. ***: $p<0.001$. (B) Control: Co-localization of internalized albumin (ALB-488) with cruzipain (CZP) in reservosomes by fluorescence microscopy.

(C) Parasites treated for 4 h with 2-BP showing no fluorescence signal of albumin (no co-localization with cruzipain). N: nucleus; k: kinetoplast. Bars=5 µm.

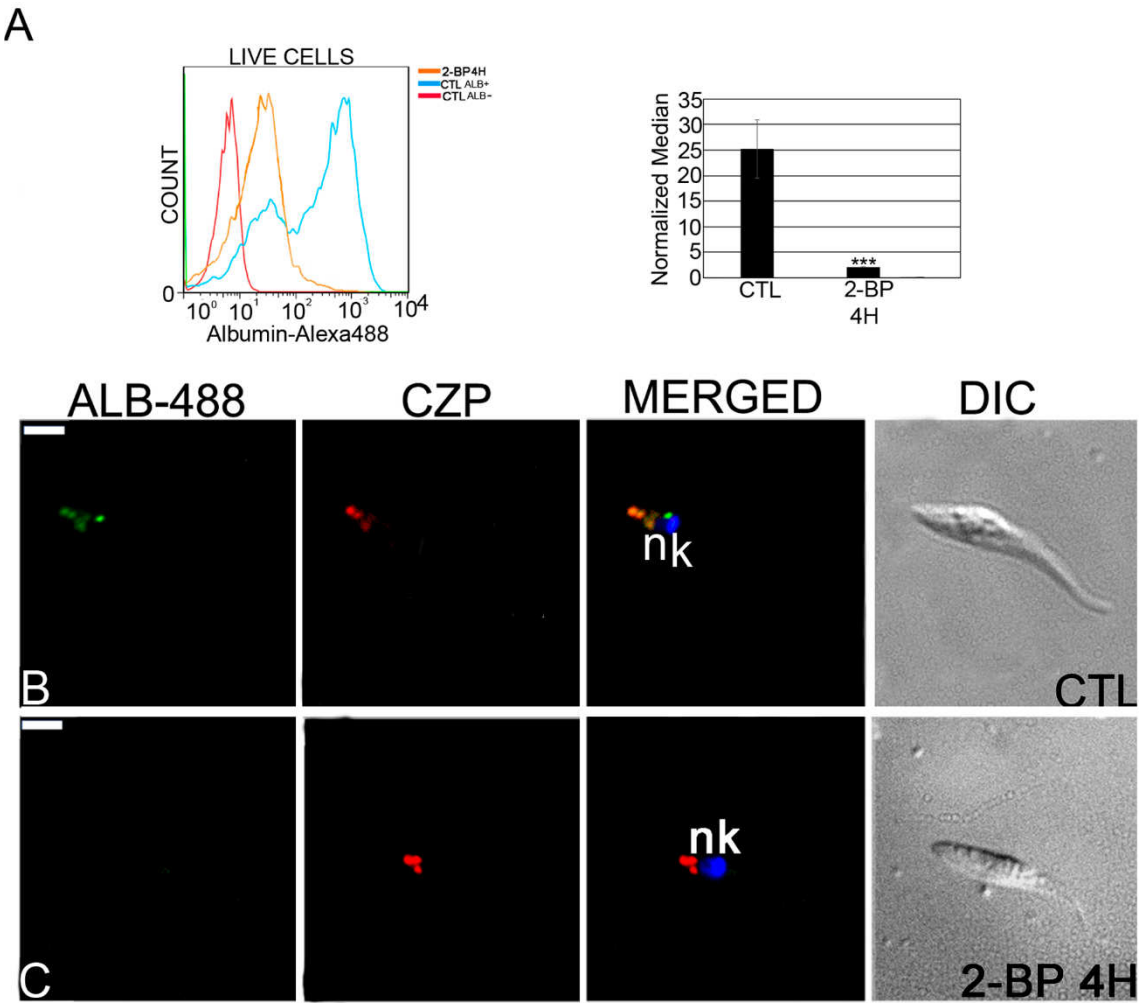

Figure 7. Metacyclogenesis of *Trypanosoma cruzi* is inhibited by 2-BP treatment.

(A) Schematic view of the metacyclogenesis experimental design. (B) Ratio of metacyclic trypomastigotes/epimastigotes after 72 h in the supernatant of TAU3AAG medium; the ratio decreased in all treatments, when compared to the untreated control. *: $p>0.005$; **: $p<0.005$; ***: $p<0.001$. (C) Giemsa-stained cells collected in the supernatant showing

morphological alterations after the different treatments. n: nucleus; k: kinetoplast. Bars=5 µm.

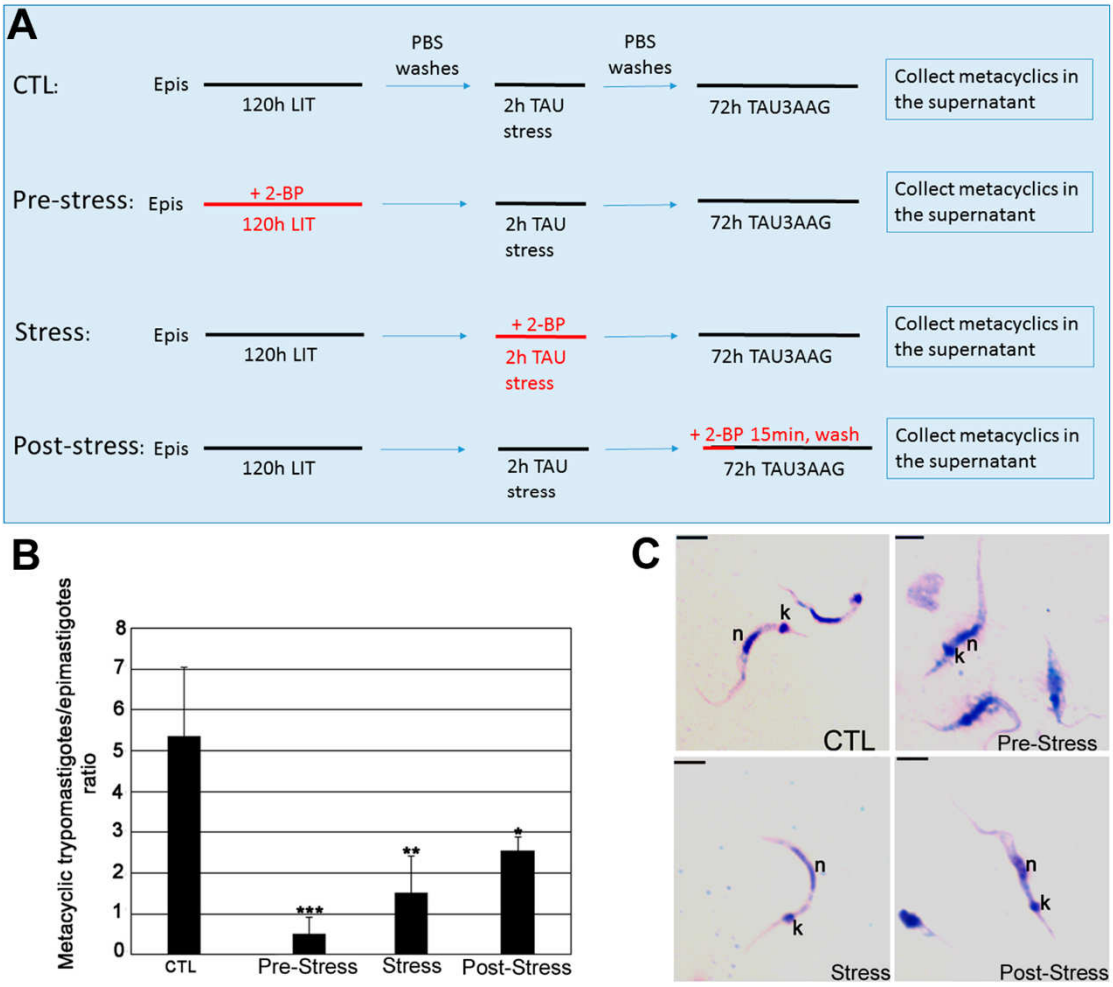

Figure 8. 2-BP treatment during metacyclogenesis alters *Trypanosoma cruzi* host cell infectivity.

(A) Number of released cell-culture trypomastigotes (CTL and 2-BP-treated groups) after Vero cell infection, showing a reduction of approximately 45.5% to 75% for the treated groups when compared to the control parasites. n=3, ***: $p<0.001$. Released cell-culture trypomastigotes (CTL and 2-BP-treated groups) as visualized by light microscopy

showing morphological alterations, such as smaller size and round nucleus, compared to the control parasites. n: nucleus; k: kinetoplast. Bars=5 µm. (B) Localization of TcFCaBP of *Trypanosoma cruzi* trypomastigotes released from Vero cells infected with 2-BP-treated metacyclic trypomastigotes (pre-stress group). CTL: Negative control showing a strong labeling in the flagellum. 2-BP: Treated parasites showing cellular (arrowhead) and partial flagellar (arrow) labeling. n: nucleus; k: kinetoplast; f: flagellum. Bars=5 µm.

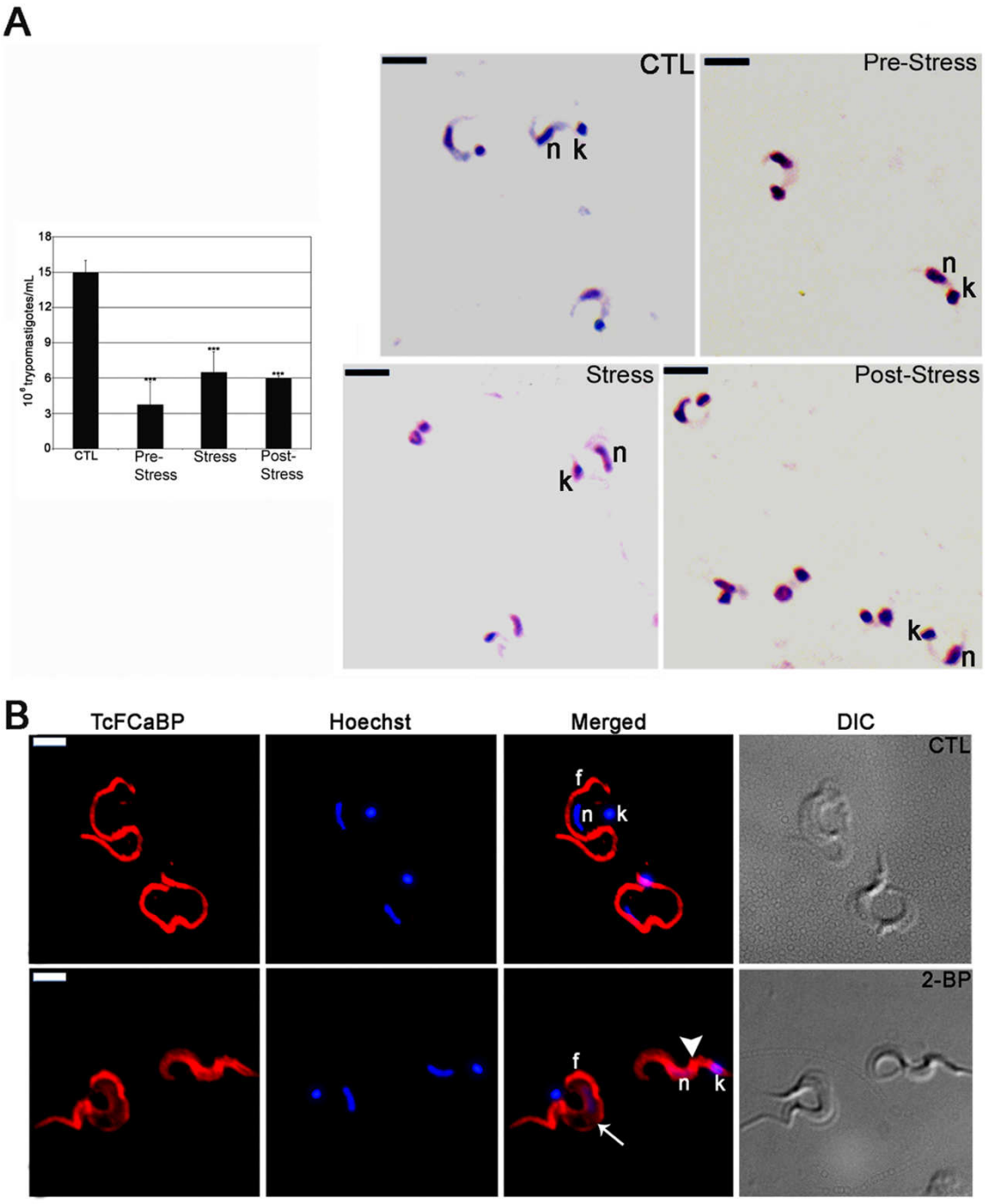

Figure 9. 2-BP treatment of culture trypomastigotes with IC_{50} 2-BP alters *Trypanosoma cruzi* host cell infectivity.

(A) 2-BP treatment before infection altered TcFCaBP flagellar localization in parasites obtained before and after infection. (B) Note the decrease in number of released trypomastigotes four days after infection. *: p>0.05 (C) Giemsa staining of released trypomastigotes showing morphological alterations. n: nucleus; k: kinetoplast. Bars=5 µm.

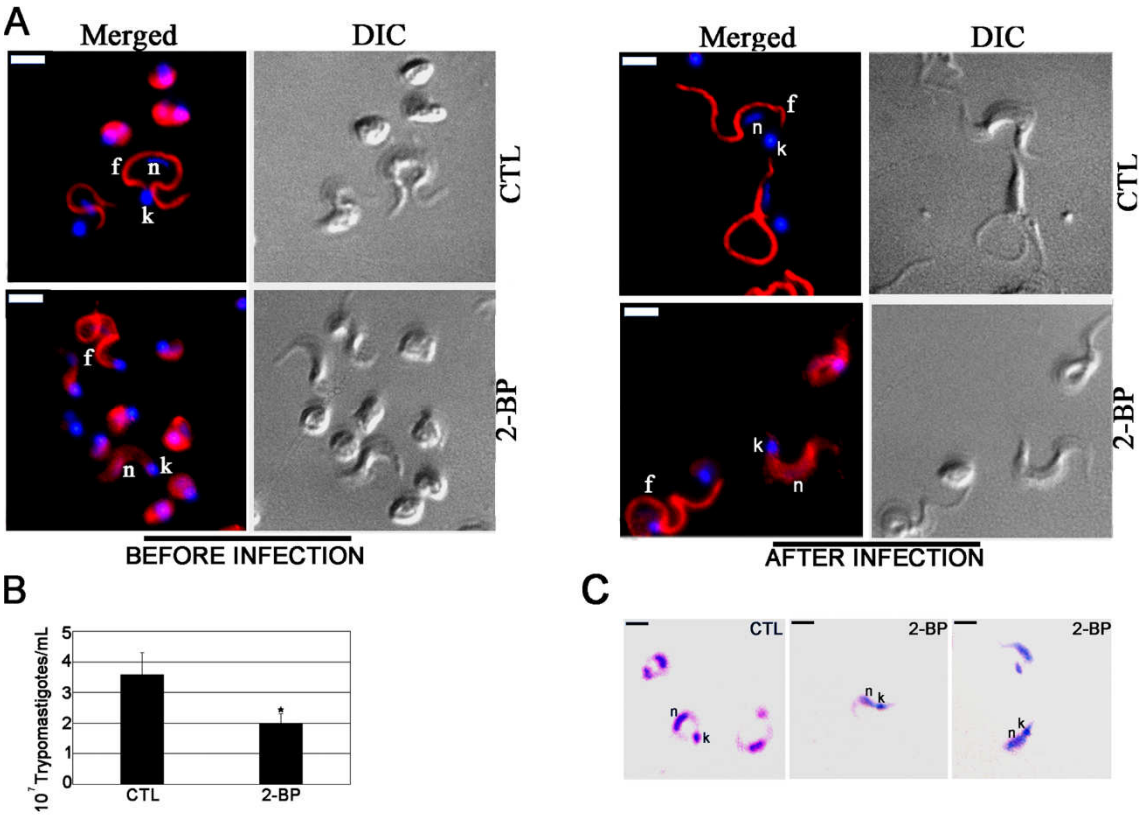

Additional Files

Additional file 1: Figure S2. 48h-old *Trypanosoma cruzi* intracellular parasites isolated by cavitation after 24 hours with 125 µM 2-BP. A) Control isolated amastigote incubated in DMEM medium with the vehicle DMSO at 0.125%;B) Treated parasite showing an intermediate morphology similar to trypomastigotes, but with kinetoplast close to the nucleus (transition form); C) Treated parasite showing the typical trypomastigote form. N= nucleus; k= kinetoplast.Bars= 5µm.

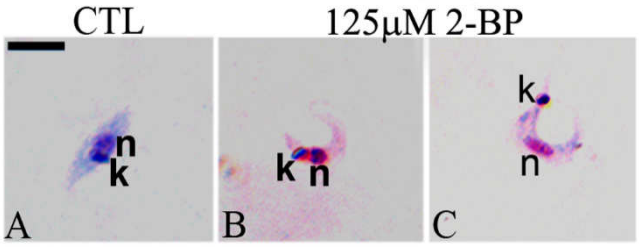

Additional file 3: Figure S3. Characterization of acid compartments in control (CTL) and 2-BP-treated epimastigotes after acridine orange (AO) staining. Note the increased AO fluorescence signal in 2-BP parasites (left panel), which corresponds to increased fluorescence in large vacuoles at the posterior cell end (right panel). Bars=5 µm.

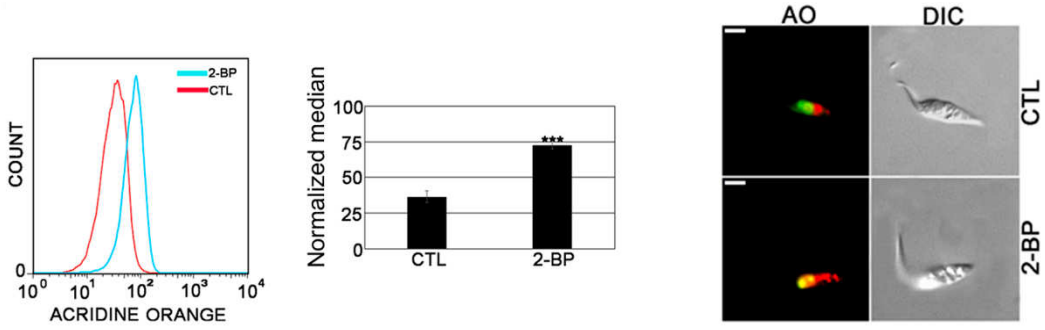

6.4. Conclusão Capítulo 3

- Os valores de CI_{50} de 2-bromopalmitato foram estimados em 130 µM em formas epimastigotas (48h), 216 nM em tripomastigotas metacíclicos (24h), 242 µM em amastigotas intracelulares isolados por cavitação (24h) e 262 µM em tripomastigotas de cultura (4h).
- A incubação de epimastigotas, por 48h, com 2-BP na concentração estimada pela CI_{50} alterou a localização de TcFCaBP, uma proteína de flagelo sabidamente palmitoilada.
- A morfologia: apareceram grandes vacúolos translúcidos na região posterior, além de alterações na ultraestrutura do complexo de Golgi.
- A endocitose de transferrina e albumina foi inibida em aproximadamente 90%.
- A metaciclogênese foi inibida em até 90% (no grupo pré-estresse).
- A infectividade foi reduzida em até 75% dos tripomastigotas metacíclicos obtidos do experimento de diferenciação e 45,5% para tripomastigotas de cultura.

VII. Capítulo 4

Palmitoil proteômica de *Trypanosoma cruzi*

Esta parte da tese teve por objetivo identificar proteínas palmitoiladas em diferentes formas evolutivas de *T. cruzi* e foi realizada no laboratório do Dr. David Morgan Engman no Cedars-Sinai Medical Center (Los Angeles, CA, EUA) durante o período de Doutorado Sanduíche por seis meses (Maio a Outubro de 2017) com bolsa PDSE CAPES (Processo 88881.135788/2016-01). A caracterização *in silico* da palmitoil proteômica de formas epimastigotas da cepa Y de *T. cruzi* foi realizada e foram identificadas 3097 proteínas, das quais: 15% foram de alta confiança ($p<0,01$), 130 (4%) tiveram média confiança ($p<0,05$) e 2501 tiveram baixa confiança ($p>0,05$). No grupo com alta confiança, 6% continham o motivo de miristoilação MG e, após predizer a função, 35% das proteínas identificadas continham função desconhecida, 13% eram de metabolismo, além de proteínas de sinalização celular e de tráfego.

Para a palmitoil proteômica de formas amastigotas intracelulares, células H9C2 foram infectadas com a cepa Y de *T. cruzi* e um total $1,2x10^9$ amastigotas intracelulares foram isolados, com uma pureza de 98% (contaminação com 2% de células hospedeiras intactas ou formas tripomastigotas). As amostras de amastigotas e de tripomastigotas concentradas estão preservadas em freezer -80ºC e serão utilizadas futuramente para análise de palmitoil proteômica através do protocolo de PalmPISC em colaboração no laboratório do Dr. David Morgan Engman.

Como estes resultados não estão compilados em forma de manuscrito, serão descritos a seguir em formato tradicional com introdução, objetivos, material e métodos, resultados e discussão e conclusões os dados obtidos.

7.1. Introdução

O sequenciamento de genomas não é o suficiente para abranger muitos dos processos biológicos. Deve-se saber, por exemplo, quais proteínas estão realmente sendo expressas, quando e em quais níveis esta expressão ocorre e quais são as suas modificações pós-transcricionais, possibilitadas pela análise dos transcritos de RNAm (transcriptômica) e, após mais avanços, a análise do conjunto de proteínas expressas a partir do genoma (proteômica) (Revisado por Humphery-Smith, 2015).

A definição do termo proteômica surgiu no ano de 1995 como sendo a caracterização em larga escala do conjunto de proteínas expressas em uma célula ou tecido (Wasinger et al., 1995). O proteoma não é estático e depende das condições e estímulos a que o organismo é exposto. Sendo assim, a proteômica visa o estudo da estrutura, função e o controle dos sistemas biológicos pela análise das várias propriedades das proteínas, incluindo também os estudos da sequência, abundância, atividade e estruturas das proteínas expressas por uma célula, assim como as modificações, interações e translocações sofridas pelas proteínas (Revisado por Humphery-Smith, 2015).

A proteômica consiste basicamente em extrair, separar, quantificar e identificar proteínas. Quando essas proteínas são intactas, o termo abordado é proteômica *top down* e quando a análise é dos seus peptídeos, ela é chamada de proteômica *bottom up*. Na proteômica *botton up*, há a digestão da proteína intacta, sendo os peptídeos analisados por espectrometria de massas (Han et al., 2008).

A proteômica *top down* tem sido empregada para o estudo da S-palmitoilação: a palmitoil proteômica. São duas as principais abordagens: 1) a técnica ABE (*Acyl Biotinyl Exchange*) utiliza a propriedade da hidroxilamida de clivar a ligação tioéster entre a cisteína e o ácido palmítico, seguido da substituição por biotina e enriquecimento utilizando estreptavidina (Figura 1.3) (Wan et al., 2007); 2) o uso do ácido graxo alcinil 17-octadecinóico (17-ODYA: 17-*octadecynoic acid*) aliado à *click chemsitry* (Martin e Cravatt, 2009). Recentemente, houve uma melhoria da abordagem ABE utilizando alterações no protocolo para espectrometria de massas (PalmPISC, do inglês *Palmitoyl Protein Identification and Site Characterization*), na qual a etapa de tripsinização é antecipada ao passo de biotinilização para que os sítios de S-palmitoilação sejam identificados (Figura 7.1) (Yang et al., 2010).

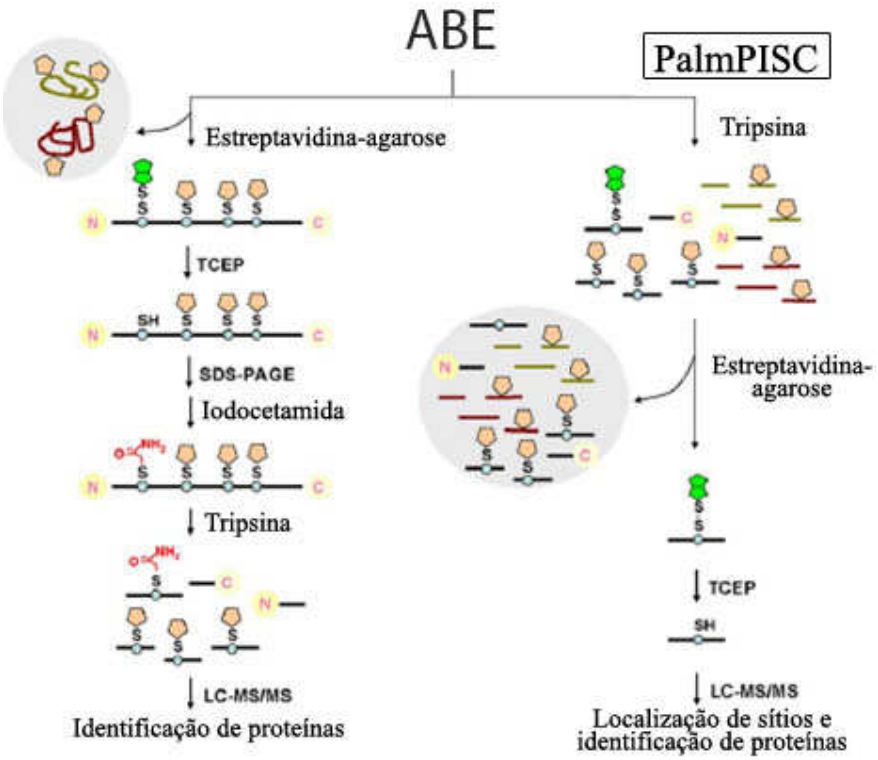

Figura 7.1. Comparação entre a preparação de amostras para *Acyl-biotinyl Exchange* (ABE) e *Palmitoyl Protein Identification and Site Characterization* (PalmPISC). Na preparação por ABE original, a amostra é tripsinizada após a coluna de afinidade da biotina com estreptavidina-agarose, e peptídeos da proteína inteira são enriquecidos e eluídos, permitindo apenas a identificação de proteínas. Na preparação PalmPISC a amostra é tripsinizada logo após a biotinilação dos tióis resultantes da quebra da ligação tioéster entre a cisteína e o ácido palmítico. Assim, após cromatografia de afinidade com estreptavidina-agarose apenas peptídeos oriundos da ligação entre a biotina e estreptavidina são enriquecidos e eluídos, e a localização dos sítios de S-palmitoilação é revelada além da identificação de protéinas. Modificado de Yang et al., 2010.

A tabela 7.1 compara dozenove estudos de larga escala em palmitoil proteômica após busca no PubMed (NCBI). Destes, onze foram em mamíferos, cinco em protozoários patogênicos, dois em plantas e um em leveduras. Treze estudos utilizaram ABE ou derivados, e seis utilizaram 17-ODYA-*click chemistry*. Apenas um dos estudos usou ambas as técnicas (Jones et al., 2012) e 212 proteínas foram enriquecidas mutualmente. O número de proteínas identificadas variou de 21 (Kostiuk et al., 2008) a 641 (Collins et al., 2017). Apenas dois estudos identificaram sítios de palmitoilação, variando de 168 (Yang et al., 2010) a 906 (Collins et al., 2017). Treze estudos realizaram validação dos dados, confirmando a palmitoilação experimentalmente de uma proteína (Nievas et al., 2018; Caballero et al., 2016; Foe et al., 2015; Hemsley et al., 2013; Jones et al., 2012; Dowal et al., 2011; Kostiuk et al., 2008), um grupo de proteínas (Morrinson et al., 2015;

Chesarino et al., 2014; Martin e Cravatt, 2009; Kang et al., 2008; Roth et al., 2006) ou utilizando outras técnicas de proteômica, tais como SILAC (Martin et al., 2012).

Tabela 7.1. Estudos de palmitoil proteômica em larga escala em diversos organismos.

Modelo de estudo	Método	Nº de proteínas identificadas\sítios	Validação	Refs
Trichomonas vaginalis	ABE	363\-	TvTSP8	Nievas et al., 2018
Mus musculus (cérebro)	ssABE*	641\906	-	Collins et al., 2017
Rattus norvegicus (cérebro)	ABE e acil RAC**	ABE 241\- Acil RAC 144\-	-	Edmonds et al., 2017
Toxoplasma gondii	ABE	401\-	ROP5	Caballero et al., 2016
Cultura celular de *Populus trichocarpa*	ABE	450\-	-	Srivastava et al., 2016
T. gondii	17-ODYA\ Click chemistry	282\-	AMA1	Foe et al., 2015
Homo sapiens (células T)	ABE	280\-	6	Morrinson et al., 2015
H. sapiens (em infecção com HIV)	17-ODYA\click chemistry	174\-	-	Colquoun et al., 2015
M. musculus (fibroblastos e células dendríticas)	17-ODYA\Click chemistry	563\-	6	Chesarino et al., 2014

Arabidosis thaliana	ABE	600	LRR-RLK	Hemsley et al., 2013
Plasmodium falciparum	ABE\17-ODYA-click chemistry	ABE 111 (alta confiança) \-17-ODYA\click chemistry 82 (alta confiança\-	202 proteínas enriquecidas mutualmente (alta e média confiança) PfGAD45	Jones et al., 2012
M. musculus (Células T)	17-ODYA\Click chemistry	165 (117 alta confiança)	Todas por SILAC	Martin et al., 2011
H. sapiens (plaquetas)	PalmPISC	215\-	TLT-1	Dowal et al., 2011
Trypanosoma brucei	ABE	124\-	-	Emmer et al., 2011
H. sapiens (balsas lipídicas)	PalmPISC	398\ 168	-	Yang et al., 2010
H. sapiens (Células T Jurkat)	17-ODYA-click chemistry	125\-	Família 3FAM108	Martin e Cravatt, 2009
R. norvegicus (mitocôndria do fígado)	17-ODYA-click chemistry	21\-	HMG65	Kostiuk et al., 2008
R. norvegicus (células neurais)	ABE	268\-	21	Kang et al., 2008
Saccharomyces cerevisiae	ABE	47	26	Roth et al., 2006

*Do inglês *site specific* ABE, permite a identificação de sítios de palmitoilação.
** Sem uso de biotina no lugar do ácido palmítico, a coluna de afinidade é baseada em beads de tiopropil, que têm afinidade com os tióis livres pós clivagem com hidroxilamida.

Nenhuma palmitoil proteômica foi realizada em *T. cruzi* e pela palmitoilação poder estar envolvida em diversos processos biológicos do parasito, o objetivo desta parte

da tese foi realizar a palmitoil proteômica de epimastigotas de *T. cruzi*, através da técnica PalmPISC.

7.2. Objetivo

Analisar a proteômica de proteínas palmitoiladas em epimastigotas de *T. cruzi*.

7.3. Objetivos específicos

1. Padronizar e realizar o enriquecimento de proteínas palmitoiladas pela metodologia "*Acyl-biotinyl Exchange*", com a melhoria da técnica (PalmPISC);

2. Identificar as proteínas palmitoiladas enriquecidas por espectrometria de massas (LC-MS/MS);

3. Analisar por bioinformática o perfil das famílias das proteínas identificadas em epimastigotas de *T. cruzi*, com validação dos dados.

7.4. Material e Métodos

7.4.1. Preparo de amostras para PalmPISC

Este protocolo de PalmPISC para análise de palmitoil proteômica foi gentilmente cedido pelo Dr. Wei Yang (Yang et al., 2010), o qual desenvolveu a abordagem PalmPISC e está em colaboração com o laboratório do Dr. David Engman.

Reagentes

- Solução neutra quebradora de pontes TCEP a 0.5 M (Pierce)
- N-etilmaleimida (Pierce)
- Hidroxilamina a 50% (Sigma)
- Biotina-HPDP (Pierce)
- Esferas (beads) de estreptavidina-agarose de alta capacidade (Pierce)
- Dimetilformamida (Sigma)

Tampões utilizados

- Tampão M: 50 mM HEPES, 10 mM NaCl, 5 mM $MgCl_2$, 0.1 mM EDTA, pH 7,4
- Tampão 4SB: 50 mM Tris-HCl, 4% SDS, 5 mM EDTA, pH 7,4
- Tampão 2SB: 50 mM Tris-HCl, 2% SDS, 5 mM EDTA, pH 7,4
- Tampão de diluição: 50 mM Tris-HCl, 150 mM NaCl, 0,2% Triton X-100, 5 mM EDTA
- Tampão de equilíbrio: 50 mM Tris-HCl, 150 mM NaCl, 0,2% Triton X-100, 0,1% SDS, 5 mM EDTA
- Tampão de lise: Tris-HCl 80 mM, SDS 4%, pH7.4

- Hidroxilamida neutra 4 M: Diluir a hidroxilamina com ddH_2O, usar 36,5% HCl para ajustar o pH para 7,4; adicionar volume apropriado de ddH_2O para uma concentração final de 4 M. Este tampão pode ser estocado a 4°C por muitos meses.

Outras soluções necessárias a serem preparadas frescas

-3,33 M N-etilmaleimida: Misturar etanol e N-etilmaleimida na proporção de 1,65 μL etanol por mg de N-etilmaleimida.

- 4 mM Biotina-HPDP em dimetilformamida: 2,2 mg de biotina-HPDP por ml de dimetilformamida.

- Tampão Biotina-HPDP/HA^+ (mL): 333 μL 4 M biotina-HPDP + 333 μL 4 M de hidroxilamina + 26,7 μL 10% Triton X-100 + 306,3 μL ddH_2O

- Tampão Biotina-HPDP/HA^- (mL): 333 μL 4 M biotina-HPDP + 333 μL 0.1 M Tris-HCl pH 7,4 + 26,7 μL 10% Triton X-100 + 306,3 μL ddH_2O

Enriquecimento de proteínas para SDS-PAGE e Western blot

As formas epimastigotas foram lisadas com tampão de lise (5x o volume da amostra) suavemente homogeneizadas em vortex, sem fervura. Os lisados foram estocados a -80°C até o uso.

A amostras em um tubo foram misturadas e a concentração de proteína determinada por Bradford. Adicionar volume apropriado do tampão 4SB para ajustar a concentração de proteína para 5,0 mg/mL.

As proteínas foram precipitadas por metanol/clorofórmio. Para cada replicata, começar com 1,0 mg de proteina e precipitar com metanol/clorofórmio de acordo com o seguinte: para cada 200 μL de solução de proteína, foram adicionados 600 μL de metanol, vortexado por 5 segundos, adicionado 150 μL de clorofórmio, vortexado por 5 segundos, adicionado 400 μL de ddH_2O, vortexado por 5 segundos. As amostras foram centrifugadas a 16.000×g por 10 min a temperatura ambiente (TA). As soluções de cima e de baixo foram removidas, sem perturbar a fase branca média (proteínas). As amostras foram centrifugadas novamente a 16.000×g por 15 segundos em TA e o sobrenadante residual removido.

Para a redução de proteína por TCEP, o pellet de proteínas foi redissolvido com 100 μL/tubo do tampão 4SB por incubação repetitiva a 37°C por 10 min e vortexando (como descrito acima). Depois da solubilização completa do pellet, foram adicionados 292 μl do tampão de diluição e as amostras hoogeneizadas em vortex por 5 segundos. Em seguida, foram adicionados 8 ml do tampão neutro quebrador de pontes TCEP a 0,5M

(concentração final 10 mM), as amostras foram vortexadas por 5 segundos e incubadas em TA por 30 min sob agitação orbital.

Para a alquilação de resíduos de cisteína não palmitoilados, foram adicionados 6 ml de N- etilmaleimida 3,33 M em etanol para cada amostra, seguido da incubação por 2,5 h em agitação orbital em TA.

As amostras foram divididas em dois tubos, identificadas como HA(+) e outro como HA(-). Foram realizadas 4-5 precipitações em methanol\clorofórmio sequenciais para remover o excesso de N-etilmaleimida, conforme descrito acima.

O pellet foi redissolvido com tampão 4SB (como descrito acima) usando 50 μL/tubo. Para os tubos HA(+), foram adicionados 150 ml de tampão biotina-HPDP/HA^+; para os tubos HA(-) adicionar 150 ml de tampão biotina-HPDP/HA^-. Foram realizardas precipitações em methanol\clorofórmio sequenciais para remover o excesso de biotina-HPDP.

Os pellets foram redissolvidos com o tampão 2SB 70 μL/tubo (mesmo procedimento descrito acima). Foi adicionado o tampão de diluição 1,330 μL para cada tubo, vortexado por 5 segundos e incubado em TA por 30 min em agitação orbital. As amostras foram centrifugadas a 16.000×g por 5 min em TA. O sobrenadante foi reservado.

As esferas de estreptavidina agarose de alta capacidade foram equilibradas. O frasco contendo as esferas por 5 vezes foi invertido gentilmente e 100 μL do conteúdo foi transferido para cada tubo Eppendorf. Um mL do tampão de equilíbrio foi adicionado para cada tubo, sendo eles invertidos por 5 vezes, centrifugados a 200×g por 1 min e descartados os sobrenadantes. O passo de lavagem foi repetido por duas vezes adicionais.

O sobrenadante de proteínas reservado anteriormente foi transferido para os tubos contendo as esferas de alta capacidade de estreptavidina-agarose equilibradas, incubados em TA por 1 h em agitação orbital, centrifugados a 200×g por 1 min e descartado o sobrenadante. As esferas com tampão de equilíbrio 1 mL/tubo foram lavadas por um total de seis vezes. Para lavagem, foi repetido o descrito para equilibrar as eferas de estreptavidina agarose.

Para a eluição das proteínas enriquecidas, foi adicionado 200 μL TCEP a 20 mM em tampão de equilíbrio para cada tubo e os mesmos incubados em TA por 30 min em agitação orbital, centrifugados a 200×g por 1 min e transferidos sobrenadante (o mais completo possível) para limpar os tubos Eppendorf. Logo depois, as amostras foram centrifugadas a 200×g por 2 min e o sobrenadante transferido, encostando nas esferas,

para limpar os tubos Eppendorf. Foram adicionados 600 μL metanol para cada tubo, vortexados por 5 segundos, adicinado 150 ml de clorofórmio, vortexados por 5 segundos, adicionar 400 μL de ddH_2O, vortexados por 5 segundos e centrifugados a 16.000×g por 10 min em TA. A fase alta foi descartada sem tocar a fase média. Foiram adicionados 800 ml de metanol para cada tubo, vortexados por 5 seg e centrifugados a 16.000×g por 10 min em TA. O sobrenadante foi descartado e seco com ar por 10 min em TA. Foram adicionados 10 μL de tampão de corrida redutor 1× para cada tubo e vortexados por 10 segundos. Agora as amostras estão prontas para SDS-PAGE e western blot, ou, em larga escala, para LC-MS\MS.

7.4.2. Análise *in silico* das proteínas identificadas no palmitoil proteoma de formas epimastigotas de *T. cruzi*

Após análise estatística por ANOVA com ajuste de Bonferroni baseada na intensidade LQF (do inglês *Label-free Quantification*), as proteínas identificadas foram separadas em três grupos: 1) alta confiança ($p<0.01$), média confiança ($p<0.05$) e baixa confiança ($p>0.05$). Em seguida, apenas as proteínas do grupo de alta confiança foram selecionadas para uma analise *in silico* mais detalhada tais como a checagem da presença destas proteínas em outras proteômicas já publicadas em *T. cruzi*, a presença do motivo MG na sequencia aminoacídica, que indica a N-miristoilação de proteínas e, com auxílio do bando de dados de tripanossomatídeos TritrypDB e protein BLAST, foi realizada a análise de Gene Ontology (GO terms) e busca de homólogos e domínios para predição da função. Importante ressaltar que as proteínas hipotéticas sem domínios conservados e homologia com proteínas conhecidas foram anotadas como de função desconhecida.

7.5. Resultados e Discussão

7.5.1. Palmitoil proteoma de epimastigotas de *T. cruzi*, cepa Y

Depois do protocolo PalmPISC para espectrometria de massas e análise dos dados por bioinformática, um total de 3097 proteínas foram identificadas em formas epimastigotas: 466 (15%) com alta confiança ($p<0,01$), 130 (4%) com confiança média ($p<0,05$) e 2501 com baixa confiança ($p>0,05$), depois de análise estatísca por ANOVA com ajuste de Bonferroni (Figura 7.2). No grupo de alta confiança, 29 proteínas (6%) continham o motivo de miristoilação MG (Figura 7.2). A miristoilação é outra modificação lipídica de proteínas, onde um ácido graxo saturado de 14 carbonos é adicionado a uma glicina N-terminal, sendo catalisada por uma única N-miristoil

transferase (Heng et al., 2013). Proteínas podem ser miristoiladas e palmitoiladas, sendo assim determinada sua localização e função (Godsel e Engman, 1999). Não foi possível identificar os sítios de palmitoilação. Mais amostras serão corridas para este fim.

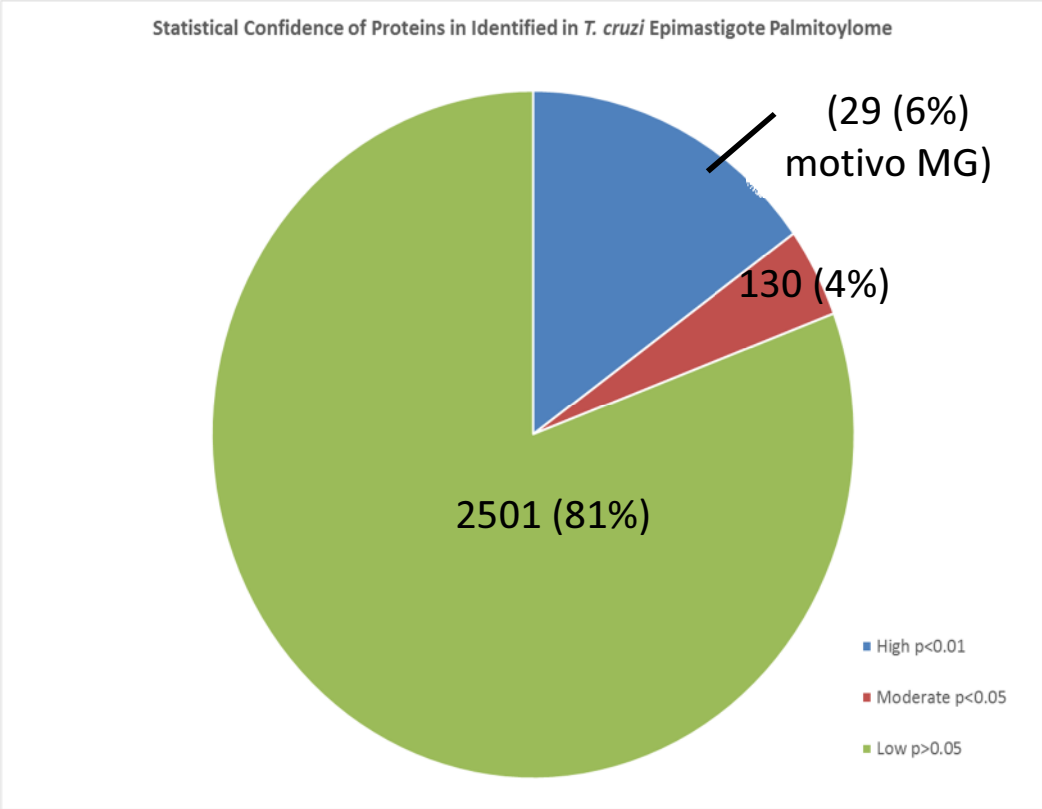

Figura 7.2. Proteínas identificadas na palmitoil proteômica de formas epimastigotas de *Trypanosoma cruzi* por PalmPISC. Das 3097 proteínas identificadas**,** 466 (15%) eram de alta confiança (p<0,01), 130 (4%) de confiança média (p<0,05) e 2501 de baixa confiança (p>0,05). No grupo de alta confiança, 29 proteínas (6%) continham o motivo de miristoilação MG.

Após análises adicionais *in silico* do grupo de alta confiança, a determinação da função protéica foi baseada nos domínios e na conservação (homologia) com proteínas de função conhecida. Um total de 152 (35%) destas proteínas possui função desconhecida (proteínas hipotéticas), seguido de proteínas de metabolismo (59 proteínas, 13%), de sinalização celular e de tráfego de vesículas (Figura 7.3). Como mais de 50% do genoma de *T. cruzi* codifica para proteínas hipotéticas (El Sayed et al., 2005), é de se esperar que proteínas hipotéticas representem uma boa porcentagem de qualquer proteoma, os outros grupos, tais como metabolismo e tráfego, são esperados numa palmitoil proteômica.

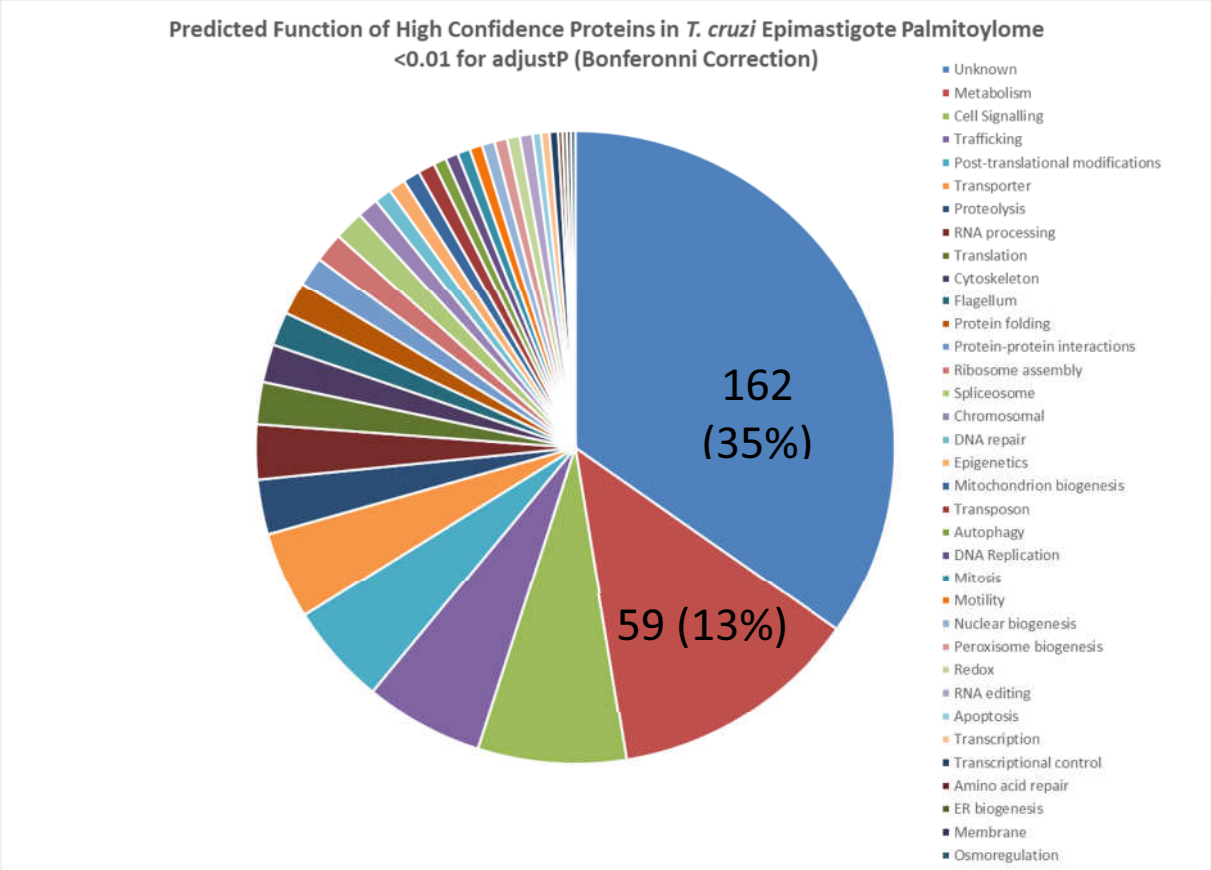

Figura 7.3. Predição *in silico* de função das proteínas identificadas por PalmPISC com alta confiança. A função foi predita com base em conservação e domínios.

A perspectiva futura é realizar a validação dos dados, o que envolve a seleção de 10-20 proteínas identificadas no grupo de alta confiança para estudos confirmatórios, os quais envolvem a geração de OGMs contendo proteínas com etiquetas para realizar (a) PalmPISC (SDS-PAGE, western blot), (b) imunofluorescência após tratamento com 2-BP para verificar alteração de localização, (c) mutação nos resíduos de cisteína e (d) nocaute por CRISPR-Cas9 ou recombinação gênica.

7.5.2. Palmitoil proteoma de amastigotas intracelulares

Células H9C2 foram infectadas com a cepa Y de *T. cruzi* e um total $1,2x10^9$ amastigotas intracelulares foram isolados por cavitação (Batista et al., 2015), com uma pureza de 98%, sendo a contaminação com 2% de células hospedeiras intactas ou formas tripomastigotas (Fig 7.4). O próximo passo será realizar o protocolo de PalmPISC com estas amastigotas e a análise dos dados, além da validação. Os pellets estão mantidos em freezer -80^{o}C.

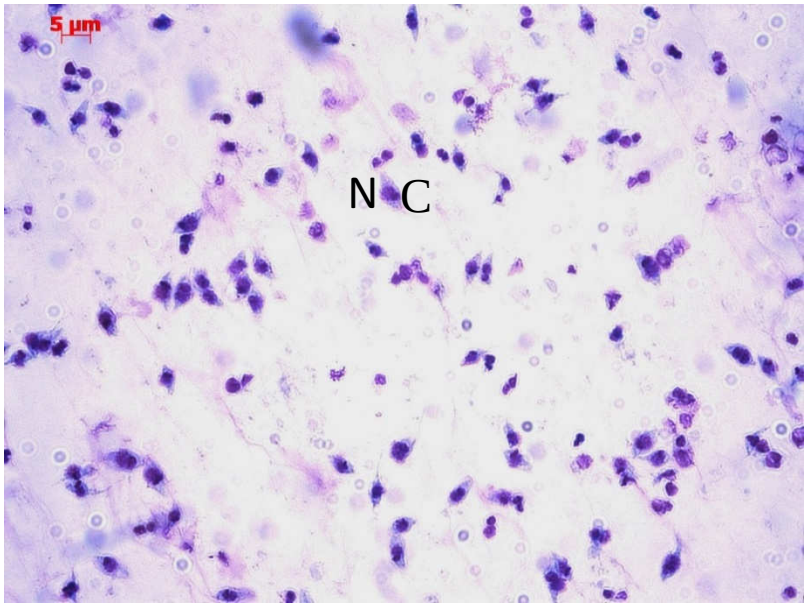

Figura 7.4. População de amastigotas intracelulares isolados pos cavitação que serão utilizados para PalmPISC. C=cinetoplasto; N= Núcleo. Barra= 5 µm.

7.5.3. Palmitoil proteoma de tripomastigotas de cultura

Também temos 5,6 x 10^9 tripomastigotas de cultura com 80% de pureza, com 20% de amastigotas extracelulares (Figura 7. 5) Próximo passo será realizar PalmPISC e análise e validação dos dados.

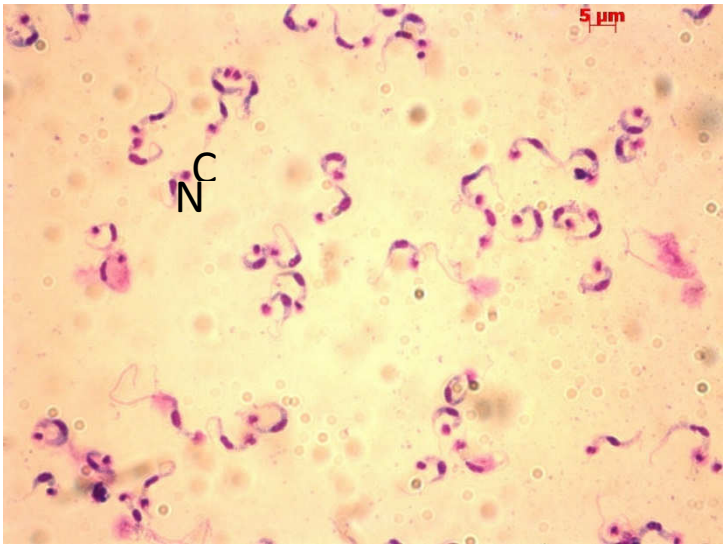

Figura 7.5. População de tripomastigotas de cultura que serão utilizados para PalmPISC. C=cinetoplasto; N= núcleo. Barra= 5 µm.

7.6. Conclusão Capítulo 4

- Após realizar PalmPISC de formas epimastigotas da cepa Y de *T. cruzi* foram identificadas 3097 proteínas: 15% foram de alta confiança, 4% tiveram média confiança e 2501 tiveram baixa confiança.
- No grupo com alta confiança, 29 proteínas (6%) continham o motivo de miristoilação MG.
- 152 (35%) proteínas identificadas continham função desconhecida, 59 (13%) eram de metabolismo, além de proteínas de sinalização celular e de tráfego.

7.7. Referências Bibliográficas

CABALLERO, M.C. et al. 2016. Identification of new palmitoylated proteins in *Toxoplasma gondii*. **Biochimical and Biophysical Acta.** 864:400-408.
Disponível em: < https://www.ncbi.nlm.nih.gov/pubmed/26825284>

CHESARINO, N.M. et al. 2014. Chemoproteomics reveal Toll-like receptor fatty acylation. **BMC Biology.** 12:91.
Disponível em: < https://www.ncbi.nlm.nih.gov/pubmed/25371237>

COLLINS, M.O. et al. 2017. Global, site-specific analysis of neuronal protein S-acylation. **Scientific Reports.** 7: 4683.
Disponível em: < https://www.ncbi.nlm.nih.gov/pubmed/28680068>

COLQUHOUN, D.R. et al. 2015. Bioorthogonal mimetics of palmitoyl-CoA and myristoyl-CoA and their subsequent isolation by click chemistry and characterization by mass spectrometry reveal novel acylated host proteins modified by HIV-infection. **Proteomics**. 15: 2066-2077.
Disponível em: < https://www.ncbi.nlm.nih.gov/pubmed/25914232 >

DOWAL, L. et al. 2011. Proteomic analysis of palmitoylated platelet proteins. **Blood.** 118: 62-63.
Disponível em: < https://www.ncbi.nlm.nih.gov/pubmed/21813449 >

EDMONDS, M.J. et al. 2017. Analysis of the brain palmitoyl-palmitoylome using both acyl-biotin exchange and acyl resin assisted capture methods. **Scientific Reports.** 7:3299.

Disponível em: < https://www.ncbi.nlm.nih.gov/pubmed/28607426 >

EL-SAYED, N.M. et al. 2005. The genome of *Trypanosoma cruzi*, etiologic agent of Chagas Disease. **Science.** 309:409-415.
Disponível em: < https://www.ncbi.nlm.nih.gov/pubmed/16020725>

EMMER, B.T. et al. 2011. Global analysis of protein palmitoylation in African trypanosomes. **Eukaryotic Cell.** 10: 455–463.
Disponível em: < https://www.ncbi.nlm.nih.gov/pubmed/21193548>

FOE, I.T. et al. 2015. Global analysis of palmitoylated proteins in *Toxoplasma gondii*. **Cell Host and Microbe.** 18: 501-511.
Disponível em: < https://www.ncbi.nlm.nih.gov/pubmed/26468752>

GODSEL, L.M. e ENGMAN, D.M. 1999. Flagellar protein localization mediated by a calcium-myristoyl/palmitoyl switch mechanism. **EMBO Journal.** 18: 2057-2065.
Disponível em: < https://www.ncbi.nlm.nih.gov/pubmed/10205160>

HAN, X. et al. 2008. Mass spectrometry for proteomics. **Current Opinion on Chemistry and Biology.** 12:483-490.
Disponível em: < https://www.ncbi.nlm.nih.gov/pubmed/18718552>

HEMSLEY, P.A. et al. 2013. Palmitoylation in plants: new insights through proteomics. **Plant Signal Behavior.** 8:25209.
Disponível em: < https://www.ncbi.nlm.nih.gov/pubmed/23759553>

HENG, J. et al. 2013. Membrane targeting of the small myristoylated protein 2 (SMP-2) in *Leishmania major*. **Molecular and Biochemical Parasitology.** 190: 1-5.
Disponível em: < https://www.ncbi.nlm.nih.gov/pubmed/23727225>

HUMPHERY-SMITH, I. 2015. The 20th anniversary of proteomics and some of its origins. **Proteomics.** 15: 1773-1776.
Disponível em: < https://www.ncbi.nlm.nih.gov/pubmed/25689367>

JONES M.L. et al. 2012. Analysis of protein palmitoylation reveals a pervasive role in Plasmodium development and Pathogenesis. **Cell Host and Microbe.** 12:246-258.
Disponível em: < https://www.ncbi.nlm.nih.gov/pubmed/22901544>

KANG, R. et al. 2008. Neural Palmitoyl-Proteomics Reveal Dynamic Synaptic Palmitoylation. **Nature.** 456:904-909.
Disponível em: < https://www.ncbi.nlm.nih.gov/pubmed/19092927>

MARTIN, B.R. e CRAVATT B.F. 2009. Large-scale profiling of palmitoylation in mammalian cells. **Nature Methods.** 6:135-138.
Disponível em: < https://www.ncbi.nlm.nih.gov/pubmed/19137006>

MARTIN, B.R. et al. 2011. Global profiling of dynamic protein palmitoylation. **Nature Methods.** 9:84-89.
Disponível em: < https://www.ncbi.nlm.nih.gov/pubmed/22056678>

MORRISON, E. et al. 2015. Quantitative analysis of the human T cell preoteome. **Scientific reports**. 5: 11598.
Disponível em: < https://www.ncbi.nlm.nih.gov/pubmed/26111759>

NIEVAS, Y.R. et al. 2018. Protein palmitoylation plays an important role in *Trichomonas vaginalis* adherence. **Molecular and Cellular Proteomics.** Doi: 10.1074\mcp.RA117.000018.
Disponível em: < https://www.ncbi.nlm.nih.gov/pubmed/29444981>

ROTH, A.F. et al. 2006. Global Analysis of Protein Palmitoylation in Yeast. **Cell.** 125:1003-1013.
Disponível em: < https://www.ncbi.nlm.nih.gov/pubmed/16751107>

SRIVASTAVA, V. et al. 2016. Proteomic Analysis of a Poplan Cell Suspense of Culture Suggestd a Major Role of S-Acylation in Diverse Cellular Processes. **Frontiers in Plant Science.**7:477.
Disponível em: < https://www.ncbi.nlm.nih.gov/pubmed/27148305>

WAN, J. et al. 2007. Palmitoylated proteins: purification and identification. **Nature Methods.** 2: 1573-1584.
Disponível em: < https://www.ncbi.nlm.nih.gov/pubmed/17585299>

WASINGER, V.C. 1995. Progress with gene product mapping of the Mollicutes: Mycoplasma genitalium. **Electrophoresis.** 16: 1090-1094.
Disponível em: < https://www.ncbi.nlm.nih.gov/pubmed/7498152>

YANG, W. et al. 2010. Proteome scale characterization of humam S-acylated proteins in lipid raft-enriched and non-raft membranes. **Molecular and Cellular Proteomics.** 9: 54-70.
Disponível em: < https://www.ncbi.nlm.nih.gov/pubmed/19801377>

YANG, W. et al. 2010. Proteome scale characterization of humam S-acylated proteins in lipid raft-enriched and non-raft membranes. **Molecular and Cellular Proteomics.** 9: 54-70.
Disponível em: < https://www.ncbi.nlm.nih.gov/pubmed/19801377>

VIII. Discussão Geral

Esta tese teve por objetivo realizar uma análise global da S-palmitoilação em *T. cruzi*, tanto em relação às proteínas que são palmitoiladas, quanto em relação às enzimas DHHC palmitoil transferases (que podem realizar este processo) e palmitoil tioesterases (que desfazem o processo).

Apesar da S-palmitoilação ser uma modificação importante em vários organismos modelos, nenhum estudo global foi realizado até o momento em *T. cruzi*. Uma das abordagens de estudos globais em S-palmitoilação concerne a identificação das enzimas envolvidas no processo, revelando suas localizações subcelulares. Identificamos 15 TcPATs e 2 PPTs no parasito, e após etapas de clonagem, transfecção e seleção de organismos geneticamente modificados (OGMs), suas localizações foram estudadas por microscopia de fluorescência. A localização das PATs concentrada na região anterior era esperada, por ser esta uma região onde ocorrem eventos importante de tráfego de proteínas, transporte de vesículas, bem como endocitose e exocitose, processos nos quais S-palmitoilação está envolvida em outros organismos. Já a localização das PPTs dispersa pelo citoplasma também era esperada, pelo fato de proteínas palmitoiladas serem destinadas a várias localidades dentro ou fora da célula. Este é um estudo inicial destas enzimas. O próximo passo será realizar estudos funcionais, tais como nocaute gênico e/ou mutações direcionadas no sítio ativo das enzimas, revelando sua relevância para a biologia do parasito.

Nesta tese também foi desenvolvida uma metodologia para isolamento de amastigotas intracelulares, para posteriores estudos biológicos, tais como endocitose, incubação com inibidor de palmitoilação e palmitoil proteômica. Foi possível obter uma população viável e purificada de amastigotas isolados por esta técnica, com marcação positiva de Ssp4, uma proteína específica da superfície destas formas. Após realizar ensaios de endocitose, foi comprovada a atividade endocítica, com co-localização de transferrina e/ou albumina com cruzipaína nos reservossomos destas formas.

Uma outra abordagem utilizada em estudos globais de S-palmitoilação é o tratamento com o inibidor de S-palmitoilação 2-bromopalmitato (2-BP) e análise dos efeitos nas células. Sabe-se que 2-BP é citotóxico, portanto ele é usado apenas para estudar a S-palmitoilação. Como este reagente nunca foi usado em *T. cruzi*, focamos em analisar seu efeito em diferentes formas do ciclo de vida, na morfologia, endocitose, diferenciação e infectividade. 2-BP demonstrou efeito em todas as formas analisadas.

Interessantemente, o CI_{50} em tripomastigotas metacíclicos foi em escala nanomolar, indicando que a S-palmitoilação possui alguma função importante nessas formas. Por microscopia eletrônica de transmissão observamos alterações na ultraestrutura do complexo de Golgi. Uma hipótese é que inibição da S-palmitoilação estaria afetando a ultraestrutura do Golgi por acúmulo de proteínas não palmitoiladas. Formas epimastigotas foram incubadas com 2-BP na concentração estimada pelo CI_{50} de 2-BP por 4 horas. Após avaliação por citometria, foi possível verificar que a endocitose de albumina e transferrina foi inibida em 90% das células, indicando que a S-palmitoilação possui um papel importante na endocitose neste parasito. Como a endocitose está relacionada ao processo de diferenciação de formas epimastigotas para tripomastigotas metacíclicas (metaciclogênese), testamos o efeito de 2-BP durante a diferenciação. A diferenciação foi alterada em até 90%, indicando que a S-palmitoilação possui um papel importante neste processo. Os tripomastigotas metacíclicos oriundos destes tratamentos também foram menos infectivos (em até 75%). Tripomastigotas de cultura tratados com o CI_{50} específica destas formas foram até 45,5% menos infectivos. Portanto, S-palmitoilação pode estar relacionada com a infectividade de *T. cruzi*. Como 2-BP é citotóxico, o próximo passo pode ser a busca de inibidores de S-palmitoilação mais específicos para *T. cruzi*, como possíveis candidatos à abordagem terapêutica. Além disso, nossos dados podem ser usados para comparação com dados proteômicos, ajudando a desvendar o papel da S-palmitoilação na biologia do *T. cruzi*.

Por fim, um estudo global importante sobre S-palmitoilação é a palmitoil proteômica, onde proteínas com esta modificação são identificadas. Com esta abordagem é possível caracterizar as diversas funções da S-palmitoilação na célula. Análise *in silico* demonstrou que 466 proteínas com diversas funções (desconhecidas, metabolismo, tráfego, entre outras) tem grande potencial de serem palmitoiladas em formas epimastigotas de *T. cruzi*. Assim, o próximo passo é a validação dos dados do palmitoil proteoma de epimastigotas de *T. cruzi*. Além disso, temos pellets congelados de amastigotas intracelulares isolados por cavitação e tripomastigotas de cultura, que aguardam o seu processamento para realizar PalmPISC e identificação das proteínas e dos sítios, além da validação.

IX. Conclusão final

Consideramos que a relevância desta tese foi iniciar estudos gerais sobre a S-palmitoilação de proteínas em *T. cruzi*. Os dados gerados nesta tese podem servir de base para estudos posteriores que visem compreender a função da S-palmitoilação na biologia do parasito, tendo em vista que: (a) este protozoário possui a maquinaria enzimática necessária para a realização desta modificação pós-traducional; (b) a inibição por 2-BP alterou diversos eventos biológicos importantes para a sobrevivência do parasito (endocitose, diferenciação e infectividade), e (c) diversas proteínas de interesse podem estar palmitoiladas e envolvidas em importantes vias metabólicas, tais como endocitose, sinalização celular e movimento flagelar, uma vez que alguns destes alvos foram identificados por palmitoil proteômica.